McKelvey School of Engineering Theses & Dissertations

McKelvey School of Engineering

Winter 12-15-2021

Advancements in Pressurized Oxy-Combustion Process: Pollutant Control and Process Development

Piyush Kumar Verma
Washington University in St. Louis

WASHINGTON UNIVERSITY IN ST. LOUIS

Department of Energy, Environmental & Chemical Engineering

McKelvey School of Engineering

Dissertation Examination Committee:

Dr. Richard L. Axelbaum, Committee Chair
Dr. Ramesh Agarwal
Dr. Klas Andersson
Dr. Young-Shin Jun
Dr. Benjamin Kumfer
Dr. Jay Turner
Dr. Grigory Yablonsky

Advancements in Pressurized Oxy-Combustion Process: Pollutant Control and Process Development

by

Piyush Kumar Verma

Prepared under the guidance of Prof. Richard L. Axelbaum

A dissertation presented to

The Graduate School

of Washington University in

partial fulfillment of the

requirements for the degree

of Doctor of Philosophy

December 2021

Saint Louis

Table of Contents

List of Figures

List of Tables

<u>Acknowledgements</u>

First and foremost, I would like to thank Prof. Richard Axelbaum, my Ph.D. advisor, for his constant guidance and support. He provided me the freedom to explore different scientific ideas, which has helped me learn and better understand my research interests. I am grateful to him for several discussions we have had over the years about scientific and non-scientific topics, which have greatly enriched my intellect. His devotion to science and his work ethic will always remain a guiding principle for me.

I am immensely thankful to all my committee members, Dr. Ramesh Agarwal, who agreed to step in at the last moment to serve as a committee member and whose lectures have been extremely valuable, Dr. Klas Andersson whose work has been critical and forms the basis of majority of this work, Dr. Young-Shin Jun for providing help with the fundamental work in her lab, and Dr. Jay Turner for his guidance. I am grateful to Dr. Ben Kumfer for constantly helping me with several aspects of this work and to Dr. Grigory Yablonsky for always providing great insights and being extremely kind. I would also like to express my gratitude to the late Dr. Ramachandran, who served as a committee member, and who was an extremely kind and brilliant mentor.

I would also like to thank all my colleagues at the Laboratory of Advanced Combustion and Energy Research, especially Dr. Zhiwei Yang, Dr. Akshay Gopan, and Dr. Dishant Khatri, without whom this work would not have been possible. I would also like to thank all my St Louis friends for making this time fun and exciting, especially, Anushree, Sayan, Nishit, Sukrant, Apoorva, and Darshit.

Finally, my gratitude goes to my college friends who motivated me to pursue a Ph.D. and made this work possible, and to my parents, Pramila Sinha and Sushil Verma, who made it all possible.

<div align="right">Piyush Kumar Verma</div>

Washington University in St Louis

December 2021

ABSTRACT OF THE DISSERTATION

Advancements in Pressurized Oxy-Combustion Process: Pollutant Control and Process
Development

by

Piyush Verma

Doctor of Philosophy in Energy, Environmental and Chemical Engineering

Washington University in St. Louis, 2021

Professor Richard Axelbaum, Chair

The emission of carbon dioxide from the power industry is one of the major causes of climate change. However, it is well established that the development of human societies across the globe depends on reliable and dispatchable power, which are generally the source of these emissions. There has been a recent growth in the integration of intermittent sources such as wind and solar which are carbon free. But these intermittent sources have significant temporal changes in power production and thus lack reliability and dispatchablity. This is a complicated problem to solve. However, flexible power plants with carbon capture and storage, are dispatchable electricity sources that precisely fit the need of the modern grid. One of the most promising carbon capture, utilization, and storage technology for coal power plants is the pressurized oxy-combustion technology. In pressurized oxy-combustion, coal is burned under elevated pressure with oxygen and recycle flue gas to produce a stream consisting mainly of CO_2 and H_2O. The moisture in the pressurized gas condenses at a higher temperature, which can be integrated to the steam cycle to increase the plant efficiency.

Staged Pressurized Oxy-Combustion (SPOC) technology developed at Washington University at St Louis is an advanced version of pressurized oxy-combustion technology. The SPOC process

has significantly higher plant efficiency compared to other pressurized combustion technologies because of reduced flue gas recycle. This work is divided into two parts to advance the understanding of pressurized oxy-combustion technology, specifically SPOC technology. The first part of the work focuses on the formation and removal of pollutants and the second part focuses on process development.

Coal combustion produces oxides of sulfur and nitrogen (SO_x and NO_x). These gases are acidic in nature and can lead to pipeline corrosion during the pressurization and transport of CO_2. Therefore there is a need to understand the formation of these gases in the combustor and their subsequent removal in a direct contact cooler (DCC). To understand the formation of SOx, NOx, and CO under pressure, we performed experiments in a 100 kWth pilot-scale combustor under a range of excess oxygen concentration and residence times. We found that the formation of SO_2 decreases with excess oxygen concentration in flue gas and pressure, potentially because of higher SO_3 formation and higher sulfur retention in the ash. The concentration of NO in the flue gas decreased with pressure but increased with excess O_2 concentration, mainly because at higher pressure, the fuel nitrogen diffusion out of the char particle is reduced, providing a higher time for reduction to N_2. Finally, we also found that the CO concentration in the flue gas decreased at a higher pressure and higher O_2 concentrations, suggesting that at higher pressure, combustion can be accomplished with lower excess oxygen, which can reduce the cost of O_2 production.

The removal of SO_x and NO_x is performed in a DCC at a temperature below 300° C. The DCC also recovers the latent heat from the moisture making the absorption in DCC high-temperature process. To develop the kinetics of the reaction between absorbed SO_2 and NO_2, (HSO_3^- and HNO_2) experiments were performed in a CSTR under a varying pH and temperature, relevant to

DCC conditions. We found that the reaction rate goes up with increasing temperature and reducing pH. Moreover, lowering the pH also led to the formation of HSO_4^- in place of a complex called HADS (hydroxyaminodisulfonic acid). A kinetic constant and temperature dependency of the reactions were obtained from the data. Based on these experiments and additional analytical analysis, the overall reaction mechanism in the DCC was reduced and a model of optimal complexity was established. The model consisted of 5 main reactions capable of predicting the kinetics inside the DCC.

To understand the transport characteristics and validate the reduced kinetic model, experiments were performed in a pilot-scale DCC. Several parameters of interest, such as pressure, oxygen concentration, inlet gas temperature, NO/SO_2 ratio, and liquid to gas ratio, were analyzed. The results suggested that pressure increased the scrubbing of both NO and SO_2. However, the impact pressure on SO_2 scrubbing increased significantly with increasing the NO to SO_2 ratio. We found that increasing the inlet gas temperature had a negative effect on both NO and SO_2 scrubbing, but the scrubbing of SO_2 through liquid-phase reactions increased with increasing NO/SO_2 ratio and temperature. Moreover, we found a significant impact of liquid to gas ratio on SO_2 scrubbing but only a mild impact on NO scrubbing. The reduced kinetics was modeled in Aspen Plus and validated against the experimental results, predicting them accurately. Finally, the reduced kinetics was used to model and optimize a full-scale DCC in Aspen Plus. An optimized model with a split water flow design increased the scrubbing efficiency of NO and SO_2 by 9% and 3%, respectively, compared to the conventional design.

The second section of the thesis focuses on the process development of the pressurized oxy-combustion process. One of the major reasons for efficiency improvement in the SPOC process is

the reduced recycle ratio. To understand the impact of recycle on oxy-combustion processes, a fundamental thermodynamic model was developed, which was complemented with a process model in Aspen plus. We found a non-linear impact of recycle ratio on the net plant efficiency of the power plant, with the impact increasing in a hyperbolic mode at a higher recycle ratio. Exergy destruction in the boiler was found to have a more significant impact on the plant efficiency than fan power consumption.

Finally, the process design and analysis of modular, pressurized air-combustion (MPAC), carbon-capture ready power plant were performed in Aspen plus to understand the plant efficiency and to provide a pathway to transition the MPAC plant to SPOC power plant. The objective was to develop a power plant that is highly efficient and flexible but can be easily converted to an SPOC power plant when economics allows for such a move. We found that the efficiency of the MPAC power plant was 1.7% higher than conventional air combustion power plants with major components similar to SPOC. A pathway to transition to SPOC was also discussed.

This combination of experimental and modeling results and analysis presented in this work hopes to push the development of SPOC process a step further.

Chapter 1. Introduction and Overview

1.1 Background and Motivation

The decarbonization of the electricity grid is a crucial step towards the net-zero emission of CO_2 [1]. The objective is to create a carbon-free grid that also provides reliable electricity at all times. Based on reliability, the electricity sources can be differentiated into intermittent sources, such as solar and wind power, and dispatchable sources, such as coal power plants with carbon capture and storage (CCUS). With the growing integration of intermittent sources in the grid, it is also essential that the dispatchable sources are not only reliable but flexible to compensate for the load changes from intermittent sources [2]. A flexible coal power plant with CCUS is a viable tool that fulfills all the requirements of a robust and clean grid while advancing the accommodation of intermittent electricity technologies. In addition, it also paves the way for continued use of the abundant coal in developing countries, such as China and India, to provide cheap and reliable power, which is critical for their growing economy. Precisely because of the underlined reasons, several agencies have projected that CCUS is a vital technology to fight global climate change [3], [4]. According to an estimate from Global CCS Institute presented in Fig 1.1, a substantial increase in CCUS technologies is required to achieve the sustainable development scenario [5].

Figure 1.1 CO_2 Capture Capacity in 2020 and 2050 by fuel and sector in the IEA Sustainable developmental scenario[5].

Oxy-combustion technology is one of the most promising technologies for CCUS [6]. In oxy-combustion, fuel is burned in the presence of oxygen and recycled flue gas to produce flue gas consisting primarily of CO_2 and H_2O [7]. After H_2O condensation and pollutant removal, a high purity stream of CO_2 is produced, which can be easily pressurized and sequestered and/or utilized. The first-generation carbon capture technologies such as atmospheric oxy-combustion, pre-combustion capture, and post-combustion capture (e.g., Amine absorption) all suffer from low efficiency and high cost because of the high parasitic loads and capital costs [8,9]. Therefore, several 2nd generation technologies for carbon capture have been proposed and are currently under development. Staged, pressurized oxy combustion (SPOC) technology, presented in Fig.1.1, conceptualized by Akshay et al.[10] is a promising 2nd generation CCUS technology owing to its high efficiency and relatively low cost and risk. The high efficiency of SPOC stems from pressurized combustion and small flue gas recycle (FGR). In pressurized oxy-combustion, coal is combusted with oxygen (and recycle flue gas) at elevated pressure (15 bar). Pressurized

2

combustion enables the recovery of the latent heat of the moisture in the flue gas by condensing moisture at high temperatures [11]. The latent heat is recovered in a direct contact cooler (DCC) and integrated into the steam cycle to increase the net plant efficiency (NPE). An additional benefit of operating under pressure is that the SO_x and NO_x in the flue gas can be scrubbed simultaneously in the DCC. This process of emission removal, which is effective only at elevated pressure, has a lower capital cost than traditional pollutants removal methods – e.g., flue gas desulfurization for SO_x removal and selective catalytic reduction (SCR) for NO_x removal. Finally, the staging of the boilers in a series-parallel combination enables a small FGR and high efficiency and ensures that all boilers operate at similar conditions [12]. In addition to the similar operating conditions and enhanced flexibility, this configuration also helps in a significant reduction of capital cost for manufacturing because of the economics of mass production.
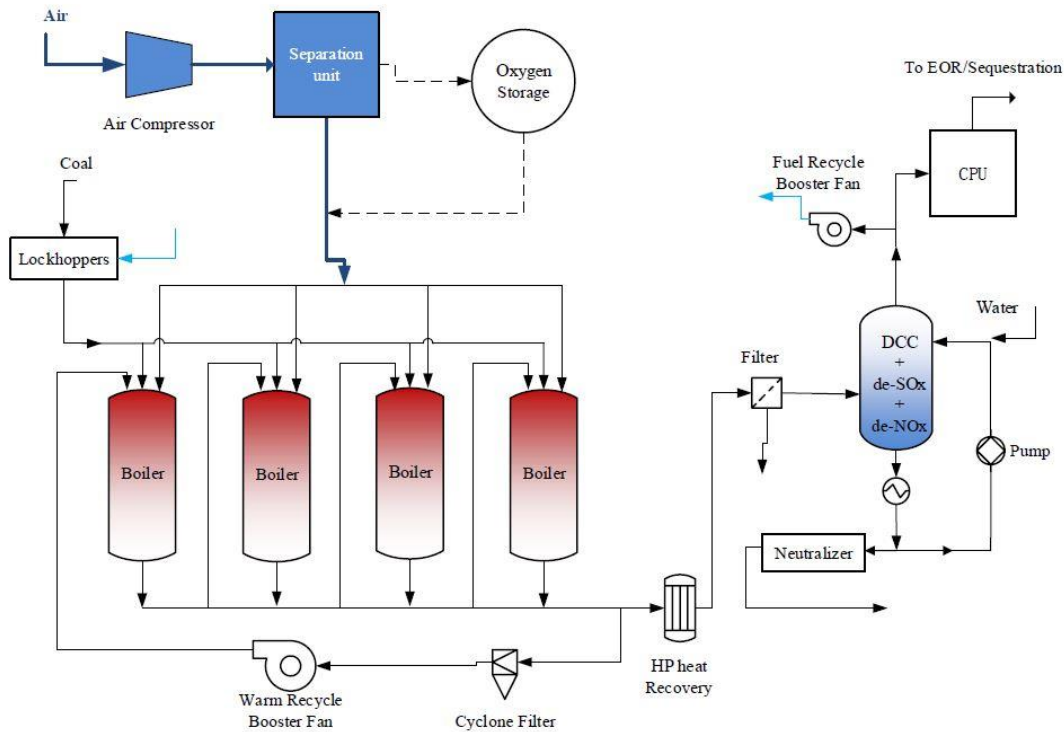
Figure 1.2. Staged pressurized oxy combustion process

3

The development of SPOC, and pressurized combustion technologies in general, is the focus of this work. This thesis explores and develops two major factors that make pressurized oxy-combustion an essential technology for CCUS. The first part focuses on understanding various aspects of SO_x-NO_x formation and removal from the flue gas of a pressurized oxy-combustion process to produce a clean CO_2 stream for sequestration. The second part focuses on the process development and intensification of the SPOC process, including understanding the impact of flue gas recycle on the plant efficiency and developing a carbon-capture ready pressurized air plant that can transition to SPOC when needed.

1.1.1 Pollutant Formation and Control

One of the most critical steps towards developing pressurized oxy-coal combustion technology for CCUS is understanding the formation and subsequent removal of pollutants from the flue gas, especially SO_x and NO_x. In conventional air combustion power plants without CCUS, the limit on the concentration of oxides of sulfur and nitrogen in the flue gas exists because of the emission regulation. However, for CCUS, limitations exist to protect the downstream equipment and pipelines used for pressurization and transportation of the CO_2. Depending on the region, the concentration standards for SO_x and NO_x can vary between 25 – 100 ppm and 100 – 150 ppm, respectively [13,14]. Therefore it is necessary to understand the formation of these pollutants in combustion to design their removal in the DCC. The first section of the thesis focuses on these two problems.

1.1.1   A) Investigation of SOx, NO_x, and CO formation in pressurized oxy-combustion

4

Combustion of coal, which contains a significant amount of sulfur and nitrogen, results in the formation of several sulfur compounds (SO_2, SO_3) and nitrogen compounds (NO, NO, NO_2, N_2O, N_2). The relative concentration of these gases depends on several factors such as pressure, stoichiometric ratio, the oxygen concentration in the flame, time-temperature profile in the boiler, etc. Since there is no N_2 in the inlet gas of the oxy-combustion process, all the N-containing gases are derived from fuel nitrogen [15]. The two pathways of NO_x formation are the gas-phase oxidation of devolatilized coal nitrogen and the heterogeneous oxidation of char nitrogen in the tail of the flame [16]. A simplified mechanism for NO_x formation from fuel-N is given in Fig. 1.3. In pressurized oxy-combustion, NO formed from this process can further react with CO and C to form reduced nitrogen species. Several studies have focused on NO_x emissions from atmospheric oxy-coal combustion. However, NO_x emissions from pressurized oxy-coal combustion are not well understood. Several factors relevant to pressurized oxy-coal combustion, such as high CO_2 concentration, higher oxygen concentration in the flame compared to air combustion, and high pressure, affect the NO_x formation, which requires further investigation.
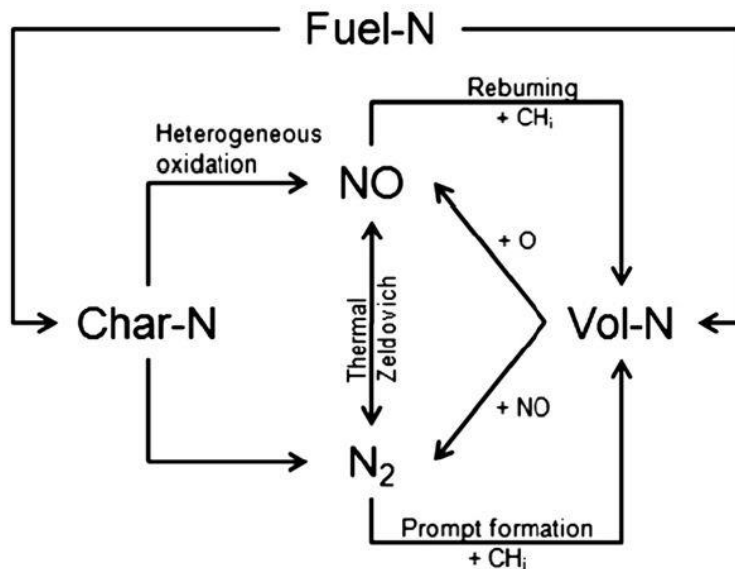
Figure 1.3 The overall mechanism of NO formation and reduction [16]

During combustion, most of the sulfur in coal is oxidized to SO_2, while a small percentage is further oxidized to SO_3. Studies of atmospheric oxy-coal combustion by various researchers suggest that the amount of SO_3 produced in oxy-coal combustion is several times more than that in air combustion [17], [18]. A review on SO_x emission in oxy-coal combustion found a 14–30% reduction in the quantity of SO_2 emission per kg of coal [19]. The study concluded that the reduction in SO_2 emission could indicate sulfuric acid condensation in the boiler. A theoretical study on the formation of SO_3 in a pressurized oxy-combustion environment by Wang et al. concluded that the interaction of SO_x and NO_x significantly accelerates the conversion rates of SO_2 to SO_3 at elevated pressures (10-15 bar) in the post flame region [20]. Ilic et al. reported that sulfur retention in ash particles also increases with the concentration of SO_2 and oxygen in the flue gas [21]. Both SO_3 formation and sulfur retention should decrease the conversion of fuel S to SO_2 in the downstream flue gas. Therefore, there is a need to understand the impact of pressure in oxy-coal combustion on the formation of SO_2. It is also prudent to analyze the effects of excess oxygen concentration in the flue, as it is relevant to design a suitable removal process.

To investigate the formation of NO_x and SO_x in the flue gas, we conducted experiments in a 100 kW_{th} pressurized oxy-coal combustor. In addition to SO_2 and NO, the formation of CO was also investigated since it is critical in understanding the reaction kinetics in the flue gas and the state of combustion.

1.1.1 B) Development of DCC for removal of SO_x and NO_x

The DCC is a reactive-absorption column designed to condense the latent heat of moisture and to remove SO_x and NO_x from the flue gas to the desired concentrations. The removal of SO_x and NO_x in the direct contact cooler can be characterized based on four major physicochemical processes – 1) The gas-phase reaction kinetics of NO_x and SO_x, 2) the interfacial absorption of SO_x and NO_x in water, 3) The liquid phase kinetic interaction between dissolved SO_x and NO_x and 4) The high-temperature condensation of the moisture from the flue gas. Therefore, the understanding and optimization of all four processes is essential for the development of DCC. The overall pathway of technological development for DCC is presented in Fig. 1.4.
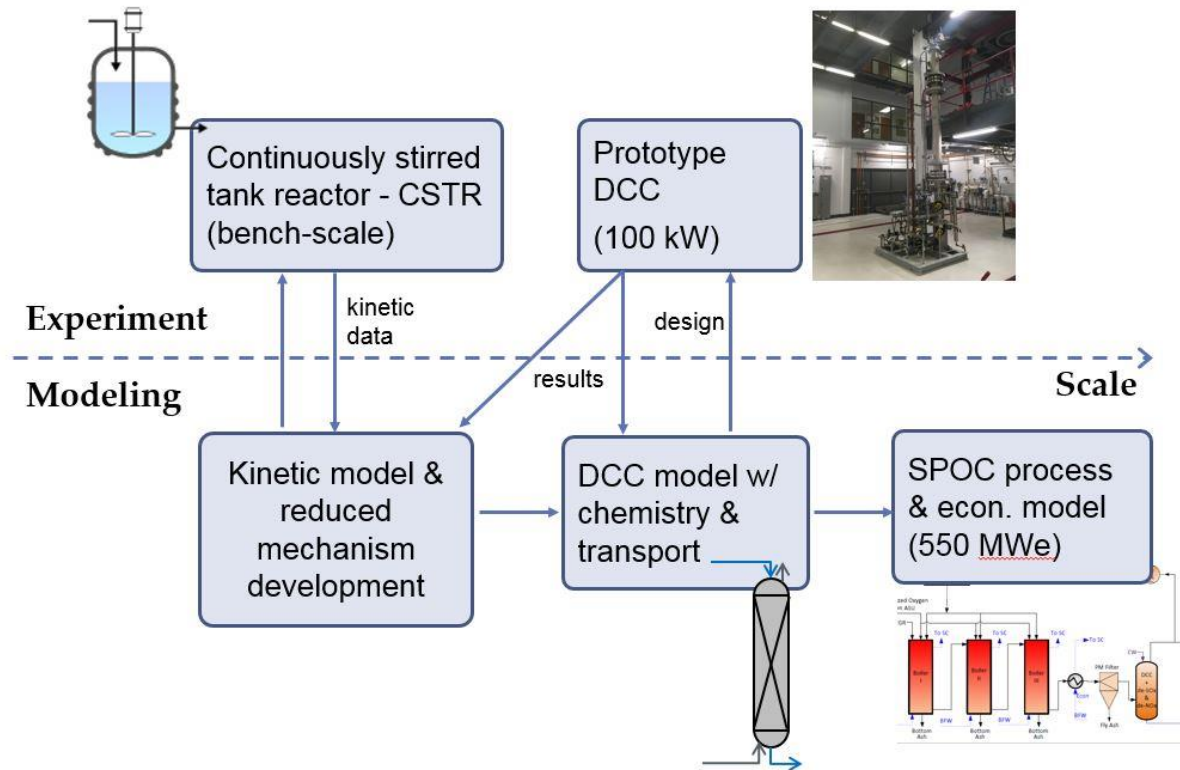
Figure 1.4. Technology development of DCC

The gas-phase chemistry mainly comprises NO oxidation to NO_2 and a small amount of N_2O_4 and N_2O_3. The oxidation kinetics of NO to NO_2 is reasonably well understood compared to the liquid phase reaction between dissolved NO_2 and SO_2 [22]. The absorption of NO_2 in water results in the formation of HNO_2 and HNO_3, and the absorption of SO_2 results in the formation of HSO_3-. While HNO_3 is relatively stable, HNO_2 reacts with HSO_3- to form several products, including HSO_4-. The most detailed chemistry of this interaction in the acidic medium was proposed by Chang et al. They reported that HNO_2 and HSO_3- react to form NSS (nitrososulfonic acid), which further reacts to form different products, depending on the pH and the relative concentration of reactants [23]. Susianto et al. further reduced the early-stage kinetics of the system into two different pathways, presented in Fig. 1.5. They reported that, in pathway 1, NSS further reacts either HSO_3- to form HADS, and in pathway 2, NSS hydrolyzes to produce HSO_4- and N_2O[24]. However, the kinetics of these reactions, especially at lower pH and a higher temperature, is not well developed. Since the removal of SO_2 depends upon the extent of liquid-phase reactions, it is imperative to understand the reaction kinetics in conditions relevant to DCC. Therefore, we conducted bench-scale liquid phase experiments to understand the kinetics of interaction between HNO_2 and HSO_3- over a range of pH and temperature.

$$NO_2^- + HSO_3^- \xrightarrow{\;\;1\;\;} HADS$$
$$\Big\downarrow 2$$
$$HSO_4^- + N_2O$$
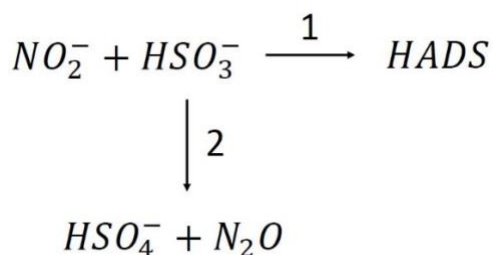
Figure 1.5 Reduced Liquid phase mechanism presented by Susianto et al[24]

An elaborate reaction mechanism for the DCC for a pressurized oxy-combustion system was first presented by Normann et al. [25]. This model, shown in Appendix A, included 34 reactions and several intermediates. This model was later reduced by Ajdari et al. to include between $7 - 12$ reactions depending on the pH of the system [26]. This model is presented in Appendix B. Although they are detailed, these models consist of several species which are difficult to measure. Therefore, in this work, we have tried to develop a novel model of optimal complexity (MOC) which meets three requirements: 1) it must be *sufficient* to model the SOx/NOx removal process accurately. 2) it must be *observable*, i.e., it must include only concentrations of substances that can be monitored during the reaction, 3) it must be *significant*, i.e., only steps with a significant contribution to the rate of the observed substances should be included in the model, and 4) it should produce an analytical equation that can be compared with experimental data. A 5-step model was developed using analysis from bench-scale experiments and analytical and modeling analysis of the reaction system.

The next step of DCC development focused on performing experiments in a pilot-scale absorption column to understand the transport and the kinetics of the system and to validate the reduced model. The experiments performed for the co-removal of SO_x and NO_x at high pressure are limited to lab-scale systems and a narrow range of system parameters [27], [28]. Additionally, no modeling or experimental studies have explored the impact of temperature on the removal kinetics. Therefore, to understand the factors relevant to the DCC of a SPOC process, we performed experiments on a pilot-scale absorption column with a 0.2 m diameter and a packing height of 2.3 m. The impact of O_2 concentration, residence time, system pressure, inlet gas temperature, SO_2/NO ratio, and liquid to gas (L/G) ratio on the scrubbing of SO_2 and NO were systematically explored using a synthetic flue gas. Moreover, experiments were designed to understand the extent to which

liquid phase interaction between HNO_2 and HSO_3^- impacts the removal of SO_2 from the flue gas. Finally, a process model of DCC was developed in Aspen Plus to validate the kinetic model based on the experiments. The model enables us to interpret the results better and to design an optimized full-scale system.

The validated kinetic model was used to develop a full-scale DCC for a 550 MWe pressurized oxy-combustion power plant in the final step of the DCC technology development. A few models have been developed for DCC using detailed kinetics, however, they have not considered the impact of moisture condensation in the column [29]. Additionally, in POC, the L/G ratio is constrained to maintain a high outlet liquid temperature, complicating the removal process. The heat transfer, the reaction kinetics, and the mass transfer process interact with each other and have different time constants. Therefore, a process model of DCC is developed and optimized in Aspen Plus for maximizing the SO_x and NO_x removal while maintaining the maximum water outlet temperature. A basic and optimized model design is compared to show how decoupling heat transfer provides better removal for the same column size and diameter. We believe that the overall development of DCC kinetics and model will be helpful to design removal process for different coal types, along with biomass combustion with carbon capture and cement plants with carbon capture using solid fuels.

1.1.2 Process Development

The second section of the thesis focuses on two central questions related to process development: 1) the impact of flue gas recycle on power plant efficiency and finding an optimum recycle ratio, and 2) developing a carbon-capture ready pressurized air-combustion power plant with high efficiency, which can transition pathway to SPOC when required.

1.1.2 A) Impact of flue gas recirculation on the efficiency of oxy-coal power plants.

In power plants, there is a material constraint on the amount of heat flux the boiler tubes can experience. In air combustion, the flux is limited because of the presence of nitrogen, however in oxy-combustion, there is no nitrogen present in the flame. Therefore, oxy-combustion typically consists of burning coal with a combination of oxygen and a large amount of recycled flue gas (60-70%), to obtain a similar heat flux profile to that of air-fired systems. As the cost of electricity from first-generation oxy-combustion is relatively high, several new oxy-combustion process concepts have been proposed in recent years, and within these, the proposed amount of flue gas recycle (FGR) has varied from near-zero to 80%. There are two impacts of the flue gas recycle on the efficiency of the plant, exergy destruction in the boiler and the power consumption by the recycle fan. Several methods , including, controlled non-stoichiometric burner design, have been proposed to reduce the recycle flue gas [30] [31]. The staging of boiler in SPOC process also results in a significant reduction of flue gas recycle [32]. However, the discussions on the effect of flue gas recycle (FGR) on the power plant efficiency are often limited to fan power consumption. Although, fan power loss is significant, it is not the most important reason for the plant efficiency reduction caused by high FGR.

In this thesis, a fundamental thermodynamic study on the impact of designing atmospheric and pressurized oxy-combustion systems with varying amount of FGR has not been properly investigated. Simple algebraic equations that can be used for quantifying the impact of FGR for any oxy-combustion plant concept are presented. The results from the model developed in ASPEN Plus are used to confirm the accuracy of the thermodynamic analysis.

1.1.2 B) Process design and analysis of a novel carbon-capture-ready process for flexible-load power generation: Modular pressurized air combustion.

The consensus on the important role of CCUS to in fighting climate change globally is clear. However, the demonstration and commercialization of the CCUS technologies, especially in power sector has been slow [33]. This is mainly because of the high cost compared to existing power plants. Without incentives for CO_2 capture, the risk associated with these high-cost technologies will continue to impede investment for large-scale demonstration, which in return limits the chances for these technologies to reduce their initial costs by technological learning[34]. In the present environment, a carbon capture ready process, which has competitive performance and economics with conventional coal plants without carbon capture, as well as critical components that are also part of a carbon capture system, would be very attractive. The benefits of such a process are twofold: 1) once this process is commercialized, the capital costs of those critical components that are shared by a carbon capture process can gradually drop due to the power of learning-by-doing; 2) when regulations or economic opportunities for CO_2 capture are in place, the installed carbon capture ready plants can be retrofit to carbon-capture plants at relatively low cost, which reduces the investment risk by minimizing the impact of future regulations or policy changes.

In this study, the process design of a modular pressurized air combustion power plant, which involves burning coal in air under pressure in parallel, modular boilers is described. After treatment, the high-pressure flue gas is passed through a series of turbines and inter-heaters to

recover most of the compression work. This work also discusses the path to convert the modular, pressurized-air combustion process to a staged, pressurized oxy-combustion process, which is one of the most promising carbon capture processes. This can be accomplished by adding a frontend air separation unit and a backend CO_2 compression and purification unit.

1.2 Dissertation Outline

This thesis contains nine chapters. Each chapter is self-contained, with an introduction, methodology, results, discussion, and conclusions section. Chapter 2 describes the formation of SO_x, NO_x, and CO in a 100 kW_{th} pressurized oxy-combustor. Chapter 3 presents the kinetic analysis of aqueous phase interactions between dissolved SO_x and NO_x in a pressurized oxy-combustion environment. Chapter 4 describes the kinetic models for DCC and presents a model of optimal complexity used for modeling the DCC. Chapter 5 focuses on the pilot-scale DCC experiments, including testing and understanding the impact of various parameters on the scrubbing efficiency of SO_x and NO_x. This chapter also presents the validation of the kinetic model developed in Chapter 4. Based on the validated model, Chapter 6 presents the full-scale DCC design and optimization. Chapters 7 and 8 focus on the process development of the SPOC process. In chapter 7, we analyze the impact of flue gas recycle on power plant efficiency. In chapter 8, a process modeling of a pressurized air power plant is presented along with a pathway to retrofit it to SPOC. Finally, chapter 9 lists the conclusions and future work to understand existing systems better and enable new work.

There are 4 appendixes referenced, the first two are referenced throughout the thesis. Appendix A presents the kinetic model presented by Normann et al [25] which forms the basis of the model

presented in this work. Appendix B presents the reduced kinetic model by Ajdari et al [26].

Appendix C contains the Curriculum Vitae and Appendix D contains the transcript.

1.3 References

[1]   J. Rissman et al., "Technologies and policies to decarbonize global industry: Review and assessment of mitigation drivers through 2070," Appl. Energy, vol. 266, no. March, p. 114848, 2020.

[2]   M. Huber, D. Dimkova, and T. Hamacher, "Integration of wind and solar power in Europe: Assessment of flexibility requirements," Energy, vol. 69, pp. 236–246, 2014.

[3]   IEA, World Energy Outlook 2015. 2015.

[4]   International Energy Agency, "Renewable Energy Essentials: Hydropower," Renew. Energy, vol. 50, no. March, pp. 1–4, 2010.

[5]   G. C. Institute, "Global Status of CCS 2020," Glob. CCS Inst., no. June, 2020.

[6]   International Energy Agengy, "Oxy Combustion Processes for CO 2 Capture from Power Plant," IEA Greenh. Gas R&D Program., p. 212, 2005.

[7]   D. McDonald, D. DeVault, and R. Varagani, "Oxy-Combustion in Pulverized Coal Power Plants for Carbon Dioxide Concentration," Electr. Power Conf., pp. 1–9, 2007.

[8]   H. Hagi, M. Nemer, Y. Le Moullec, and C. Bouallou, "Towards second generation oxy-pulverized coal power plants: Energy penalty reduction potential of pressurized oxy-combustion systems," Energy Procedia, vol. 63, pp. 431–439, 2014.

[9]   H. Hagi, Y. Le Moullec, M. Nemer, and C. Bouallou, "Performance assessment of first generation oxy-coal power plants through an exergy-based process integration methodology," Energy, vol. 69, pp. 272–284, 2014.

[10]   A. Gopan, B. M. Kumfer, J. Phillips, D. Thimsen, R. Smith, and R. L. Axelbaum, "Process design and performance analysis of a Staged, Pressurized Oxy-Combustion (SPOC) power plant for carbon capture," Appl. Energy, vol. 125, pp. 179–188, 2014.

[11]   A. Gopan, B. M. Kumfer, and R. L. Axelbaum, "Effect of operating pressure and fuel moisture on net plant efficiency of a staged, pressurized oxy-combustion power plant," Int. J. Greenh. Gas Control, vol. 39, pp. 390–396, 2015.

[12]   S. Hume, "Enabling Staged Pressurized Oxy-Combustion: Improving Flexibility and Performance at Reduced Cost," 2019.

[13]   E. de Visser et al., "Dynamis CO2 quality recommendations," Int. J. Greenh. Gas Control, vol. 2, no. 4, pp. 478–484, 2008.

[14]   B. Paschke and A. Kather, "Corrosion of pipeline and compressor materials due to impurities in separated CO2 from fossil-fuelled power plants," Energy Procedia, vol. 23, pp. 207–215, 2012.

[15]   P. Glarborg, A. D. Jensen, and J. E. Johnsson, "Fuel nitrogen conversion in solid fuel fired systems," vol. 29, pp. 89–113, 2003.

[16]   M. B. Toftegaard, J. Brix, P. A. Jensen, P. Glarborg, and A. D. Jensen, "Oxy-fuel combustion of solid fuels," Prog. Energy Combust. Sci., vol. 36, no. 5, pp. 581–625, 2010.

[17]   D. Fleig, K. Andersson, F. Normann, and F. Johnsson, "SO3 Formation under oxyfuel combustion conditions," Ind. Eng. Chem. Res., vol. 50, no. 14, pp. 8505–8514, 2011.

[18]   J. Ahn, R. Okerlund, A. Fry, and E. G. Eddings, "International Journal of Greenhouse Gas Control Sulfur trioxide formation during oxy-coal combustion," Int. J. Greenh. Gas Control, vol. 5, pp. S127–S135, 2011.

[19]   R. Stanger and T. Wall, "Sulphur impacts during pulverised coal combustion in oxy-fuel technology for carbon capture and storage," Prog. Energy Combust. Sci., vol. 37, no. 1, pp. 69–88, 2011.

[20]   X. Wang, A. Adeosun, G. Yablonsky, A. Gopan, P. Du, and R. L. Axelbaum, "Synergistic SOx/NOx chemistry leading to enhanced SO3 and NO2 formation during pressurized oxy-combustion," React. Kinet. Mech. Catal., no. 2, 2017.

[21]   M. Ili, B. Grubor, and V. Manovi, "Sulfur retention by ash during coal combustion . Part I . A model of char particle combustion," vol. 68, no. 2, pp. 137–145, 2003.

[22]   H. Tsukahara, T. Ishida, and M. Mayumi, "Gas-phase oxidation of nitric oxide: Chemical kinetics and rate constant," Nitric Oxide - Biol. Chem., vol. 3, no. 3, pp. 191–198, 1999.

[23]   S. G. Chang, D. Littlejohn, and N. H. Lin, "Kinetics of Reactions in a Wet Flue Gas Simultaneous Desulfurization and Denitrification System," Am. Chem. Soc., pp. 127–152, 1982.

[24]   M. S. Pétrissans and A. Zoulalian, "Influence of the pH on the Interactions between Nitrite and Sulfite Ions . Kinetic of the Reaction at pH 4 and 5," Ind. Eng. Chem, vol. 40, pp. 6068–6072, 2001.

[25]   F. Normann, E. Jansson, T. Petersson, and K. Andersson, "Nitrogen and sulphur chemistry in pressurised flue gas systems: A comparison of modelling and experiments," Int. J. Greenh. Gas Control, vol. 12, no. 2, pp. 26–34, 2013.

[26]   S. Ajdari, F. Normann, K. Andersson, and F. Johnsson, "Reduced Mechanism for Nitrogen and Sulfur Chemistry in Pressurized Flue Gas Systems," Ind. Eng. Chem. Res., vol. 55, no. 19, pp. 5514–5525, 2016.

[27]   L. T. Murciano, V. White, F. Petrocelli, and D. Chadwick, "Sour compression process for the removal of SOx and NOx from oxyfuel-derived CO2," Energy Procedia, vol. 4, no. x, pp. 908–916, 2011.

[28]   V. White, A. Wright, S. Tappe, and J. Yan, "The Air Products Vattenfall oxyfuel CO2compression and purification pilot plant at schwarze pumpe," Energy Procedia, vol. 37, no. x, pp. 1490–1499, 2013.

[29]   C. Iloeje, R. Field, and A. F. Ghoniem, "Modeling and parametric analysis of nitrogen and sulfur oxide removal from oxy-combustion flue gas using a single column absorber," Fuel, vol. 160, no. X, pp. 178–188, 2015.

[30]   V. Becher, J. P. Bohn, A. Goanta, and H. Spliethoff, "A combustion concept for oxyfuel processes with low recirculation rate - Experimental validation," Combust. Flame, vol. 158, no. 8, pp. 1542–1552, 2011.

[31]   H. Kobayashi and L. E. Bool, "12 - Direct oxy-coal combustion with minimum or no flue gas recycle," in Woodhead Publishing Series in Energy, L. B. T.-O.-F. C. for P. G. and C. D. (CO2) C. Zheng, Ed. Woodhead Publishing, 2011, pp. 259–272.

[32]   F. Xia, Z. Yang, A. Adeosun, A. Gopan, B. M. Kumfer, and R. L. Axelbaum, "Pressurized oxy-combustion with low flue gas recycle: Computational fluid dynamic simulations of radiant boilers," Fuel, vol. 181, pp. 1170–1178, 2016.

[33]   E. R. Ochu and S. J. Friedmann, "CCUS in a net-zero U . S . power sector : Policy design , rates , and project finance," Electr. J., vol. 34, no. 7, p. 107000, 2021.

[34]   E. S. Rubin, M. R. Taylor, S. Yeh, and D. A. Hounshell, "Learning curves for environmental technology and their importance for climate policy analysis," Energy, vol. 29, no. 9–10, pp. 1551–1559, 2004.

Chapter 2. Understanding SO$_x$, NO$_x$, and CO formation in 100 kW$_{th}$ pressurized oxy-coal combustor.

2.1 Introduction

The global energy market has been driven towards a low-carbon future to minimize the environmental impact of electricity generation. Renewable energy, especially wind and solar, has been growing at an unprecedented rate in the last decade. However, the intermittent and seasonal nature of wind and solar power presents a major challenge to grid reliability [1]. To protect the grid, dispatchable low-carbon sources are required, which will largely come from carbon-capture-equipped fossil-fuel plants [2], especially for industrial countries like the US and China. Based on projections from the International Energy Agency, coal will continue to be a major fuel source in the world in the long term due to its abundance and low price [3]. Future coal plants will need to be not only efficient and low carbon but also flexible in order to meet the demands of a highly variable grid [4].

Carbon capture technologies for coal plants can be grouped into three categories: pre-combustion capture, post-combustion capture (PCC), and oxy-combustion. All three are expensive, but oxy-combustion has been shown to be competitive with the other two in terms of plant efficiency and cost [5]. In recent years, pressurized oxy-combustion (POC) received much attention due to its potential for improved plant efficiency and reduced costs compared with conventional atmospheric oxy-combustion [6]. The basis of POC is that since the CO$_2$ product of a carbon capture plant must ultimately be pressurized for geo-sequestration or enhanced oil recovery (EOR), there is minimal

17

net pumping cost for operating under pressure because it requires about the same amount of energy to compress the O_2 stream as it does the CO_2 stream. However, under elevated pressure, the moisture in the flue gas can be condensed at a higher temperature, enabling the recovery of the latent heat of the moisture, which improves plant efficiency [7]. Moreover, under elevated pressure, SO$_X$ and NO$_X$ can be removed by a simple water wash column [8], which significantly reduces the capital and operational cost compared with traditional pollutant removal units – e.g., flue gas desulfurization (FGD) for SOx removal and selective catalytic reduction (SCR) for NOx removal [9]. The staged pressurized oxy-combustion process (SPOC), which is one of the most promising POC technologies because of its high efficiency, is presented in Fig. 2.1. The efficiency improvement is accomplished by minimizing FGR and operating with a dry feed. Process analysis has shown that FGR reduces plant efficiency, but the impact is minimal for FGR below 30% [10]. Thus, the SPOC process limits FGR to 30% and utilizes a staged combustion concept to control combustion temperature in the boiler without resorting to slurry feed, which reduces efficiency.
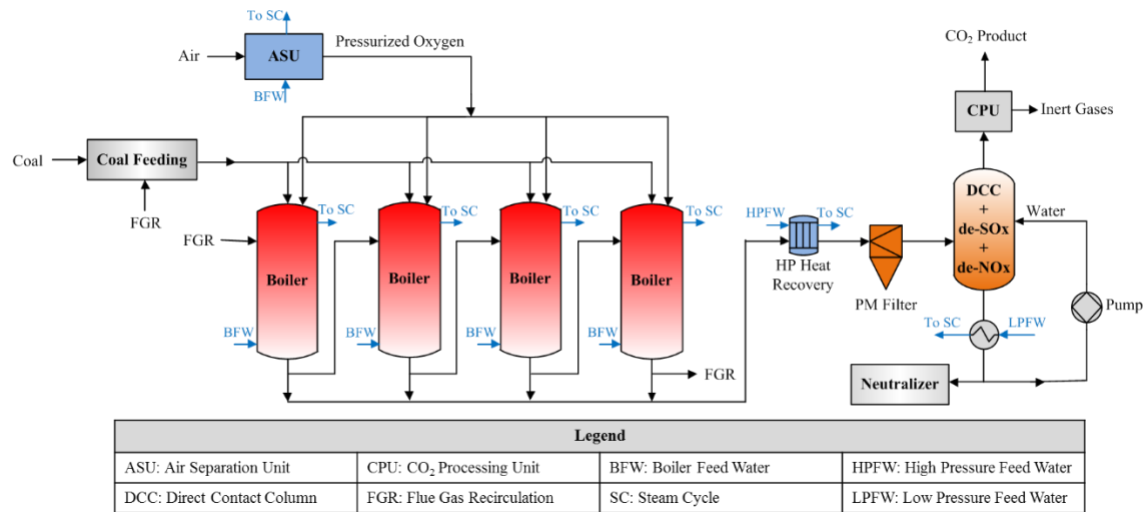
Figure 2.1 Simplified process flow diagram for a four-stage modular SPOC process.

High pressure and combustion atmosphere have a significant impact on the emissions of pollutants. However, there are limited experiments to understand the emission of CO, SO_x, and NO_x for a pulverized pressurized oxy-coal combustion, especially at a large scale. Lab-scale studies provide some important understanding of the directional influence of various factors on pollutant emission. Hu et al. conducted lab-scale oxy-combustion experiments and reported that NO_x emission was a weak function of inlet oxygen concentration but a strong function of equivalence ratio[11]. They concluded that more fuel-N was converted to NO_x due to the oxidizing atmosphere, resulting in a high NO_x emission index. They also found that SO_2 concentration increases with the increase in equivalence ratio in the fuel-lean region. Croiset et al. performed. experiment in a 0.21 MW combustor with 5% excess oxygen[12]. Their results suggest that flame temperature strongly impacts NO_x emission, as their NO_x emission increased with increasing oxygen concentration in the inlet gas. They found a weak impact of flame oxygen concentration on the emission of SO_2. In an experiment by Fleig et al. in a lab-scale combustor in an oxy-combustion environment with 4% excess oxygen, they concluded that S to SO_2 conversion is a function of combustion temperature, with SO_2 release increasing at higher temperatures [13]. They also reported that the %S conversion SO_2 is reduced significantly in oxy-combustion experiments. Apart from higher retention, higher SO_3 was also observed in this experiment, mainly increasing in the oxy-fuel condition in the post-flame region. Kaznac et al. performed similar experiments in an electrically heated laboratory drop-tube furnace [14]. They reported that the conversion of sulfur to SO_2 was higher for low oxygen concentrations and decreased sharply with oxygen. For low sulfur coals, the conversion was well below 50%. Similarly, the N to NO conversion was also low and increased marginally with oxygen concentration. Zan et al. performed oxy-combustion experiments in a pressurized tube furnace and measured the emission of NOx with change in pressure, tube temperature, and

19

moisture in the flue gas[15]. They reported that an increase in pressure suppresses NO formation by a reduction with char and CO and higher residence time.

Up till now, there have been very few experimental studies on dry-feed oxy-coal combustion under pressure, especially in pilot-scale combustors. Pilot-scale testing is critical to the development of the dry-feed, pressurized PC boiler for the POC process. It demonstrates the conceptual design and provides a deeper understanding of the combustion characteristics. The goal of this work is to presents the first experimental results of pilot-scale, dry-feed, oxy-coal combustion under pressure. The experiments were conducted on a 100 kW$_{th}$ pressurized combustor designed and constructed at WUSTL. This work aims to understand the formation of SO_x, NO_x, and CO in the flue gas under varying combustion parameters. Because the power consumed in oxygen production in the ASU is one of the biggest factors that reduces the efficiency of the POC power plant, the impact of excess oxygen on the SO_x, NO_x and CO formation is explored in detail. Moreover, the impact of pressure is also investigated to understand an optimum pressure for better combustion characteristics and SO_x and NO_x formation. We believe that the understanding the formation of these pollutants will lead to a better design of both combustion and removal processes.

2.2   Experimental Methods

The POC facility at WUSTL is rated at 20 bar and 100 kW$_{th}$ thermal input. Figure 2.2 shows a schematic of the entire facility. O_2 and CO_2 are both provided by bulk liquid tanks. Methane is used for ignition and preheating before switching to coal and is supplied by high-pressure cylinders. Coal feeding is designed as a batch process to avoid the need for a lock hopper system. The screw feeder delivers coal to a linear vibratory feeder contained in an 8" transfer pipe during

20

operation. A small CO_2 stream flows through the coal pressure vessel, the transfer pipe, and the burner to assist with coal transport. The refractory-lined furnace is contained at the center of the main pressure vessel. A stream of CO_2 purge gas is fed into the annular space between the furnace and pressure vessel wall from the top of the vessel and leaves the vessel from the bottom. During operation, the pressure outside the furnace is kept equal or slightly higher than that inside of the furnace, such that flue gas leakage to the pressure vessel can be avoided. The flue gas from the furnace is cooled by a water spray generated by six nozzles in the water quench section. In all the experiments, a mixture of 70 vol% CO_2/30 vol% O_2 has been used as oxidizers for ignition. After ignition, the furnace is preheated for about 2 hours using the gaseous flame at around 50 kWth. Then the fuel is gradually switched to coal. Powder River Basin coal is used for the experiments, with the proximate and ultimate analyses provided in Table 2.1.
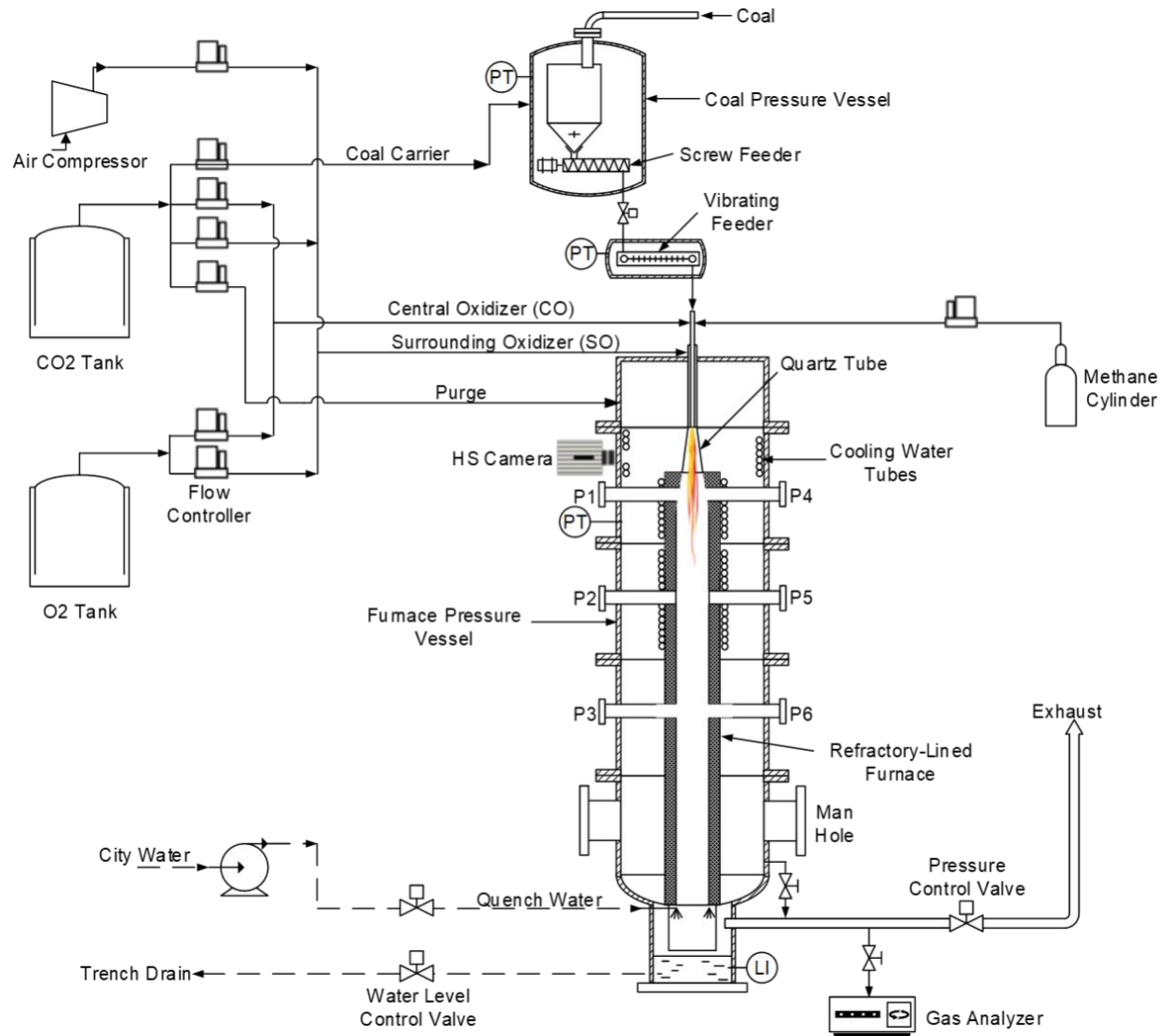
Figure 2.2 Schematic of the 100 kW$_{th}$, pressurized, oxy-fuel combustion research facility

An oil-cooled bottom sampling probe, maintained between 225 – 240 °C, is used to sample the flue gas. The oil temperature is chosen to avoid the condensation of SO_3 in the sampling probe. The gas coming out of the probe is filtered in a candle filter to remove and collect the ash particles. A small flow rate ($<$ 2 slpm) of flue gas is depressurized and condensed to remove the acids in the ice-cooled condensation tank. A Testo gas analyzer is used to analyze the concentration of NO, NO_2, SO_2, CO and O_2

Table 2.1 Main properties of the coal used in the experiment

Proximate analysis (wt% ar)				Ultimate analysis (wt% daf)					HHV (MJ/kg)
Moisture	VM	FC	Ash	C	H	O	N	S	
27.42	31.65	36.43	4.5	73.81	5.01	19.91	0.95	0.32	20.47
Particle size distribution									
Particle size (µm)		44	75	105	150	250			
Cumulative distribution %		53	62	70	80	95			

2.3 Results and Discussion

2.3.1 CO formation

Figure 2.3 (a) presents the change in concentration of CO with flue gas oxygen concentration at 10 bar and 15 bar. The experiments were repeated at least twice to establish the reproducibly of the results. The residence time in the combustor was kept approximately constant in both the cases to just compare the impact of pressure. The oxygen concentration in the flame was maintained around 30% in all cases. The flue gas excess oxygen concentration was changed by changing the stoichiometric ratio of the flame. It is evident that the at low excess oxygen concentration ($< 2\%$ v/v) the CO formation at 10 bar is very high compared to 15 bar. At an O_2 concentration of 1% v/v in the flue gas, the concentration of CO changes from around 600 ppm to around 3800 ppm. The gasification reaction (R1) is enhanced at higher pressure, leading to higher CO production via char reacting with CO_2. The gasification is slower at 10 bar compared to 15 bar, and continues for much longer time, limiting the time for CO oxidation(R2). Moreover, a higher O_2 partial pressure in the flue gas at 15 bar compared to 10 bar leads to a faster combustion of CO. Additionally, higher pressure also results in a lower equilibrium concentration of CO, shifting the equilibrium towards CO_2.

$$C + CO_2 \rightarrow 2CO \qquad\qquad\qquad\qquad\qquad\qquad\qquad\qquad\qquad (R1)$$

$$CO + \frac{1}{2}O_2 \rightarrow CO_2 \;\ldots\ldots\ldots\ldots\ldots\ldots\ldots\ldots\ldots \qquad\qquad\qquad\qquad \ldots\ldots\ldots(R2)$$
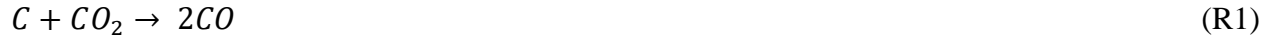
In the previous study on the same system, Yang et al. found that at 15 bar, 1% O_2 concentration in the exit flue gas led to almost complete combustion of coal particles[16]. Therefore, it should be noted that, at higher pressure the combustor can be operated at much lower O_2 excess oxygen concentration than what is generally accepted in current power plants (3 – 5 % v/v), effectively reducing the cost from air separation unit.

(a)
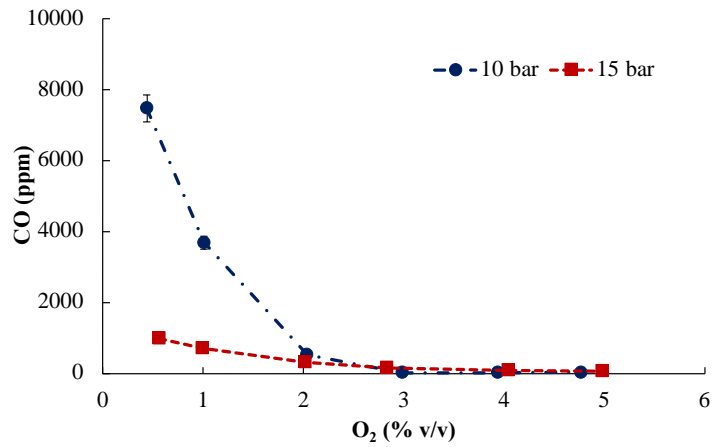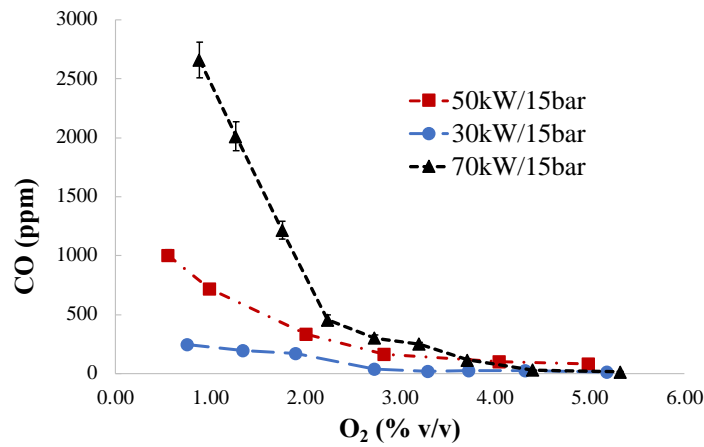
Figure 2.3 Impact of O_2 concertation on CO formation for a) different pressures b) different residence time

Figure 2.3 (b) presents the impact of residence time on CO concentration in the flue gas. At 15 bar, the total flow of thermal input was systematically reduced, which effectively changes the residence time in the combustor. At 70 kW_{th} condition, the residence time is too low for CO to oxidize completely at lower O_2 concentrations. However, above a concentration of 3% v/v of O_2, the residence time was enough to obtain a similar CO concentration in each case. As expected, at 30 kW_{th} load, which had the longest residence time, the CO concentration remained low even for very low concentration of oxygen. It should be noted that, apart from residence time, this profile also includes the impact of combustor wall temperature. At 70 $kW_{th,}$ the wall temperatures were 50 °C higher than 50 kWth, and almost 150 °C degrees higher than 30 kWth. However, this makes the trends even more impactful because n at lower wall temperatures, the combustion was completed at 30 kW_{th}, a higher wall temperature, similar to 70 kW_{th}, would result in even lower CO in the flue gas.

2.3.2 NO formation
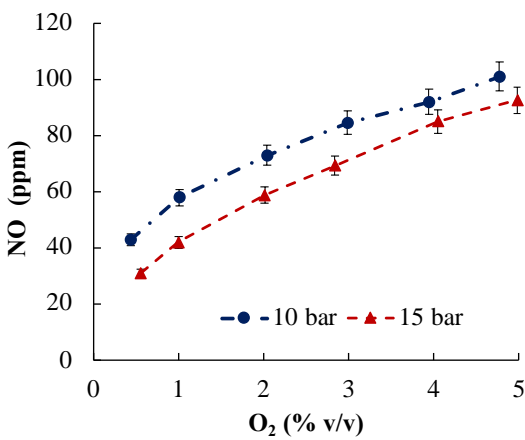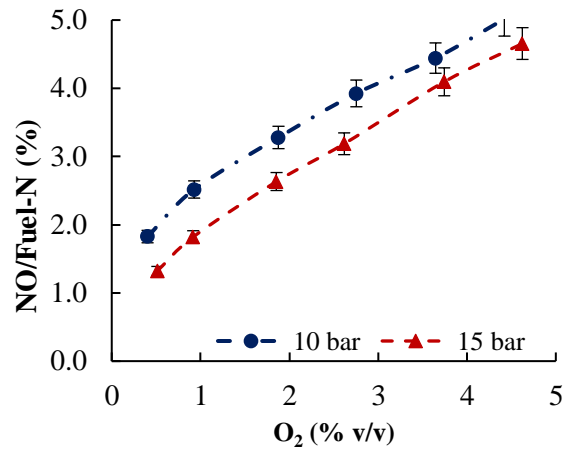
(a)   (b)

Figure 2.4 Impact of O_2 concentration on NO formation at 10 and 15 bar

Figure 2.4 (a) presents the impact of pressure of NO concentration in the flue gas. The conditions were maintained similar to the description in Section 2.3.1 for CO formation. At both pressures, NO formation increases with the increase in O_2 concentration in the flue gas. There is a 3 to 4 times increase in NO concentration when O_2 concentration changes from 1 to 5% v/v. Higher oxygen leads to higher NO formation because of a shorter time for coal burnout. The reducing species are oxidized quickly, leading to higher NO concentrations. This trend is visible at both 10 bar and 15 bar experiments. However, the NO formation at 15 bar decreases as compared to 10 bar for a similar O_2 concentration in the flue gas. There are two main reasons for this- 1) At higher pressures, there is a higher resistance to NO diffusion out of the char particle, which results in a longer residence time of NO inside the char, resulting in a reduction from char and forming N_2. 2) At higher pressures, the CO concentration in the flame region is higher because of the gasification reaction. It has been observed that CO reduces NO to N_2 at higher pressure.

Figure 2.4(b) presents the percent of fuel-N converted to NO. Although the fraction of fuel-N converted to NO increases with increasing O_2 concentration in the flue gas, it is still below 5% for an oxygen concentration of around 5%. Other studies have observed low fuel-N to NO conversion. For example, Kaznac et al. [14] observed 25 – 30% conversion at atmospheric pressure and CO2 environment in a drop tube furnace, and Lupianez et al. [18] found around 10 – 25% conversion of fuel-N to NO in a fluidized bed combustor. It is clear that a significant reduction in NO formation can be seen at high pressures, CO_2 combustion environment compared to atmospheric pressure combustion, potentially owing to a higher diffusion of CO in the char particles and lack of thermal NO_x.

The flue gas was also analyzed for NO_2 concentration in each experiment. Less than 5 ppm of NO_2 was observed at a very high oxygen concentration in the flue gas (10% v/v O_2), but that could be a result of oxidation of NO to NO_2 in the sampling probe. The concentration of N_2O was not measured in these experiments. Studies have reported some formation of N_2O in oxy-combustion, however significantly lower than atmospheric oxy-combustion. The concentration of N_2O will be studied in future experiments.

2.3.3 SO_2 formation
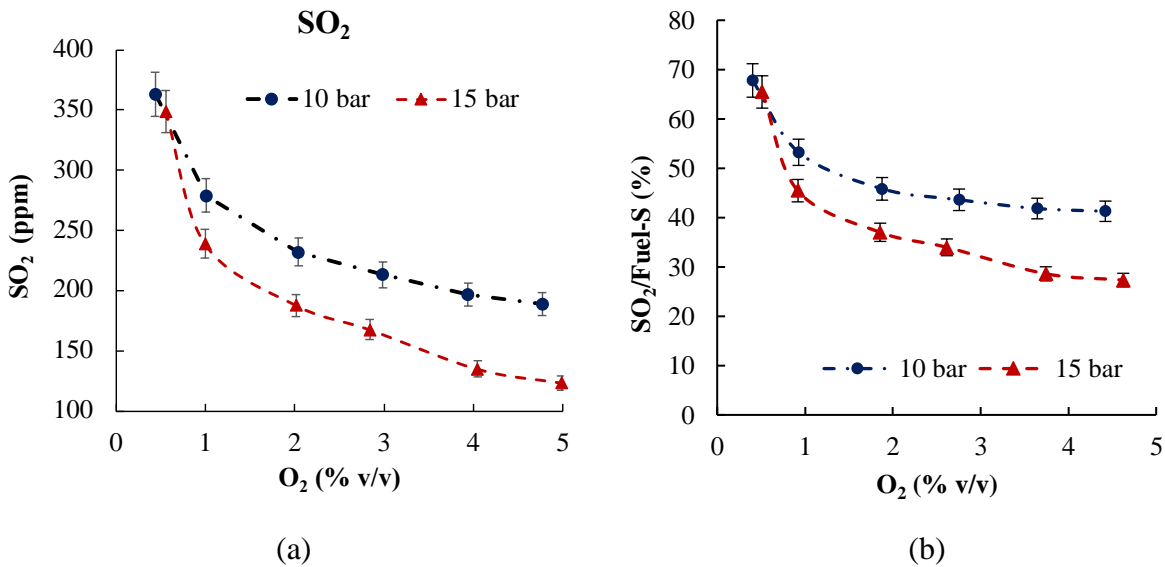
Figure 2.5 Impact of O_2 concentration on SO_2 formation at 10 and 15 bar

Figure 2.5(a) presents the change of SO_2 concentration with flue gas O_2 concentration at two different pressures. The experimental procedure for these experiments were the same as that of CO formation experiments discussed in Section 2.3.1. The amount of SO_2 in the flue gas goes down with oxygen concentration at both 10bar and 15 bar pressures. However, the impact is much stronger at 15 bar. At a stoichiometric ratio close to 1, corresponding to a very small O_2 concentration in the flue gas, the SO_2 concentration in the gas was very high. This is mainly because, in the absence of oxygen, both SO_3 formation and retention of sulfur in ash are very low. However, at higher oxygen concentrations, there is a higher potential for SO_3 formation. This effect is even higher at 15 bar, compared to 10 bar, mainly because of interaction with NO in the post flame region as described by Wang et al. [8].

Figure 2.5 (b) presents the fraction of fuel-S converted to SO_2. Comparing close to 3% O_2 concentration in the flue gas, at 10 bar, 44% fuel-S is converted to SO_2 compared to 33% at 15 bar. Fleig et al. reported close to 45% conversion of fuel-S to SO_2 at atmospheric pressure oxy-

28

combustion at an oxygen concentration of 30% in the flame [19]. At similar conditions, we see a significant reduction at higher pressure. However, considering the impact of coal type in SO_2 formation, it is difficult to make a direct comparison. Similar values have been reported for other oxy-combustion experiments, ranging from 30 – 60% depending on the coal type. In an atmospheric oxy-combustion experiment performed for a similar PRB coal, Ahn et al., found close to 20% conversion of fuel-S to SO_2. However, close to 40% sulfur was retained in the ash[17]. Additionally, at high pressure, the partial pressure of SO_2 in the flue gas is high, which results in a higher potential for sulfation. It has also been reported that $CaSO_4$ decomposition is reduced at higher SO_2 concentrations. Therefore, the impact of pressure on fuel-S conversion to SO_2 may be because of several factors and not a result of SO_3 formation alone.

It has been reported that higher pressure also results in higher diffusion of SO_2 and O_2 in the ash particles, which results in larger retention of sulfur in the ash particles. Although the experiments did not measure ash sulfur retention systematically, an SEM-EDX analysis of the ash collected from the filter at 15 bar and 3% O_2 concentration revealed significant retention of sulfur in ash. Since only a small amount of ash was collected on the filter, it is difficult to generalize the retention of sulfur to total ash in coal, however, based on retention of sulfur in similar coal combustion experiments, and it is probable that retention is the bigger factor[17]. Further studies are required to verify this hypothesis.

2.4 Conclusion

The investigation of the formation of CO, NO and SO_2 in the pressurized oxy-combustion is important to understand the combustion characteristics and to design a removal process. To

understand the formation of SOx, NOx, and CO under pressure, we performed experiments in a 100 kWth pilot-scale combustor under a range of excess oxygen concentration and residence time. The results suggest that CO concentration in the flue gas decreased at a higher pressure and at higher O_2 concentrations because of the impact of gasification of char in the presence of CO_2 and higher O_2 partial pressure in the gas. This implies that combustion at 15 bar can be accomplished with lower excess oxygen (1% v/v), which can reduce the cost of O_2 production compared to atmospheric oxy-combustion where 3 – 5 % excess O_2 is required.

The study also found a significant reduction in NO formation at higher pressure. This is mainly because at higher pressure, there is a reduction in the diffusion rate of fuel nitrogen out of the char particle, extending the residence time for potential reduction to N_2. The concentration of NO went up with excess O_2 concentration in the flue gas, suggesting that lower O_2 is better for NO emission. However, very low NO concentration may be a potential problem for SO_2 removal in the direct contact cooler. Finally, SO_2 concentration decreased with excess O_2 concentration in flue gas at both 10 bar and 15 bar. This is mainly because at higher pressure, there is higher retention of sulfur in ash and also higher SO_3 formation. A higher O_2 concentration also resulted in lower SO_2 formation, which agrees with the hypothesis since higher O_2 enhances both SO_3 formation and retention. Further studies are suggested to understand the formation of N_2O, SO_3, and ash sulfur retention as they may be critical for understanding the overall balance of sulfur and nitrogen.

2.5 References

[1]   S. C. Johnson, J. D. Rhodes, and M. E. Webber, "Understanding the impact of non-synchronous wind and solar generation on grid stability and identifying mitigation pathways," Appl. Energy, vol. 262, no. 15, p. 114492, 2020.

[2] N. A. Sepulveda, J. D. Jenkins, F. J. de Sisternes, and R. K. Lester, "The Role of Firm Low-Carbon Electricity Resources in Deep Decarbonization of Power Generation," Joule, vol. 2, no. 11, pp. 2403–2420, 2018.

[3] International Energy Agency, "World Energy Outlook 2018: Highlights," vol. 32, no. 0, pp. 23–28, 2018.

[4] P. Vithayasrichareon, J. Riesz, and I. MacGill, "Operational flexibility of future generation portfolios with high renewables," Appl. Energy, 2017.

[5] C. Yin and J. Yan, "Oxy-fuel combustion of pulverized fuels: Combustion fundamentals and modeling," Appl. Energy, vol. 162, no. Supplement C, pp. 742–762, 2016.

[6] H. Zebian and A. Mitsos, "Pressurized oxy-coal combustion: Ideally flexible to uncertainties," Energy, 2013.

[7] A. Gopan, B. M. Kumfer, J. Phillips, D. Thimsen, R. Smith, and R. L. Axelbaum, "Process design and performance analysis of a Staged, Pressurized Oxy-Combustion (SPOC) power plant for carbon capture," Appl. Energy, vol. 125, pp. 179–188, 2014.

[8] X. Wang, A. Adeosun, G. Yablonsky, A. Gopan, P. Du, and R. L. Axelbaum, "Synergistic SOx/NOx chemistry leading to enhanced SO3 and NO2 formation during pressurized oxy-combustion," React. Kinet. Mech. Catal., no. 2, 2017.

[9] P. Verma et al., "Optimizing complexity in the kinetic modelling of integrated flue gas purification for pressurized oxy-combustion," Chem. Eng. J., vol. 383, Mar. 2020.

[10] A. Gopan, P. Verma, Z. Yang, and R. L. Axelbaum, "Quantitative analysis of the impact of flue gas recirculation on the efficiency of oxy-coal power plants," Int. J. Greenh. Gas Control, vol. 95, no. December 2019, p. 102936, 2020.

[11] Y. Hu, S. Naito, N. Kobayashi, and M. Hasatani, "CO 2 , NO x and SO 2 emissions from the combustion of coal with high oxygen concentration gases," vol. 79, no. x, pp. 1925–1932, 2000.

[12] E. Croiset and K. V Thambimuthu, "NO x and SO 2 emissions from O 2 / CO 2 recycle coal combustion," vol. 80, no. x, pp. 2117–2121, 2001.

[13] D. Fleig, F. Normann, K. Andersson, F. Johnsson, and B. Leckner, "The fate of sulphur during oxy-fuel combustion of lignite," Energy Procedia, vol. 1, no. 1, pp. 383–390, 2009.

[14] F. Kazanc, R. Khatami, P. Manoel Crnkovic, and Y. A. Levendis, "Emissions of NOx and SO2 from coals of various ranks, bagasse, and coal-bagasse blends burning in O2/N2 and O2/CO2 environments.," Energy and Fuels, vol. 25, no. 7, pp. 2850–2861, 2011.

[15] H. Zan, X. Chen, J. Ma, D. Liu, and Y. Wu, "Experimental Study of NO x Formation in a High-Steam Atmosphere During a Pressurized Oxygen-Fuel Combustion Process," no. x, 2020.

[16]   Z. Yang et al., "Experimental study and demonstration of pilot-scale, dry feed, oxy-coal combustion under pressure," Appl. Energy, vol. 285, no. August 2020, p. 116367, 2021.

[17]   J. Ahn, R. Okerlund, A. Fry, and E. G. Eddings, "Sulfur trioxide formation during oxy-coal combustion," Int. J. Greenh. Gas Control, vol. 5, no. SUPPL. 1, pp. S127–S135, 2011.

[18]   ]C. Lupiáñez, I. Guedea, I. Bolea, L.I. Díez, L.M. Romeo, Experimental study of SO2 and NOx emissions in fluidized bed oxy-fuel combustion, Fuel Process. Technol. 106 (2013) 587–594

[19]   D. Fleig, K. Andersson, F. Johnsson, B. Leckner, Conversion of sulfur during pulverized oxy-coal combustion, Energy and Fuels. 25 (2011) 647–655

Chapter 3. Kinetic analysis of aqueous phase interactions between dissolved SO_x and NO_x in a pressurized oxy-combustion environment

3.1 Introduction

Pressurized oxy-combustion (POC) of coal is a promising technology for efficient power generation with carbon capture, utilization, and storage (CCUS)[1]. In POC, coal is combusted at elevated pressure with oxygen to produce a flue gas stream primarily comprising of CO_2 and H_2O. Due to high pressure, the moisture in the flue gas can be condensed at a higher temperature to recover the latent heat, enhancing the efficiency of the POC power plant[2]. Depending on the amount of sulfur and nitrogen present in the coal, the flue gas also contains oxides of sulfur and nitrogen, predominantly SO_2 and NO[3]. At low temperatures, SO_x and NO_x form corrosive acids such as H_2SO_4 and HNO_3 in the presence of water vapor and oxygen. The condensation of these acids carries the potential to severely damage the metallic equipment, such as pipes and compressors[4]. Therefore, it is critical to remove the SO_x and NO_x from the flue gas to avoid damage during compression and transportation of the product CO_2 stream[5].

Several researchers have proposed a direct contact cooler (DCC) - a reactive-absorption column that uses water to remove SO_x and NO_x from the flue gas[6,7]. Since the latent heat recovery is not an objective for atmospheric pressure oxy-combustion power plants, the liquid to the gas ratio (L/G) in the column is not constrained. Hence, the DCC is designed as a low-temperature process with higher L/G flexibility. However, for the POC power plant, the increase in power plant

efficiency depends on the outlet DCC water temperature; therefore, the L/G in the column must be maintained as low as possible. The L/G constraint presents an additional complication of high-temperature SO_x and NO_x removal. This also poses a limit on the pH of the water inside the column, which impacts both the absorption and the reaction kinetics. The conditions inside the DCC of a POC power plant can range from the pH of 2 to 4 and temperatures of $25 - 160°C$ [2,8].

There are four major physicochemical phenomena taking place inside the DCC: 1) the reaction of NO in the gas phase producing NO_2, 2) the absorption of NO_2 in water to form HNO_2 and HNO_3, 3) the absorption of SO_2 in water to form HSO_3^- and, 4) the aqueous-phase reactions between the dissolved HSO_3^- and HNO_2. While the first three phenomena have been investigated in detail by several researchers[9][10], the liquid phase chemical reactions between HNO_2 and HSO_3^- lack comprehensive understanding, especially in conditions relevant to the DCC. Since the reaction between HSO_3^- and HNO_2 enhances the absorption of SO_2 and NO_2, understanding the liquid phase kinetics is vital for designing an effective scrubbing process[11].

$$
\begin{array}{c}
\underset{\text{Nitrous acid}}{HNO_2} \xrightleftharpoons[]{HSO_3^-} \underset{\substack{\text{Nitrososulfonic}\\\text{acid}}}{HO_3SNO} \xrightleftharpoons[]{HSO_3^-} \underset{\substack{\text{Hydroxylamine}\\\text{disulfonic acid}}}{(HO_3S)_2NOH} \xrightleftharpoons[]{HSO_3^-} \underset{\substack{\text{Amine trisulfonic}\\\text{acid}}}{(HO_3S)_3N}
\end{array}
$$

$$
NO + HSO_4^- \xleftarrow{HNO_2} \qquad HSO_4^- \xdownarrow{H^+} \qquad HSO_4^- \xdownarrow{H^+} \qquad HSO_4^- \xdownarrow{H^+}
$$

$$
+ \qquad\qquad + \qquad\qquad +
$$

$$
\underset{\substack{\text{Hyponitrous}\\\text{acid}}}{H_2N_2O_2} \xleftarrow{HNO_2} \underset{\substack{\text{Hydroxylamine}\\\text{monosulfonic acid}}}{(HO_3S)NHOH} \xrightarrow{HSO_3^-} \underset{\substack{\text{Amine}\\\text{disulfonic acid}}}{NH(HSO_3)_2}
$$

$$
N_2 + HNO_3 + H_2O \xleftarrow{HNO_2} \qquad N_2O \xdownarrow{H^+}\;{}_{HNO_2} \qquad HSO_4^- \xdownarrow{H^+}\;{}_{HSO_3^-} \qquad HSO_4^- \xdownarrow{H^+}
$$

$$
+ \qquad\qquad +
$$

$$
\underset{\text{Hydroxylamine}}{NH_2OH} \xrightarrow{SO_2} \underset{\text{Sulfamic acid}}{(NH_2)(HSO_3)}
$$

$$
\;{}_{SO_2} \qquad H^+ \qquad {}_{HNO_2}
$$

$$
NH^+ + HSO_4^- \qquad N_2 + HSO_4^-
$$

Figure 3.1. Liquid phase reaction mechanism between HSO_3^- and HNO_2 proposed by Chang et al. [12]

Chang et al. proposed a comprehensive liquid phase reaction mechanism between HSO_3^- and HNO_2, which included all possible intermediates and products[12]. The mechanism is presented in Fig. 3.1. They reported that in the first step, HNO_2 (aq) and HSO_3^-(aq) react form nitrososulfonic acid (NSS (aq)). NSS further reacts according to one or more of the three pathways depending on the pH of the solution and the relative concentrations of the reactants: (1) Reaction with HSO_3^-(aq) to produce hydroxylamine disulfonate (HADS), (2) Acidic hydrolysis to form HSO_4^-(aq) and hyponitrous acid ($H_2N_2O_2$(aq)), which subsequently decomposes to produce N_2O (g) and, (3) Reaction with HNO_2(aq) to form HSO_4^-(aq) and NO (g). Based on the conclusion from Chang et al., Oblath et al. [13,14] conducted multiple studies to understand the impact of pH and measure the kinetic constant of the three reaction pathways. They found that above the pH of 4, NSS(aq) only reacted with HSO_3^-(aq) to produce HADS(aq) and reported the reaction mechanism and kinetic constants. They also noted that below the pH of 3.2, there was a significant formation of N_2O(aq) because of the acidic hydrolysis of NSS(aq). While this study provided a good insight into the reaction products at different pH values, detailed kinetics below the pH of 4 were not studied. Moreover, since their experiments were limited to room temperature, they did not address the stability of HADS as a function of temperature.

$$HNO_2(aq) + HSO_3^-(aq) \xrightarrow{\;1\;} NSS(aq) \xrightarrow{\;2\;} HADS(aq) \longrightarrow Y(aq)$$

$$\downarrow 3$$

$$N_2O(g)$$
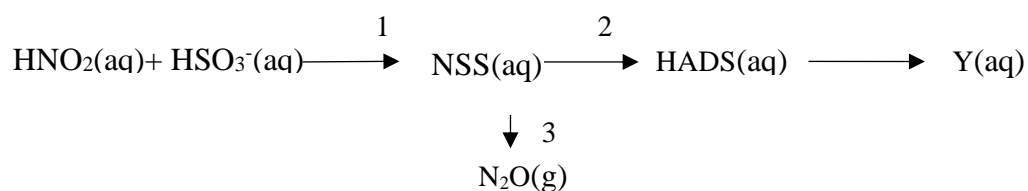
Figure 3.2 Liquid phase mechanism presented by Susianto et al. [15]. Y represents the product of its acidic hydrolysis, whose composition is ill-defined.

Building on the previous work by Chang et al. and Oblath et al.[12,13], Susianto et al.[15] conducted liquid phase experiments to investigate reactions between nitrite and sulfite ions relevant to flue gas systems. They did not observe NO (g) formation at a pH range between 2 – 4 and, therefore, discarded the viability of the reaction between NSS(aq) and HNO_2(aq) under these conditions. They effectively reduced the reaction mechanism from Chang et al. to two parallel reactions, shown in Fig. 3.2. Three major findings from this work were reported: (1) At room temperature (25 °C), at a pH less than 1, the reaction between HNO_2 (aq) and HSO_3^-(aq) is fast, and all nitrite ion is converted to N_2O(g) and HSO_4^-(aq) (pathway 3 in Fig. 2); (2) Between pH 1 and 4, all three reactions take place simultaneously; and (3) When pH is close to 4, nitrite ions can be completely converted into HADS(aq) and no N_2O(g) is produced (pathway 2 in Fig. 2). The also provided the kinetic constant for the formation of HADS (aq) at the pH of 4 but did not discuss the kinetics at higher temperatures.

The kinetic studies in the literature are limited to the interactions of HSO_3^- and HNO_2 at room temperature and comparatively high pH (> 4)[13]. Hence, there is a distinct lack of kinetic data for the conditions relevant to DCC operation. In this work, we evaluate the reaction dependencies and kinetic constant for the reaction between HNO_2 (aq) and HSO_3^-(aq) in the conditions relevant to the flue gas of pressurized oxy-combustion. We discuss the effect of temperature (between 21 and 80°C) and pH (between 2.5 and 4) on the two viable reaction pathways. Moreover, we analyze the relative formation of HADS and HSO_4^- with the change in pH and temperature and present the relative kinetic constants for the reactions. Additionally, a qualitative analysis of the stability of HADS at higher temperatures is presented. An improved understanding of the liquid phase chemistry obtained from this study should help design an efficient scrubbing system, which

remains one of the critical steps in developing POC for carbon capture, utilization, and sequestration (CCUS) EOR.

3.2 Materials and Methods

The reactions were studied in the aqueous phase (aq) using a 100 mL stirred borosilicate reactor. A water bath was employed for the temperature control of the reactor. Aqueous solutions for HSO_3^-, HNO_2, and HNO_3 were prepared by dissolving $NaHSO_3$ (A.C.S Reagent Grade), $NaNO_2$ (A.C.S Reagent Grade), and $NaNO_3$ (A.C.S. Reagent Grade), respectively in de-ionized water. The initial pH for the solution was attained using a standard solution of phosphoric acid and NaOH, owing to their non-reactivity with any other compound in the reaction system[15]. The pH of the solution was continuously measured using a pH meter. To study the reactions with relevant concentrations to POC, initial molar concentrations of 3×10^{-3}M HNO_2 and HSO_3^- were used for all the reactions. The reactor was tightly sealed to avoid evaporation at high temperatures. Samples were taken on an average of every 15 – 20 seconds over 5 minutes and capped and stored for analysis. For accuracy, at least two replication for each experiment were performed.

The storage methodology was adapted from Susianto et al.[15], which uses a combination of 1×10^{-3} M (A.C.S Reagent Grade) D-mannitol solution at a pH of 12. The high pH seizes the sulfite and nitrite interactions, and D-Mannitol prevents sulfite oxidation to sulfate, providing a stable solution for sample storage. All solutions were analyzed within 6 – 8 hours of initial storage. Each sample was analyzed in an Ion Chromatograph (Dionex ICS-1600) with an IonPac AG22 column and an ASRS 300 Suppressor capable of quantifying HNO_2, HNO_3, HSO_3^- and HSO_4^- concentrations. This column was unable to detect the presence of HADS. The accurate

determination of the initial ion concentration coupled with a sulfur and nitrogen mass balance was used to reasonably estimate the HADS formation.

3.3 Results and Discussions

3.3.1 The effect of pH on the reaction between HNO_2 and HSO_3^-
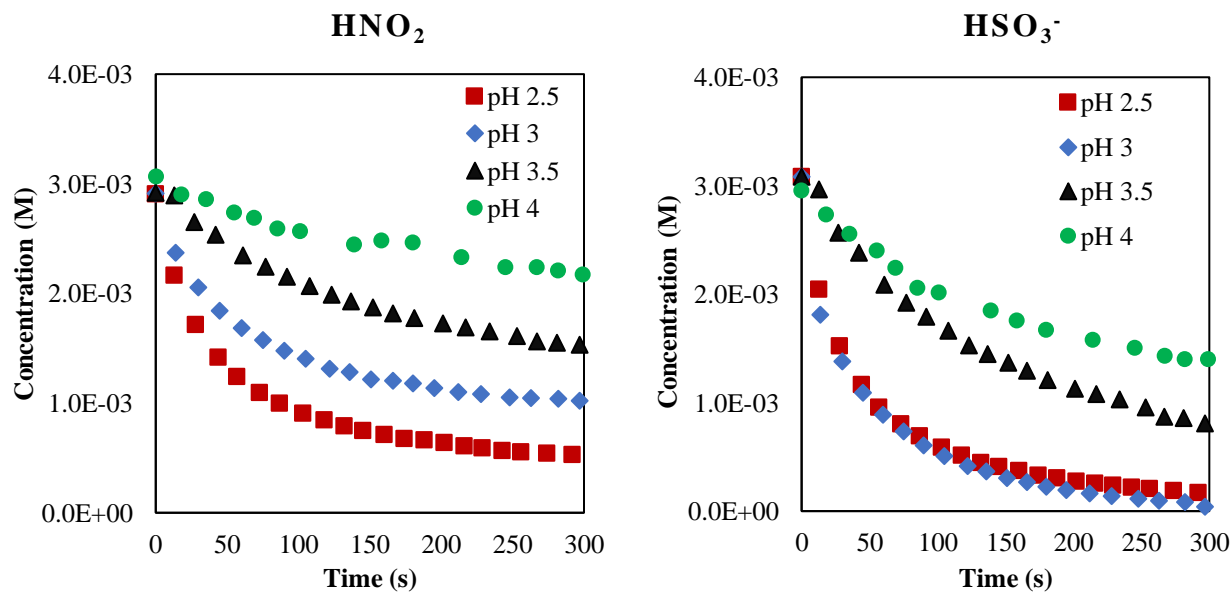
Figure 3.3. The effect of pH on HNO_2 and HSO_3^- consumption rates at 22 °C.

The experiments were conducted by mixing the initial moles of HNO_2 and HSO_3^- in a stirred batch reactor and taking a sample an average of every 15 seconds. The experiments at each condition were repeated twice to ensure reproducibility. From the perspective of the gas cleanup process, the main objective is the rate of consumption of HSO_3^- in the liquid phase. The consumption of HSO_3^- via reaction with HNO_2 will increase the dissolution of SO_2 to maintain the gas-liquid equilibrium

between SO_2 and HSO_3^-. The results presented in Fig. 3.3 clearly illustrate that the rate of consumption of HSO_3^- goes up as the pH of the system goes down, giving a clear assertion that a low pH is good for removal of SO_2, barring other factors. The same trend can be seen for the consumption of HNO_2 as pH goes down from 4 to 2.5. This indicates that the rate of the first reaction (R1) is depended on the H^+ concentration in solutions. However, from our analysis and experimental design, it is hard to conclude if H^+ acts as a catalyst or a reactant, as it is complicated to differentiate the acid consumption in Reaction 1 and Reaction 3.

$$HNO_2 + HSO_3^- \rightarrow NOSO_3^- \ (NSS) \ + H_2O \tag{R1}$$

$$NOSO_3^- + HSO_3^- \rightarrow HON(SO_3)_2^{2-} \ (HADS) \tag{R2}$$

$$NOSO_3^- + \frac{1}{2}H_2O \rightarrow 1/2N_2O + HSO_4^- \tag{R3}$$
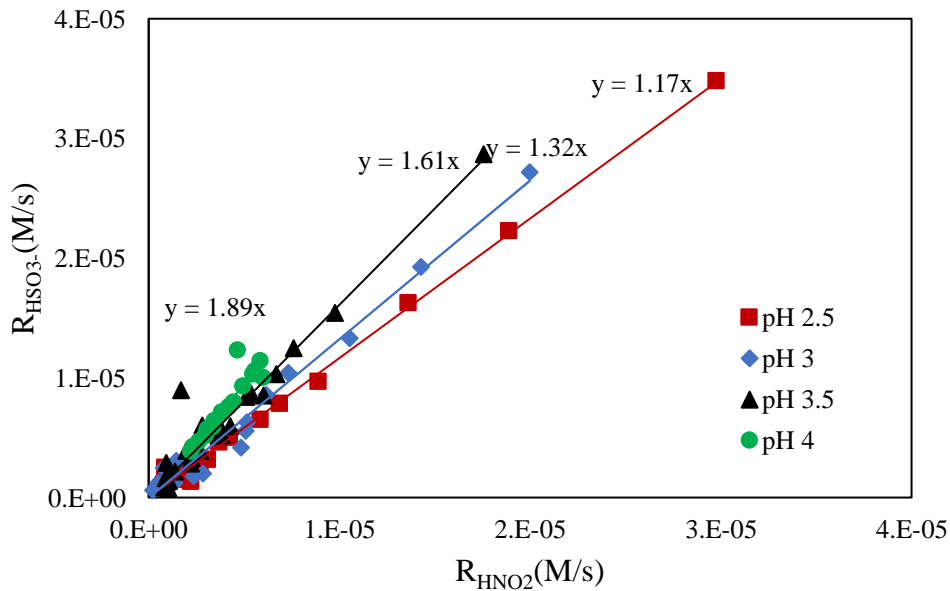
Figure 3.4 Correlation between the rate of consumption of HNO_2 and HSO_3^- at 22 °C.

To understand the reaction order dependencies of the species we plotted the concentration of HNO_2 against HSO_3^-, presented in Fig. 3.4. As evident from the plot, at every pH, although the slope changes, the strong linear correlations between HNO_2 and HSO_3^-. The slope merely represents the stoichiometry of the overall reaction, the straight line confirms that both HSO_3^- and HNO_2 are consumed in the reaction with the same order, even at pH as low as 2.5. This result is corroborated by the hypothesis from Oblath et al.[14], which states that Reaction 1 is slower than 2 and 3 and hence the rate of Reaction 1 alone can sufficiently account for the rate of consumption for both the reactants. Although Oblath et al. performed the analysis only up to a pH of 3.2, this study confirms that Reaction 1 remains the slower reaction for as low as pH of 2.5. This also makes the individual calculation of rate constants for Reactions 2 and 3 difficult.

$$-\frac{d[HNO_2]}{dt} = R_1 = -\frac{1}{\nu}\frac{d[HSO_3^-]}{dt}$$
(Eq. 3.1)

Since both reactants are consumed at same reaction rate, Equation 1 mathematically represents the kinetic dependency of the rate of consumption of HNO_2 with HSO_3^-, where ν is the stoichiometric constant for the global consumption of HSO_3^- per mole of HNO_2. The slopes from Fig. 4 represents the overall stoichiometry of the three reactions system. At a pH of 4, the consumption of HSO_3^- per mole of HNO_2 is around 1.89, and it starts to go down, as the pH drops, to a value of almost 1.17 at a pH of 2.5. This suggests that in the 2nd part of the reaction system, with Reaction 2 competing in parallel with Reaction 3, the reaction shifts from Reaction 2 to Reaction 3 as the pH of the system goes down. A value of 2 would represent only the formation of HADS, which makes the result consistent with the results observed by Susianto et al., above pH 4[15].
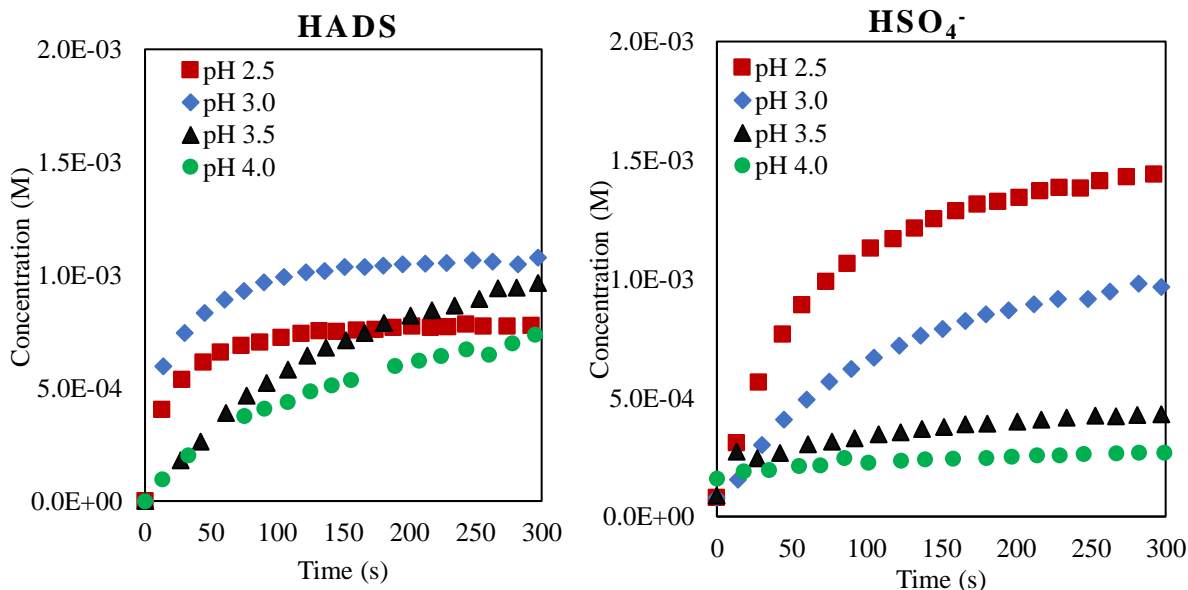
Figure 3.5. The effect of pH on HSO_4^- and HADS formation rate at 22 °C.

The products of the reaction system are also a good fingerprint for a better understanding of the competing Reactions 2 and 3. The production of HSO_4^- and HADS is presented in Fig. 3.5, which shows that a decrease in pH results in an increase in HSO_4^- formation rate, indicating that the Reaction 3 pathway is more prevalent at lower pH, which is corroborated by results from Pires et al.[16], where they found that the rate of formation of N_2O is a maximum at pH of 0.

The formation of HADS in Fig. 5 shows a more complex dependence on pH with the rate of Reaction 1 going up as the pH goes down with a reduction in the ratio of HADS/HSO_4^-, as the selectivity shifts towards Reaction 3. The rate of formation of HADS before 50 seconds, is higher at lower pH (2.5 and 3) compared to higher pH, but the final concentration of HADS plateaus as HSO_4^- formation is selectively preferred at lower pH values. However, HADS production rate remains constant at higher pH values (3.5 and 4), and the overall concentration of HADS continues to climb without a significant reduction till 300s. It also implies that while the formation of HADS

41

is favored at higher pH, it is overall a slower process compared to the formation of HSO_4^-, as H^+ favor both Reactions 1 and 3. The split between Reaction 2 and Reaction 3, can be presented as a function of HSO_3^- and H^+, and the rate of the overall consumption of the reactants can be correlated with H^+ concentration, along with the concentrations of HSO_3^- and HNO_2. The analysis of the rate constants is presented in Section 3.3.

3.3.2   The effect of temperature
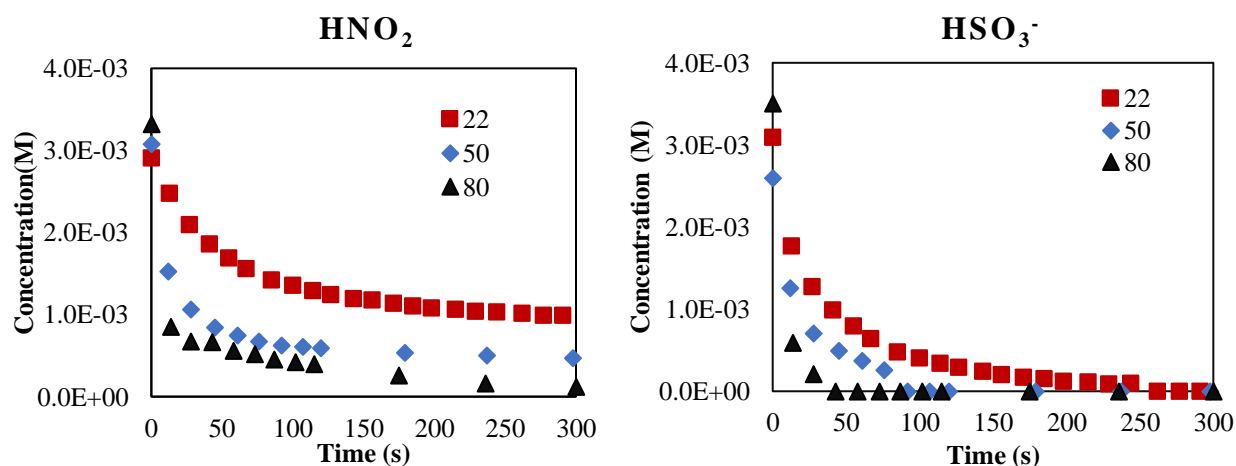
Figure 3.6. The effect of temperature on the consumption of on HSO_3^- and HNO_2 at a pH of 3.

The high temperature experiments were conducted in a stirred batch reactor placed in a water bath to maintain a constant temperature. The experiments were conducted twice for every condition to ensure reproducibility. The increase in temperature results in an increased reaction rates for both HSO_3^- and HNO_2. As evident from Fig. 3.6, HSO_3^- is consumed in under 40 s at a temperature of $80\,°C$. In respect to an overall removal of SO_2 from the gas phase, there are two opposing dynamics at play here. Higher temperature typically reduces gas absorption in the liquid phase, which should reduce SO_2 absorption barring any liquid phase interaction of the absorbed SO_2. However, as seen

in Fig. 3.6, higher temperature enhances liquid phase consumption of HSO_3^- through reaction with HNO_2. With an increases in the consumption rate, for a given residence time, the absorption of SO_2 will increase through the liquid phase reaction pathway. The effective rate of absorption of SO_2 in a steady state process, will result from the combination of both the two competing dynamics. The same can be said for the temperature dependence of the absorption of NO_2 and the rate of liquid phase reaction. Moreover, the analysis of the rate of the consumption of HNO_2 and HSO_3^- suggest that the rate order remains the same, denoting that the formation of NSS remains the slower step. Additionally, comparing the rates of consumption of the reactants at different temperatures, similar to Fig. 3.5, suggests that the ratio of consumption of HSO_3^- to HNO_2 ranges between 1.32 and 1.22. Although there is a slight decrease at higher temperatures, the calculation was performed using fewer points (just 3 points for 80 ℃) because the reaction completes very fast. Hence, it can be safely assumed that split between HSO_4^- and HADS remains almost in the same range up to a temperature of 80 ℃.
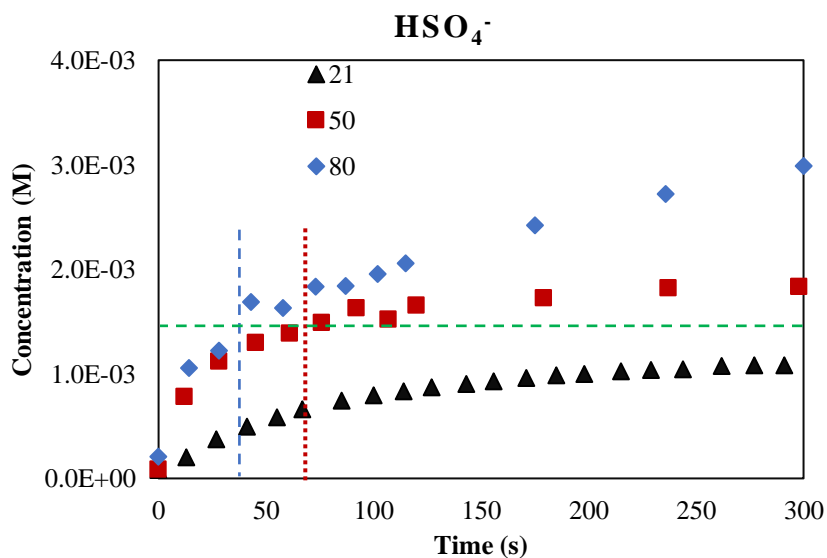
Figure 3.7. The effect of temperature on the formation of HSO_4^- for an extended time period. The lines mark the point where all of HSO3- was consumed.

It is also observed in Fig. 3.6(a) that at higher temperatures, the consumption of HNO_2 shows and interesting trend after the reaction of HSO_3^- is completed (i.e., all the HSO_3^- is consumed). The concentrations of HNO_2 continued to go down slowly with time, however not with the same rate as that of Reaction 1. Additionally, the concentrations of HSO_4^- also slowly increased after the complete consumption of HSO_3^-. These trends for an extended time range are not accounted in the reaction mechanism comprising of Reaction 1−3. In Fig. 3.7, the straight lines mark the time at which HSO_3^- is fully consumed for the temperature of $50\,^{\circ}C$ and $80\,^{\circ}C$, as well as the concentration of HSO_4^- at that point. It is evident from the figure that a further reaction is taking place resulting in the formation of HSO_4^- in conjunction with the consumption of HNO_2. The mole balance for the consumption of HNO_2 from Fig. 3.6(a) and the formation of HSO_4^- in Fig 3.7, suggest that for each mole of HNO_2 consumed two moles for HSO_4^- is produced. Because the only source of sulfur in the solution at this point is HADS, (with a 1:2 nitrogen to sulfur ratio), it appears that further reaction of HADS is taking place at higher temperatures. According to the reaction mechanism developed Chang et al.[12] presented in Fig. 2, there are two potential reaction pathways that could result is this observation. The first pathway is based on a reverse breakdown reaction of HADS to produce NSS and HSO_3^-, where NSS then reacts according to Reaction 3 in our mechanism to form HSO_4^- and N_2O, and the produced HSO_3^- reacts with excess HNO_2 to form NSS again and follow the same path (Reaction 1 and 3). In the second potential pathway, HADS goes through acidic hydrolysis to form hydroxylamine monosulfonic acid (HAMS) and HSO_4^- (Reaction 4). HAMS then reacts with HNO_2 to form $H_2N_2O_2$ (Reaction 5), which then hydrolyses to form N_2O (Reactions 6 and 7). Both Ajdari et al. [17] and Susianto et al. [15] considered this pathway, but since their work was limited to room temperature experiments, they did not observe this trend and

deemed the pathway less relevant. However, both reaction pathways result in the same overall reaction; consumption of one mole of HNO_2 every two moles of HSO_4^- produced.

$$HON(SO_3)_2^{2-} + H^+ \rightarrow HSO_4^- + (HO_3S)NHOH \text{ (HAMS)} \tag{R4}$$

$$(HO_3S)NHOH + HNO_2 \rightarrow HSO_4^- + H_2N_2O_2 \tag{R5}$$

$$H_2N_2O_2 + H^+ \rightarrow N_2O + H_2O \tag{R6}$$

$$HON(SO_3)_2^{2-} + HNO_2 \rightarrow N_2O + H_2O \tag{R7}$$
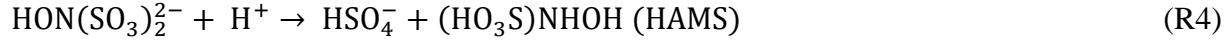
Considering the rate of 1st and 2nd part of the reaction, before and after the total consumption of HSO_3^-, at higher temperatures, the important thing to note is that no net formation of HSO_3^- is observed, and more sulfur(IV) is oxidized to sulfate(VI). Hence the 2nd part of the reaction would not have an impact on the removal of SO_2 from flue gas. However, the influence of temperature on the complex HADS requires further investigation to determine the final product formation.

3.3.3 Reaction rate analysis

3.3.3.1 Estimation of the rate constant for the production of NSS

In Section 3.1, the analysis from Fig. 4 confirmed that the formation of NSS (Reaction 1) is the rate-limiting step for the overall system, and hence, the rates of Reactions 2 and 3 cannot be determined independently. Moreover, the rate of Reaction 1 is of paramount importance for gas cleanup systems. Oblath et al.[13] and Susianto et al.[15] analyzed this reaction in the pH range of 4 – 6.5 and established the formation of NSS is first order in HNO_2, HSO_3^- and H^+. The analysis in our study confirms that the order of the reaction remains constant for the formation of NSS up to a pH of 2.5. Hence, the rate of formation of NSS of NSS can be represented by Equation 2,

45

$$\frac{d[NSS]}{dt} = R_1 = - \frac{d[HNO_2]}{dt} = k_1[HNO_2][HSO_3^-][H^+] \tag{Eq. 3.2}$$

To calculate the rate constant for reaction 1, the rate of change of HNO_2 was used and the rate

constant was then confirmed using the rate of change of HSO_3^- with the stoichiometric dependency

developed in Section 3.1. The reaction rate constant for the formation of NSS comes out to be,

$(5.374 \pm 0.5) \times 10^3$ $L^2mol^{-2}s^{-1}$. Susianto et al. calculated the rate constant of formation of

HADS at a pH of 4 to be 4×10^3 $L^2mol^{-2}s^{-1}$, with the hypothesis that HADS is the only product

of the reaction. In this study, we observed the formation of HSO_4^- at a pH of 4, similar to the

observations by Oblath et al, however the amount of HSO_4^- remained small compared to HADS

formation[14,15].
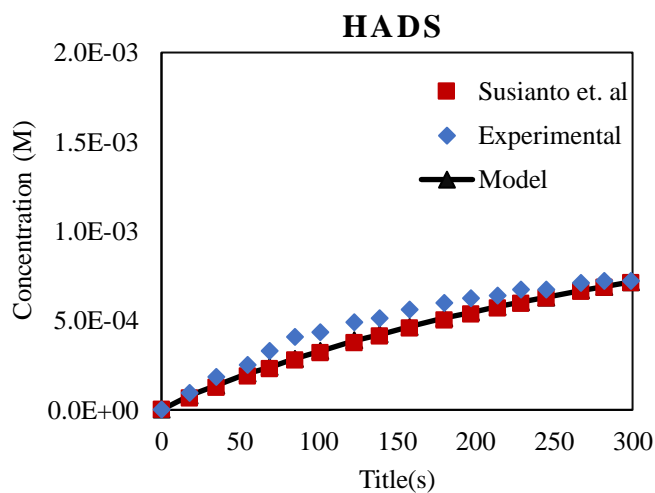
Figure 3.8 A comparison between our experimental data and HADS prediction from kinetic constants at a pH of 4.

In Fig. 3.8, the HADS concentrations obtained from the experiment at pH 4, is compared with the

calculated HADS concentration using the kinetic constant reported by Susianto et al. and the

kinetic constant developed in this study[15]. The calculated concentration of HADS using the

constant by Susianto et al. and this study, provide a close estimation of HADS. Both the constants, slightly underestimate the concentration of HADS at pH 4. The rest of the products at various pH values, can be estimated from the kinetic constant developed in this study using the value of k_1, along with the stoichiometry calculated in Fig. 3.4.

3.3.3.2 Estimation of the relative rate constants of Reactions 2 and 3

As discussed in Section 3.1, the rate constants for Reactions 2 and 3 are difficult to calculate, however, the data can be used to estimate the ratio of rate constants for two reactions. Considering both reactions to be first order with NSS; the equation can be presented as;

$$\frac{d[HADS]}{dt} = k_2[NSS][HSO_3^-] \tag{Eq. 3.3}$$

$$\frac{d[HSO_4^-]}{dt} = k_3[NSS][H^+] \tag{Eq. 3.4}$$

Hence,

$$\frac{k_2}{k_3} = \left(\frac{d[HADS]}{dt} \Big/ \frac{d[HSO_4^-]}{dt}\right)\left(\frac{H^+}{HSO_3^-}\right) \tag{Eq. 3.5}$$

Using this equation for every pH, the value of $\frac{k_2}{k_3}$, comes out to be 1.09 ± 0.4.

3.3.3.3 Estimation of the temperature dependence of the rate constant for the production of NSS
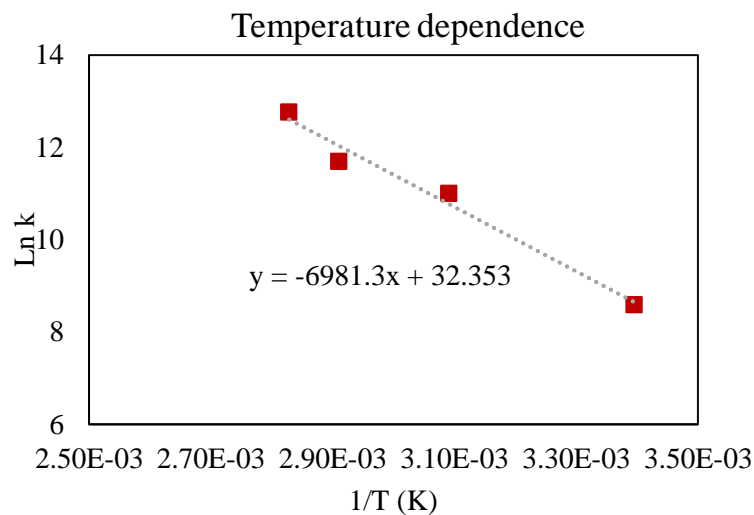
Figure 3.9 Temperature dependence of rate constant

Finally, the temperature dependence of the rate constant for Reaction 1 was calculated using the experimental data from the temperature range of 21–80 °C. According to the Arrhenius law, the slope represents the value of E_a/R, while the intercept represents the value of the pre-exponential factor, presented in Fig. 9. The rate constant can be expressed as $k_1 = 1.12 \times 10^{14} \exp\left(-\frac{6981}{T}\right) L^2 mol^{-2} s^{-1}$. Because the absolute value of rate constants for Reaction 2 and Reaction 3, are unavailable, the estimation of their individual temperature dependence will require further investigation. However, it is not necessary for the purposes of this analysis since Reaction 1 is controlling the rate.

3.4 Conclusions

The reaction mechanism between absorbed SO_2 and NO_2 in water is a complicated phenomenon, consisting of multiple steps and several chemical intermediate species. However, the complicated mechanism can be reduced to the combination of three important reactions: (1) The reaction of HSO_3^- and HNO_2 in presence of H^+ to produce NSS, (2) Reaction of NSS with another mole of HSO_3^- to produced HADS, and (3) The acidic hydrolysis of NSS to produce HSO_4^-. In this study, the experimental investigation of the reaction kinetics of this reaction system was performed, to understand the effect of pH and temperature on the system and to quantify the rate constants required for modeling and optimization the system.

The effect of pH was studied in the range of 2.5 – 4, which is the most relevant to the scrubbing process. First, based on the correlation between the consumption rate of both the reactants, we concluded that formation of NSS (Reaction 1) is the limiting step for the kinetic system for the entire pH range, and the rate of this reaction increases as the pH is reduced. Second, the production of HADS (Reaction 2) is favored over the production of HSO_4^- (Reaction 3) at higher pH and vice versa, with the concentrations of major products shifting slowly from HADS to HSO_4^- as the pH is reduced.

The effect of temperature on the reaction system was studied between the temperatures of 21– 80 ℃, at a pH of 3. Increase in temperature results in the increase of reaction rate for NSS production, which remains the rate-limiting step. Additionally, the split between HADS and HSO_4^- formation only changes slightly with HSO_4^- being favored at higher temperatures. The reaction rate constant for NSS formation (Reaction 1) is presented and compared with the models present in literature. The relative rate constant for HADS and HSO_4^- (Reaction 2 and 3) is also presented, as individual

49

rate constant determination was not possible. Finally, the temperature dependence of the rate constant for Reaction 1 is presented. The liquid phase interaction between SO_x and NO_x at high temperature had not been studied before and was one of the major roadblocks for the development of the kinetic model for high-temperature scrubbing process. The development of reaction mechanisms and rate constants for a wide range of temperature and pH, helps in the development of an optimized direct contact column for pressurized oxy-combustion systems, advancing a step further in the commercialization of carbon capture technologies.

3.5 References

[1]   H. Hagi, M. Nemer, Y. Le Moullec, C. Bouallou, Towards second generation oxy-pulverized coal power plants: Energy penalty reduction potential of pressurized oxy-combustion systems, Energy Procedia. 63 (2014) 431–439.

[2]   A. Gopan, B.M. Kumfer, R.L. Axelbaum, Effect of operating pressure and fuel moisture on net plant efficiency of a staged, pressurized oxy-combustion power plant, Int. J. Greenh. Gas Control. 39 (2015) 390–396.

[3]   Y. Hu, J. Yan, Characterization of flue gas in oxy-coal combustion processes for CO2 capture, Appl. Energy. 90 (2012) 113–121.

[4]   N.G. Vannerberg, T. Sydberger, Reaction between SO2 and wet metal surfaces, Corros. Sci. 10 (1970) 43–49.

[5]   B. Paschke, A. Kather, Corrosion of pipeline and compressor materials due to impurities in separated CO2 from fossil-fuelled power plants, Energy Procedia. 23 (2012) 207–215.

[6]   A. Gopan, B.M. Kumfer, J. Phillips, D. Thimsen, R. Smith, R.L. Axelbaum, Process design and performance analysis of a Staged, Pressurized Oxy-Combustion (SPOC) power plant for carbon capture, Appl. Energy. 125 (2014) 179–188.

[7]   T.Z. Tumsa, S.H. Lee, F. Normann, K. Andersson, S. Ajdari, W. Yang, Concomitant removal of NOx and SOx from a pressurized oxy-fuel combustion process using a direct contact column, Chem. Eng. Res. Des. 131 (2018) 626–634.

[8]   V. White, A. Wright, S. Tappe, J. Yan, The Air Products Vattenfall oxyfuel CO2compression and purification pilot plant at schwarze pumpe, Energy Procedia. 37 (2013) 1490–1499.

[9]   H. Tsukahara, T. Ishida, M. Mayumi, Gas-phase oxidation of nitric oxide: Chemical kinetics and rate constant, Nitric Oxide - Biol. Chem. 3 (1999) 191–198.

[10]   F.P. Terraglio, R.M. Manganelli, The absorption of atmospheric sulfur dioxide by water solutions, J. Air Pollut. Control Assoc. 17 (1967) 403–406.

[11]   F. Normann, E. Jansson, T. Petersson, K. Andersson, Nitrogen and sulphur chemistry in pressurised flue gas systems: A comparison of modelling and experiments, Int. J. Greenh. Gas Control. 12 (2013) 26–34.

[12]   S.G. Chang, D. Littlejohn, N.H. Lin, Kinetics of Reactions in a Wet Flue Gas Simultaneous Desulfurization and Denitrification System, Am. Chem. Soc. (1982) 127–152.

[13]   S.B. Oblath, S.S. Markowitz, T. Novakov, S.G. Chang, Kinetics of the formation of hydroxylamine disulfonate by reaction of nitrite with sulfites, J. Phys. Chem. 85 (1981) 1017–1021.

[14]   S.B. Oblath, S.S. Markowltz, T. Novakov, S.G. Chang, Kinetics of the initial reaction of nitrite ion in bisulfite solutions, J. Phys. Chem. 86 (1982) 4853–4857.

[15]   M.S. Pétrissans, A. Zoulalian, Influence of the pH on the Interactions between Nitrite and Sulfite Ions . Kinetic of the Reaction at pH 4 and 5, Ind. Eng. Chem. 40 (2001) 6068–6072.

[16]   M. Pires, M.J. Rossi, The heterogeneous formation of N2O in the presence of acidic solutions: Experiments and modeling, Int. J. Chem. Kinet. 29 (1997) 869–891.

[17]   S. Ajdari, F. Normann, K. Andersson, F. Johnsson, Reduced Mechanism for Nitrogen and
        Sulfur Chemistry in Pressurized Flue Gas Systems, Ind. Eng. Chem. Res. 55 (2016)
        5514–5525.

Chapter 4. Optimizing Complexity in the Kinetic Modelling of Integrated Flue Gas Purification for Pressurized Oxy-Combustion

4.1 Introduction

Coal combustion remains an important source of power generation in many countries, resulting in large emissions of CO_2 [1]. The reduction of CO_2 emissions from coal-fired power plants is deemed to be vital to mitigate the impact of climate change[2]. Carbon Capture Utilization and Storage (CCUS) is considered an essential approach to reducing carbon dioxide emissions. In CCUS, CO_2 is captured from the power plant and stored in suitable underground geological formations or utilized for enhanced oil recovery (EOR) [3,4]. Among the various approaches for capturing CO_2, oxy-combustion is particularly promising [2]. With first-generation oxy-combustion technologies, combustion occurs at near atmospheric pressure using a combination of pure oxygen and recycled flue gas, generating a relatively pure CO_2 stream with water vapor and other species (oxygen, SO_x, NO_x, HCl, and Hg) [5]. The flue gas is purified and compressed to make it suitable for sequestration or EOR [6]. The compression process requires the removal of SOx and NOx from the CO_2 stream to avoid acidic corrosion in the equipment and piping. In traditional air-fired power plants, flue gas purification consist of separate processes for removal of NO_x and SO_x. Typically, a selective catalytic reactor or selective non-catalytic reactor, SCR or SNCR, is used for removal of nitrogen oxides, while sulfur oxides are scrubbed with alkali earth salts. These methods require large, costly equipment, parasitic loads and chemicals. Therefore, a low-cost method of flue gas purification in oxy-combustion is needed for controlling and improving the process efficiency.

In recent years, the integrated removal of SO_x and NO_x via compression of the oxy-combustion flue gas to a pressure of 15-30 bar has been proposed. Advantages include: 1) the process is more economical than separate removal for NO_x and SO_x because of the decrease in capital costs, as the amount of large equipment is reduced; 2) the scrubbing water also cools the gas, which removes the heat of compression; and 3) mercury can be removed simultaneously by reacting with nitric acids [7]. However, a major challenge of the process is the presence of moisture during compression, which can lead to acid condensation and corrosion in the equipment (sour gas compression). On the other hand, pressurized oxy-combustion (POC) offers an attractive solution to this problem because pressurizing the oxygen before combustion removes the need for compression before integrated NO_x and SO_x removal. NO_x and SO_x can be removed simultaneously in one device, a Direct Contact Cooler, or DCC, where at the same time the latent heat from the flue gas moisture is recovered. A detailed pressurized oxy-combustion power plant is presented in Figure 4.1. In addition to the benefits of SO_x/NO_x removal under pressure, the overall efficiency for the POC process is further increased because of the latent heat recovery in the DCC [8].
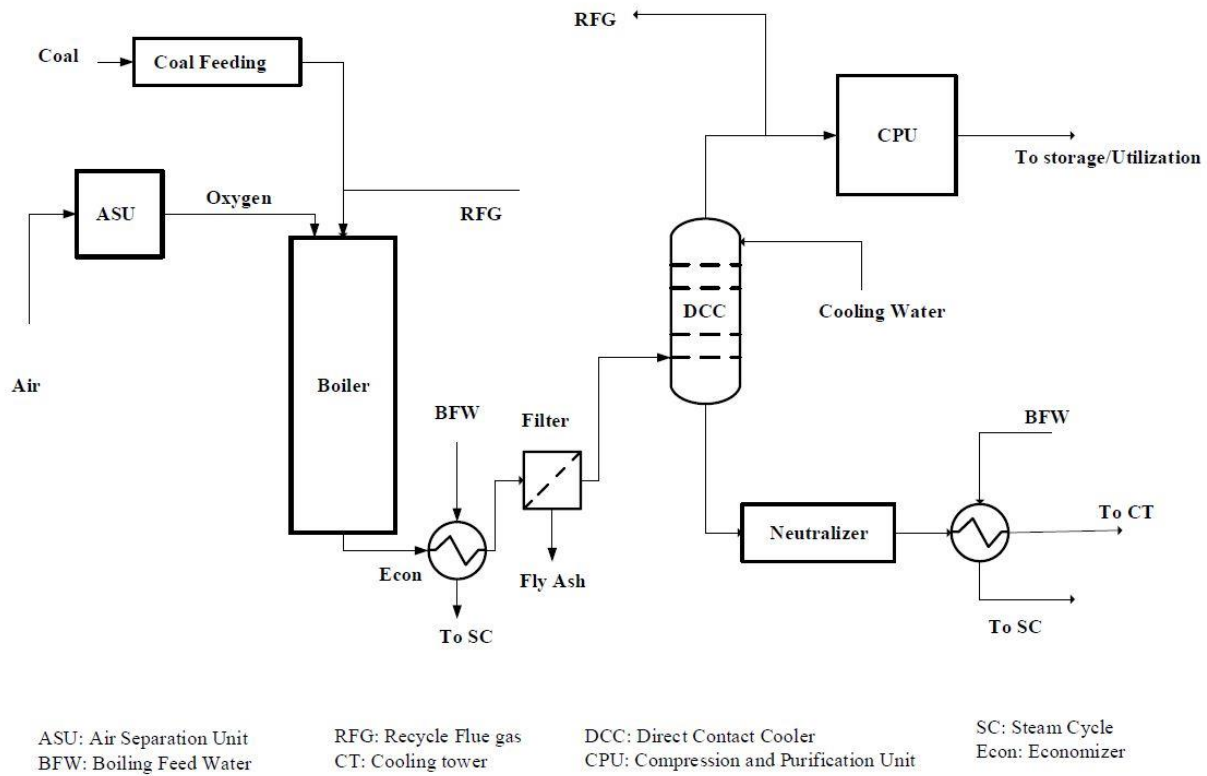
Figure 4.1 Pressurized Oxy-Combustion process. Adopted from Akshay et al. [8]

For the development of an optimized and efficient industrial-scale process of integrated SOx and NOx removal, there is a need to understand and simplify the kinetic behavior of various reactions taking place in the Direct Contact Column. The goal of this chapter is to develop a novel model of optimal complexity (MOC). Such a reduced model should meet three requirements: 1) it must be *sufficient* to accurately model the SOx/NOx removal process, i.e. the steps must reflect the main physio-chemical processes in the system. 2) it must be *observable*, i.e. it must include only concentrations of substances that can be monitored during the reaction, 3) it must be *significant*, i.e. only steps with a significant contribution to the rate of the observed substances should be included in the model, and 4) it should produce an analytical equation that can be compared with

experimental data. The novelty of this work is the development of the MOC, which includes

oxidation of NOx in the gas phase, dissolution of the corresponding oxides in water, as well as the

liquid-phase reaction, i.e., the reaction of NO- and SO- containing substances in water. Although

Normann et al. [9] and Ajdari et al. [11] have presented detailed reaction mechanisms, they were

overloaded with unknown intermediates. In this work, we have developed a model of optimal

complexity presented in terms of observed concentrations, which allows us to deduce the physico-

chemical characteristics of the system. It also allows us to derive analytical expressions for the

process and enhances our understanding of the system.

4.2 Review of kinetic models
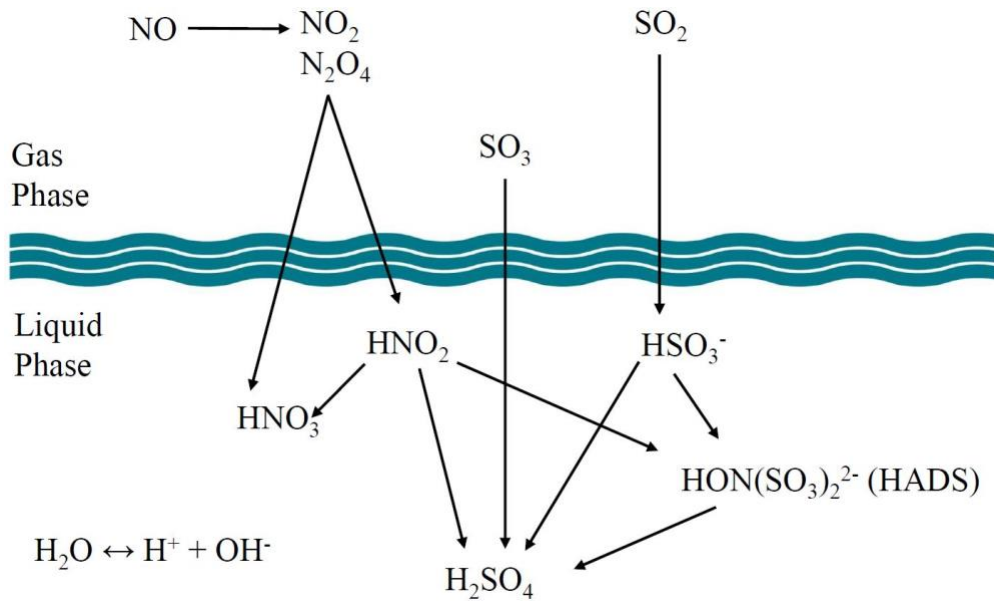
Figure 4.2 Overview of SOx/NOx absorption system.

The most elaborate mechanism and model for integrated SO_x and NO_x removal from high-pressure

flue gas was proposed by Normann et al. [9]. They discussed 34 major reactions in this mechanism

and performed kinetic modelling on 22 reactions (Appendix A). In Normann's model, the formation reaction of N_2O_3 and N_2O_4 was considered even though a majority of studies suggest that they are not available in significant quantities. In the liquid phase, Normann et al. [9] considered two different mechanisms of interactions between the NO- and SO- containing substances; the lead-chamber mechanism and the Raschig mechanism. The lead-chamber mechanism is presented by the following set of steps, in which NO works as a catalyst.

$2NO + O_2 \rightarrow 2NO_2$

$2NO_2 \, (N_2O_4) + H_2O \rightarrow HNO_2 + HNO_3$

$H_2SO_4 + HNO_2 \rightarrow HNSO_5 + H_2O$

$H_2SO_3 + 2HNSO_5 + H_2O \rightarrow 3H_2SO_4 + 2NO$
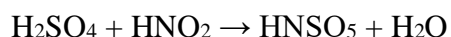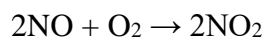
Raschig mechanism is the following:

$HNO_2 + HSO_3^- \rightarrow NOSO_3^- + H_2O$

$NOSO_3^- + H^+ \, (+ H_2O) \rightarrow HNO + H_2SO_4$

$NOSO_3^- + HSO_3^- \rightarrow HNO(SO_3)_2^{2-}$

$HNO + HNO \rightarrow N_2O + H_2O$

$HNO(SO_3)_2^{2-} + H^+ \rightarrow HNOHSO_3^- + H^+ + HSO_4^-$
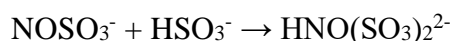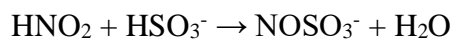
In this mechanism, HNO_2 reacts with HSO_3^- also N_2O is a product of the final step.

Which of the two mechanisms is dominating and more responsible for kinetic behavior in the liquid phase is still debated in the literature. Normann et al. verified their modelling results based on the experimental data obtained by Murciano et al. under different pressure, residence times and SOx and NOx concentrations [10]. Normann's model is detailed but complicated, containing

species whose concentrations are difficult to measure in real experimental studies. Among the 39 species in this model, there are only 10 that can be experimentally measured. Thus, this mechanism could benefit from a significant model reduction since reduced mechanisms are more suitable for engineering modelling, and they are easier to understand, holding the potential to be modeled analytically.

To simplify the Normann model and eliminate the uncertainties related to assumed intermediates, Ajdari et al. proposed a reduced mechanism (Appendix B) [11]. In this mechanism, NO oxidation was the rate-limiting reaction in the gas phase, while liquid phase reactions were sensitive to the pH value, which can be considered as a parameter of the kinetic model. The first stage of simplification was done using sensitivity analysis [11]. The number of species and reactions was significantly reduced – from 39 to 20 species and from 34 to 12 reactions, respectively. They reported that the gas-phase reactions between NO_2 and NO to form N_2O_3 and N_2O_4 are insignificant. Ajdari et al. did not consider the lead-chamber mechanism to be significant. Depending on the pH-value, different liquid phase reactions were considered limiting. The pH-specific mechanisms related to different pH-values (1, 2, 4 and 5) were established (Appendix B). The two major liquid phase mechanisms described by Ajdari et al. are in a significant agreement with the results presented by different authors [11, 12, and 13]. In the final reduced mechanism, which included the pH-specific mechanism, the number of species was reduced to between 14 and 17 and the number of reactions to 7 or 8.

4.3 Proposed Mechanism and Model

The process of SOx and NOx removal from the flue gas is depicted in Figure 2. The interaction between various SOx and NOx species in gas and liquid phases can be categorized under three kinetic subsystems: 1) The gas-phase NOx reactions, its dissolution and subsequent reaction with water. 2)The dissolution of SO_2 and its subsequent reaction with water and, 3) The interactions between SO- and NO-containing species in the aqueous phase.

4.3.1 Kinetics of NOx reaction

This mechanism reflects only two nitrogen oxides (NO and NO_2) because the other oxides (N_2O_3 and N_2O_4) are not observed experimentally. Similar to Ajdari et al. [11], the mechanism presented in this study does not consider the lead-chamber mechanism. Gas-phase chemistry of NO oxidation has been extensively studied and is reasonably well understood. A comprehensive review of the rate of NO oxidation in the dry gas phase was done by Tsukahara et al. [11]. They reported that the reaction is a third-order homogenous reaction, with the Arrhenius equation, k ($L^2.mol^{-2}.s^{-1}$) $= 1.2x10^3 \exp\left(\frac{530}{T}\right)$ being the best fit between the temperature of 273 to 600 K.

$$2NO(g) + O_2(g) \rightarrow 2NO_2 (g) \tag{R1}$$

Lee et al. studied reaction kinetics of NO_2 with the liquid water at low partial pressure and reported that the reaction has second-order kinetics with a rate constant of 10^8 $M^{-1}s^{-1}$ at room temperature [16, 20].

$$2NO_2(g)+H_2O(aq) \rightarrow HNO_2(aq) + HNO_3(aq) \tag{R2}$$

In the literature, dissociation of HNO_2 in liquid phase with the production of NO is considered as part of the mechanism.
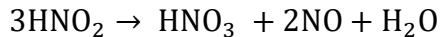
$$3HNO_2 \rightarrow HNO_3 + 2NO + H_2O \hspace{6cm} R_{diss}$$

To experimentally verify this reaction as part of the mechanism, we conducted gas-liquid experiments with NOx. The experiments were performed in a 15 bara pressure vessel with a 50 mL mixture of NO/O_2 with 250 mL of deionized water. The change in concentrations of the dissolved species (HNO_2 and HNO_3) with time was investigated via ion chromatography. In Figure 4.3, the liquid phase shows an approximate 1:1 ratio between HNO_2:HNO_3 concentrations, which does not change at residence times up to 60 minutes. The 1:1 ratio suggests that the dissociation of HNO_2 (R_{diss}) does not occur to any observable extent in these conditions. This was also confirmed by the gas phase analysis of the system where no NO was observed in the gas phase. These results confirmed that reaction R_{diss} can be excluded from the reduced mechanism.
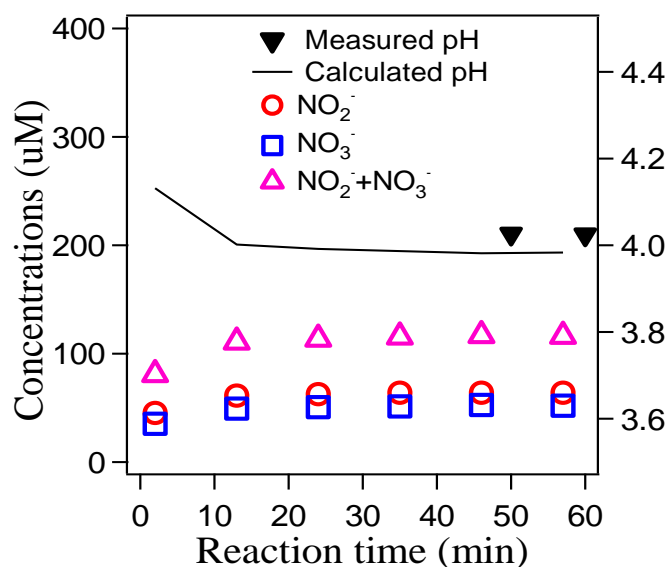
Figure 4.3 HNO_2 and HNO_3 liquid ion formation from 900 ppm NO/ 3% O_2

Because of the experimental results obtained above (1:1 ratio between HNO_2:HNO_3 concentrations), the reaction $2NO_2 + H_2O \rightarrow HNO_2 + HNO_3$ is considered to be significant. It is one of physico-chemical grounds of our mechanism.

61

4.3.2   Kinetics of SOx reaction

$$SO_2(g) + H_2O \ (aq) \leftrightarrow HSO_3^-(aq) + H^+ (aq) \tag{R3}$$

Wang et al. studied kinetics of the "sulfur dioxide-water" reaction using the radioactive tracer technique and reported a rate constant of $0.57 \times 10^7 \ s^{-1}$ [13]. This reaction is very fast and should be considered as an equilibrium reaction [23], which makes this subsystem very fast as compared to Subsystem I.

SO_3 exists in the form of H_2SO_4 in the flue gas at the temperature range of interest [14]. It is extremely soluble in water and is assumed to be removed in the first stage of the column. In the literature, it is well accepted that SO_3 does not react with any of the other species hence it is not considered as a variable in any model. [15]

4.3.3   Interaction of SO- and NO- containing species in the liquid phase

$$NO_2^- + HSO_3^- \xrightarrow{\ 1\ } HADS$$
$$\downarrow 2$$
$$HSO_4^- + N_2O$$
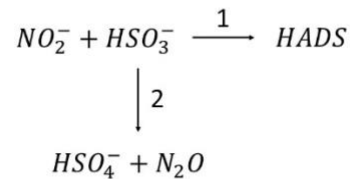
Figure 4.4 Reduced liquid phase mechanism presented by Susianto et al.[17]

In accordance with Susianto et al[17]. , the interaction between HNO_2 and HSO_3^-can be presented by two parallel reactions,

HNO_2 (aq) + HSO_3^- (aq) → HSO_4^-(aq) + ½ N_2O(g) + 0.5 H_2O(aq)   (R4)

HNO_2 (aq) + $2HSO_3^-$(aq) → HADS(aq) + H_2O(aq)   (R5)

where HADS is hydroxylamine disulfonic acid. The slow reaction of the further transformation of HADS is neglected. Based on analysis from Chang et al.[18] and Susianto et al. formulated three major findings:

1) Between pH 1 and 4, both reactions take place simultaneously: production of nitrous oxide along with sulfuric acid, production of HADS. Trends in N_2O production and HADS hydrolysis run contrary to the trend in the pH: they decrease as pH increases.

2) At room temperature (25 °C), when the pH is very low (pH<1), the reaction between nitrite and sulfite ions is fast, and nitrite ions are converted to nitrous oxide and sulfuric acid [18].

3) When the pH is close to 4, nitrite ions can be completely converted into HADS and no N_2O is produced [19].

To validate the work by Susianto et al. at conditions suitable for oxy-combustion flue gas environment, additional experiments at a temperature of 25 ºC and pH of 4, were performed [19]. It was shown that the apparent kinetic orders and dependencies of the two reactions are the same, however, the stoichiometry is different. Decomposition of HADS is negligible, and only two reactions R4 and R5 are considered to be significant for these interactions. This result is another foundation of our kinetic model.

Finally, our whole mechanism, which consists of 5 steps for the pH range of 3 to 4 is presented in Table 4.1. This mechanism and model meet the requirements of optimal complexity described in Section 1 - all steps have physical meaning, all variables that are included in the kinetic model can

be related to experimentally measured concentrations, and the mechanism consists only of steps significant to the overall process.

Table 4.1 Reactions Mechanism and Kinetics

	Reaction	Rate (M/s)	Reference
1	$2NO + O_2 \rightarrow 2NO_2$	$1.2 \times 10^3 \exp\left(\frac{530}{T}\right)[NO]^2[O_2]$	[11]
2	$2NO_2 + H_2O \rightarrow HNO_2 + HNO_3$	$10^8[NO_2]^2$	[16, 20]
3	$SO_2 + H_2O \leftrightarrow HSO_3^- + H^+$	$0.57 \times 10^7([SO_2] - \frac{[HSO_3^-][H^+]}{K_{eq}})$	[17, 21, 23][a]
4	$HNO_2 + HSO_3^- \rightarrow HSO_4^- + \frac{1}{2} N_2O + 0.5 H_2O$	$0.223[HSO_3^-][HNO_2^-]$	[18][b]
5	$HNO_2 + 2HSO_3^- \rightarrow HADS + H_2O$	$3.7 \times 10^8[HSO_3^-][HNO_2^-] \exp\left(-\frac{6100}{T}\right)$	[22][b]

[a]The value of K_{eq} is taken from Eigen et al. [23]

[b]Rate of reactions have been modified considering concentrations of H^+ as parameter for pH 4.

4.4 Kinetic Modeling

In this chapter, the results of two modelling approaches are presented: 1) an analytical analysis yielding equations related to sub-models, which correspond to separate 'blocks', and 2) a numerical analysis related to the kinetic model for the entire complex system.

4.4.1 Kinetic Model: Analytical results

Table 4.2 Variable, Parameters and Rate of reactions used in analysis

Variables	Parameters	Rate of Reaction

$x_1 = [NO]$	$K_1 = k_1[O_2]$	$r_1 = K_1 x_1^2$
$x_2 = [NO_2]$	$K_2 = k_2[H_2O]$	$r_2 = K_2 x_2^2$
$x_3 = [HNO_2]$	$K_3^+ = k_3^+[H_2O]$	$r_3 = K_3^+ y_1 - K_3^- y_2 y_3$
$x_4 = [HNO_3]$	$K_3^- = k_3^-$	$r_4 = K_4 x_3 y_2$
$y_1 = [SO_2]$	$K_4 = k_4$	$r_5 = K_5 x_3 y_2$
$y_2 = [HSO_3^-]$	$K_5 = k_5$	
$y_3 = [H^+]$		

5   *Concentrations of oxygen and water are considered constant

This section presents the mathematical framework and results without detailed derivation of expression and analysis.

Subsystem I

Subsystem I consider the gas-phase NOx reactions, its dissolution and subsequent reaction with water, as a separate system. It is assumed that this system contains solely irreversible reactions as shown below.

2NO + O₂ → 2NO₂

2NO₂ + H₂O (l) → HNO₂ + HNO₃
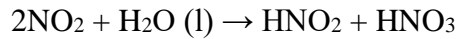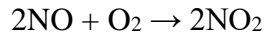
The parameter $u = \sqrt{4K_2/K_1 + 1}$ is introduced into the set of ordinary differential equations (ODEs) that describe the kinetics,

$$\frac{dx_1}{dt} = -2K_1 x_1^2 \tag{1}$$

$$\frac{dx_2}{dt} = 2K_1\left(x_1^2 - \frac{u^2 - 1}{4}x_2^2\right) \tag{2}$$

$$\frac{dx_3}{dt} = \frac{dx_4}{dt} = \frac{u^2 - 1}{4}x_2^2 \tag{3}$$

This set of ODEs (1), (2), (3), along with a mass conservation law $x_1(t) + x_2(t) + x_3(t) + x_4(t) = x_1(0) + x_2(0) + x_3(0) + x_4(0) = x_0$ describe a solvable initial value problem. The solutions are the analytic expressions of the concentrations, where the new variable $\tau = 2x_1(0)K_1 t + 1$,

$$x_1(t) = \frac{x_1(0)}{2x_1(0)K_1 t + 1} \tag{4}$$

$$x_2(t) = \frac{2x_1(0)([2x_1(0) + x_2(0)(u+1)]\tau^u - [2x_1(0) - x_2(0)(u-1)])}{\tau([2x_1(0) + x_2(0)(u+1)](u-1)\tau^u + [2x_1(0) - x_2(0)(u-1)](u+1))} \tag{5}$$

$$x_3(t) = x_3(0) + \frac{x_1(0)^2 K_1 t}{2x_1(0)K_1 t + 1} + \frac{x_2(0) - x_2(t)}{2} \tag{6}$$

$$x_4(t) = x_4(0) + \frac{x_1(0)^2 K_1 t}{2x_1(0)K_1 t + 1} + \frac{x_2(0) - x_2(t)}{2} \tag{7}$$

This expression can be modified taking into account that R1 is slow and R2 is very fast. We can assume that NO2 (x_2) is characterized by quasi-steady-state behavior. Therefore, one can obtain,

$$\dot{x}_2 \approx 0 \Rightarrow r_2 = r_1, \tag{8}$$

$$x_2 = x_1\sqrt{\frac{K_1}{K_2}} \tag{9}$$

x_1, x_2 and x_4 do not depend on the other variables, and their explicit expressions are the same as expressions obtained in the previous analysis of Subsystem I, see equations (4), (6) and (7).

Subsystem II

Subsystem II considers the gas-phase SOx reactions, its dissolution and subsequent reaction with water, as another separate system. The kinetics of this reaction is described analytically for the reversible case.

$SO_2 + H_2O \leftrightarrow HSO_3^- + H^+$

The corresponding set of ODEs is,

$$\frac{dy_1}{dt} = -K_3^+ y_1 + K_3^- y_2 y_3 \tag{10}$$

$$\frac{dy_2}{dt} = \frac{dy_3}{dt} = K_3^+ y_1 - K_3^- y_2 y_3 \tag{11}$$

This set of ODEs along with the mass conservation laws $2y_1(t) + y_2(t) + y_3(t) = 2y_1(0) + y_2(0) + y_3(0) = 2y_0$ form an initial value problem. If, furthermore, $y_2(0) = y_3(0) = 0$ then the initial value problem has the following solutions,

$$y_1(t) = \frac{y_0\big((v+1)\exp(-K_3^+ vt) + (v-1)\big)}{(v+1) + (v-1)\exp(-K_3^+ vt)} \tag{12}$$

$$y_2(t) = y_3(t) = \frac{2y_0\big(1 - \exp(-K_3^+ vt)\big)}{(v+1) + (v-1)\exp(-K_3^+ vt)} \tag{13}$$

$$v = \sqrt{4K_{3,eq}^{-1} y_{1,0} + 1} \tag{14}$$

Subsystem III

Finally, Subsystem III considers the interactions between SO- and NO- containing species in the aqueous solution. Under the assumption that Subsystem I and II reached their conclusion or equilibrium, this third set of reactions can be analyzed independently.

$HNO_2 + HSO_3^- \rightarrow HSO_4^- + \frac{1}{2} N_2O + 0.5 H_2O$

$HNO_2 + 2HSO_3^- \rightarrow HADS + H_2O$
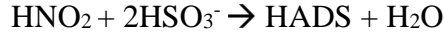
The concentrations in Subsystem III will be marked with a hat so as to differentiate them from their counterparts in Subsystems I and II. The variables here are $\widehat{x_3} = [HNO_2]$ and $\widehat{y_2} = [HSO_3^-]$. The rates of the two reactions are given below.

$$r_4 = K_4 \widehat{x_3} \widehat{y_2} \tag{15}$$

$$r_5 = K_5 \widehat{x_3} \widehat{y_2} \tag{16}$$

The approach to analyzing this subsystem is to solve the following ODEs consecutively

$$\frac{d\widehat{x_3}}{d\widehat{y_2}} = \frac{r_4 + r_5}{r_4 + 2r_5} = \frac{K_4 + K_5}{K_4 + 2K_5} \tag{17}$$

$$\frac{d\widehat{y_2}}{dt} = -(r_4 + 2r_5) = -(K_4 + 2K_5)\widehat{x_3}(\widehat{y_2})\widehat{y_2} \tag{18}$$

The initial concentrations for this subsystem are taken from the previous two subsystems, i.e. $\widehat{x_3}(0) = x_3(\infty)$ and $\widehat{y_2}(0) = y_2(\infty)$. The final solutions of this system are given below,

$$\widehat{x_3}(t) = \frac{\Delta \widehat{x_3}(0)}{\widehat{x_3}(0) - \gamma \widehat{y_2}(0)\exp(-\Delta k_y t)} \tag{19}$$

$$\widehat{y_2}(t) = \frac{\Delta \widehat{y_2}(0)\exp(-\Delta k_y t)}{\widehat{x_3}(0) - \gamma \widehat{y_2}(0)\exp(-\Delta k_y t)} \tag{20}$$

where $k_x = K_4 + K_5$, $k_y = K_4 + 2K_5$, $\gamma = k_x/k_y$ and $\Delta = \widehat{x_3}(0) - \gamma \widehat{y_2}(0)$.

Combined model for the whole system

The full reaction system is presented in Table 1. The ODE and initial conditions are presented in Table 3. In the analysis of our whole system, we consider two physico-chemical assumptions, based on the preliminary information which is presented in the review of experiment and models,

1) Quasi-steady state regime for NO_2 (used previously in the analysis of Subsystem I).

Table 4.3 ODE and initial condition for the full system

Ordinary Differential Equation	Initial Condition
$\dot{x}_1 = -2r_1$ $\dot{x}_2 = 2(r_1 - r_2)$ $\dot{x}_3 = r_2 - r_4 - r_5$ $\dot{x}_4 = r_2$ $\dot{y}_1 = -r_3$ $\dot{y}_2 = r_3 - r_4 - 2r_5$ $\dot{y}_3 = r_3$	$x_1(0) = x_{1,0}$ $x_2(0) = 0$ $x_3(0) = 0$ $x_4(0) = 0$ $y_1(0) = y_{1,0}$ $y_2(0) = 0$ $y_3(0) = 0$

2) Equilibrium of SO_2 dissolution (Reaction 3), as the dissolution reaches equilibrium very fast.

$$\dot{x}_2 \approx 0 \Rightarrow r_2 = r_1 \tag{21}$$

$$r_3 \approx 0 \tag{22}$$

Under these assumptions the concentrations x_1, x_2 and x_4 are identical to the expressions obtained for the Subsystem I, Equations (4), (6) and (7). The concentrations of y_1 and y_3 are determined using the equilibrium concentrations of System II, Equations (12) and (13), as initial concentrations. The results are as follows,

$$y_1(0) = y_{1,eq} = y_{1,0} + \frac{K_{3,eq}}{2}\left(1 - \sqrt{4K_{3,eq}^{-1}y_{1,0} + 1}\right) \tag{23}$$

$$y_1(t) = \frac{K_{3,eq}^{-1}y_{1,0}y_2(t)}{1 + K_{3,eq}^{-1}y_{1,0}y_2(t)} \tag{24}$$

$$y_3(0) = y_{3,eq} = \frac{K_{3,eq}}{2}\left(\sqrt{4K_{3,eq}^{-1}y_{1,0} + 1} - 1\right) \tag{25}$$

$$y_3(t) = \frac{y_{1,0}}{1 + K_{3,eq}^{-1}y_{1,0}y_2(t)} \tag{26}$$

The remaining ordinary differential equations are,

$$\dot{x}_3 = r_1 - r_4 - r_5 \tag{27}$$

$$\dot{y}_2 = -r_4 - 2r_5 \tag{28}$$

With the adjusted initial conditions,

$$x_3(0) = 0 \tag{29}$$

$$y_2(0) = y_{2,eq} = y_{3,eq}, \tag{30}$$

defining $k_x = K_4 + K_5$ and $k_y = K_4 + 2K_5$, the rate r_1 is given explicitly using the analytic solution of x_1,

The solution of x_3 as a function of $y_2(t)$,

$$x_3(y_2) = \frac{k_x(2K_1x_{1,0}t + 1)(y_2 - y_{2,eq}) + k_y K_1 x_{1,0}^2 t}{k_y(2K_1x_{1,0}t + 1)} \tag{31}$$

The expression $y_2(t)$ is needed to determine the concentrations x_3, y_1 and y_3. The final step is to solve this last initial value problem,

$$\dot{y}_2 = -k_y x_3(y_2) y_2 \tag{32}$$

$$y_2(0) = y_{2,eq} \tag{33}$$

An explicit solution for this initial value problem is not presented. The solution includes an integral as shown below,

$$y_2(t) = \frac{y_{2,eq}(2K_1 x_{1,0}t + 1)^{\frac{k_y}{4K_1}} \exp\left(\left(k_x y_{2,eq} - \frac{k_y}{2} x_{1,0}\right)t\right)}{1 + \int_0^t k_x (2K_1 x_{1,0}\tau + 1)^{\frac{k_y}{4K_1}} \exp\left(\left(k_x y_{2,eq} - \frac{k_y}{2} x_{1,0}\right)\tau\right) d\tau} \tag{34}$$

4.4.2 Kinetic Model: Numerical Result and Comparison

The reactor is modelled as a two-phase batch reactor of constant volume. The liquid and gas phases are assumed to be perfectly mixed. Rigorously, the overall balance in the gas-phase is modelled as:

$$\frac{dC_{g,i}}{dt} = \sum v_{i,j} R_{g,j} - R_{mass\ transfer,i} \tag{35}$$

where $C_{g,i}$ is the concentration of species i in the gas phase at any given time t, $v_{i,j}$ is the stoichiometric coefficient of component i in the reaction j, $R_{g,j}$ is the rate of gas-phase reaction j, and $R_{mass\ transfer,i}$ is the rate of mass transfer. Consequently, the liquid phase overall balance is modelled as:

$$\frac{dC_{l,i}}{dt} = \sum v_{i,j} R_{l,j} - (R_{mass\ transfer,i}) V_{gas}/V_{liq} \tag{36}$$

where V_{gas} and V_{liq} are the volume of gas and liquid phases, respectively, which are assumed to be constant throughout the process. $R_{l,j}$ is the rate of liquid-phase reaction j. In this modelling, the

value of the mass transfer coefficient is considered high enough to make the system limited by chemical kinetics, not mass-transfer.

Table 4.4 Input variable for the model.

Temperature	25 ^{0}C
Pressure	15 bar
SO$_2$ Concentration	900 ppm (v)
NO$_2$ Concentration	200 ppm (v)
NO Concentration	700 ppm (v)
O$_2$ Concentration	3%
L/G ratio (mass/mass)	1.5

In our numerical analysis, we analyzed the kinetic models both for independent subsystems and the whole system. The simplified kinetic model presented in Table 4.1 was used for numerical simulation and the initial input variables for the model are presented in Table 4.4. The values of different variables are considered typical for the pressurized oxy-combustion process. The L/G ratio is fixed based on the cooling water requirement for the latent heat removal in the pressurized oxy-combustion process [20]. Figure 4.5 compares the concentration profiles of species in gas and liquid phases for Subsystem I obtained from the analytical solution of Subsystem I with the numerical results for the whole system. Since NO$_2$ concentrations are quite small compared to NO and HNO$_2$ concentrations, they are presented separately for better understanding. The kinetic behavior of Subsystem I is driven by a combination of fast dissolution of NO$_2$ in water to form HNO$_2$ and slow oxidation of NO to NO$_2$. Because of the two competing reactions – NO$_2$ formation and consumption – it goes through a small maximum. Subsequently, NO$_2$ can be considered as

72

being in quasi-steady state regarding NO because of the fast Reaction 2, and the concentration of

NO_2 can be represented by, $[NO_2] = [NO]\sqrt{\frac{K_1}{K_2}}$. For NO and NO_2 the analytical solutions of

Subsystem I are exactly comparable to their numerical solution of the whole system. The temporal

domain in which the solution for HNO_2 in Subsystem I is valid is less than 2 seconds.
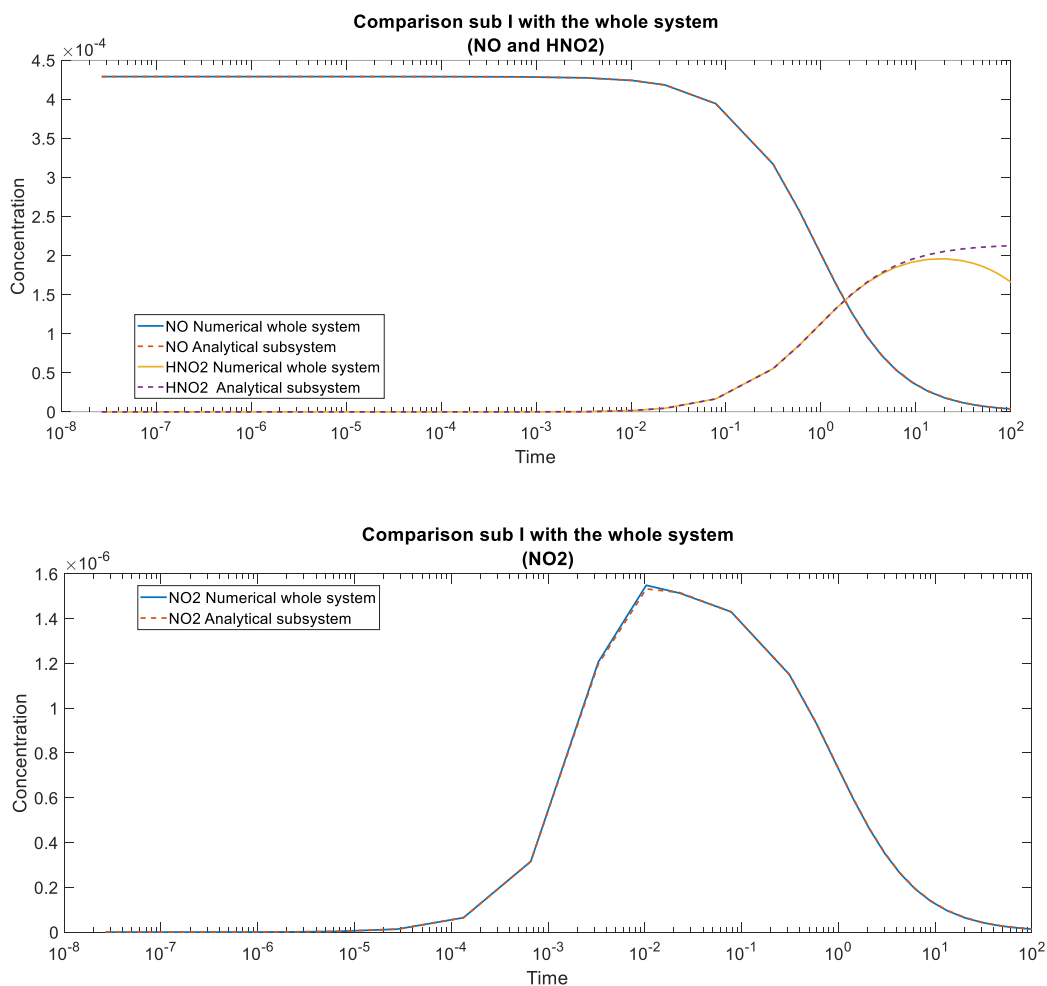
Figure 4.5 Concentration profile comparison for Subsystem I with the numerical solution for the whole system. (a) Concentration profile for NO and HNO_2, (b) Concentration profile for NO_2.

In this calculation, the initial NO_x-mixture contains only NO. If the mixture contained both NO and NO_2, a temporal dependence will not be characterized by a maximum. For the numerical solution of the whole system, the HNO_2 concentration is a result of the two consecutive reactions, the formation of HNO_2 from NO oxidation and the reaction of HNO_2 with HSO_3^-. The presence of a maximum in HNO_2 explains this phenomenon of consecutive reactions.
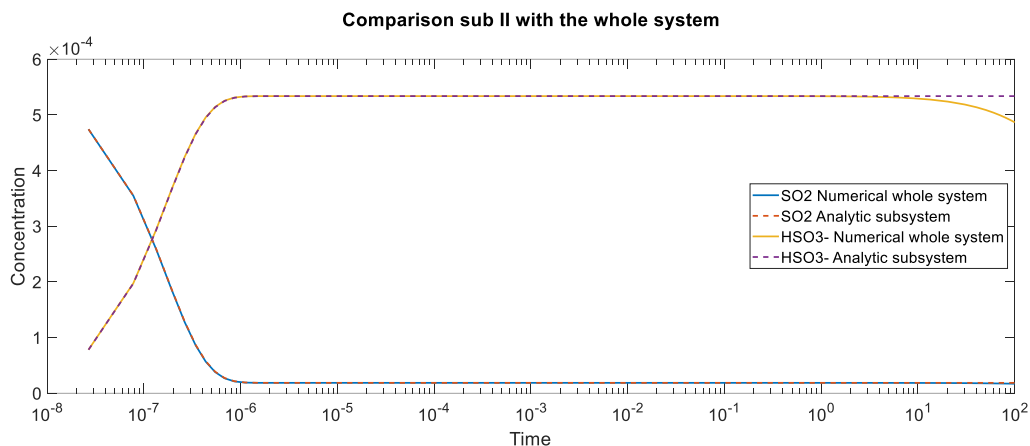
Figure 4.6 Concentration profile comparison for Subsystem II with the numerical solution for the whole system.

Subsystem II (Figure 4.6), the SO_2 dissolution system, reaches equilibrium very quickly. There are no gas side reactions to have an impact on the subsequent reaction of HSO_3^-. For the whole system, SO_2 quickly dissolves to form HSO_3^-, which then reacts in the liquid phase. This system remains in equilibrium between HSO_3^- and SO_2. The validity of the analytical solution of Subsystem II exists up until 10 seconds, before the consumption of HSO_3^- in Subsystem III becomes significant.
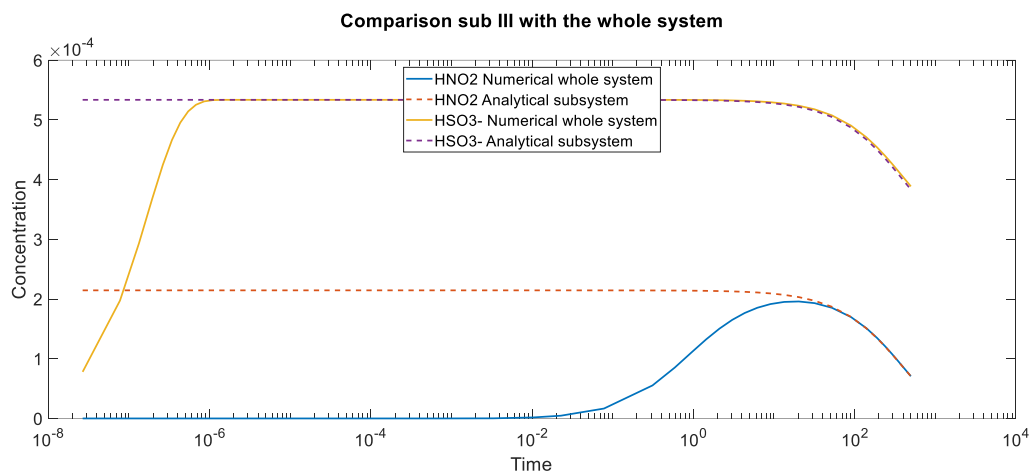
Figure 4.7 Concentration profile comparison for Subsystem III with the numerical solution for the whole system.

Subsystem III is presented in Figure 4.7, which presents the liquid phase reactions between HNO_2 and HSO_3^- if they start from the given initial concentrations. The results are consistent with the experimental fact [19] that rate dependencies for the two reactions have the same kinetic order, but different stoichiometry. For Subsystem III, its validity compared to the whole system exists after approximately 50 seconds.

4.5 Discussions and Conclusions

Based on the experimental facts and mathematical analysis we built a model of optimal complexity in terms of only measured species. The kinetic model of the whole system consists of three subsystems i.e. NOx gas-liquid reactions, SO_x gas-liquid and the liquid phase interactions between SO- and NO-containing species. The NO oxidation to NO_2 can be considered as a limiting process which determines the removal of NOx from the flue gas. The gas-phase oxidation of NO to NO_2 is very slow in comparison with the dissolution of NO_2. Typically, under these conditions, the

75

concentration of NO_2 can be considered as quasi-steady state species. In this situation, the concentration of NO, NO_2 and HNO_3 can be calculated using only Subsystem I (NO-subsystem). Therefore, these concentrations are "uncoupled variables". Only the concentration of HNO_2 is a "coupled variable," relating to the kinetic behavior of the whole system. Also, it is negligible in comparison with the concentration of NO, and the production of HNO_2 and HNO_3 can be treated as the direct process of NO oxidation. SO_2 dissolution (Subsystem II) is very fast in comparison with other reactions achieving equilibrium in almost 1 sec at the given temperature. This reaction can be treated separately from other 'blocks'. So, the initial concentration of HSO_3^- for the whole system can be defined through equilibrium, related to the initial concentration of SO_2. The concentration of HSO_3^- is then governed by the slow Subsystem III reaction of NO- and SO-containing substances. Interaction between NO and SO containing substances in the liquid phase can be described by two reactions with the same apparent kinetic orders, but different stoichiometries.

Finally, the obtained reduced mechanism consists of only 5 reactions – in comparison with the 7-step Ajdari's mechanism. All NO_x- SO_x interactions can be essentially grasped by a sequence of 4 irreversible reactions and the fast reversible 'SO_2-water' equilibrium. NO (Subsystem I) and SO_2 (Subsystem II) decrease during the reaction. NO_2 and HNO_2 (Subsystem I and III) and HSO_3^- (Subsystem II and III) go through a maximum, as illustrated in the results. While the model is grounded in data obtained in the domain of pH 4–5, the advantage of the model of optimal complexity is reflected in the conclusions presented above, which were deduced based on its analysis. Notably, the model is able to explain important physico-chemical changes of the system

in terms of only measurable species. Additionally, the model makes it easier to obtain an analytical solution of some subsystems.

4.6 References

[1]   IEA, *World Energy Outlook 2015*. 2015.

[2]   B. J. P. Buhre, L. K. Elliott, C. D. Sheng, R. P. Gupta, and T. F. Wall, "Oxy-fuel combustion technology for coal-fired power generation," *Prog. Energy Combust. Sci.*, vol. 31, no. 4, pp. 283–307, 2005.

[3]   R. Soundararajan and T. Gundersen, "Coal based power plants using oxy-combustion for CO2capture: Pressurized coal combustion to reduce capture penalty," *Appl. Therm. Eng.*, vol. 61, no. 1, pp. 115–122, 2013.

[4]   Y. S. Jun, D. E. Giammar, and C. J. Werth, "Impacts of geochemical reactions on geologic carbon sequestration," *Environ. Sci. Technol.*, vol. 47, no. 1, pp. 3–8, 2013.

[5]   L. Chen, S. Z. Yong, and A. F. Ghoniem, "Oxy-fuel combustion of pulverized coal: Characterization, fundamentals, stabilization and CFD modeling," *Prog. Energy Combust. Sci.*, vol. 38, no. 2, pp. 156–214, 2012.

[6]   G. Scheffknecht, L. Al-Makhadmeh, U. Schnell, and J. Maier, "Oxy-fuel coal combustion-A review of the current state-of-the-art," *Int. J. Greenh. Gas Control*, vol. 5, no. SUPPL. 1, pp. 16–35, 2011.

[7]   R. John and G. Gb, "(12) United States Patent FOREIGN PATENT DOCUMENTS CO at styled U . S . Patent," vol. 2, no. 12, 2008.

[8]   A. Gopan, B. M. Kumfer, J. Phillips, D. Thimsen, R. Smith, and R. L. Axelbaum, "Process design and performance analysis of a Staged, Pressurized Oxy-Combustion (SPOC) power plant for carbon capture," *Appl. Energy*, vol. 125, pp. 179–188, 2014.

[9]   F. Normann, E. Jansson, T. Petersson, and K. Andersson, "Nitrogen and sulphur chemistry in pressurised flue gas systems: A comparison of modelling and experiments," *Int. J. Greenh. Gas Control*, vol. 12, no. 2, pp. 26–34, 2013.

[10]   L. T. Murciano, V. White, F. Petrocelli, and D. Chadwick, "Sour compression process for the removal of SOx and NOx from oxyfuel-derived CO2," *Energy Procedia*, vol. 4, no. x, pp. 908–916, 2011.

[11]   H. Tsukahara, T. Ishida, and M. Mayumi, "Gas-phase oxidation of nitric oxide: Chemical kinetics and rate constant," *Nitric Oxide - Biol. Chem.*, vol. 3, no. 3, pp. 191–198, 1999.

[12]   Y. N. Lee and S. E. Schwartz, "Reaction kinetics of nitrogen dioxide with liquid water at low partial pressure," *J. Phys. Chem.*, vol. 85, no. 7, pp. 840–848, 1981.

[13]   A. Solution and R. Tracers, "Kinetic Study of Sulfur Dioxide in," no. 3, pp. 574–580, 1964.

[14]   E. Vainio, D. Fleig, A. Brink, K. Andersson, F. Johnsson, and M. Hupa, "Experimental Evaluation and Field Application of a Salt Method for SO $_3$ Measurement in Flue Gases," *Energy & Fuels*, vol. 27, no. 5, pp. 2767–2775, 2013.

[15]   S. Ajdari, F. Normann, K. Andersson, and F. Johnsson, "Reduced Mechanism for Nitrogen and Sulfur Chemistry in Pressurized Flue Gas Systems," *Ind. Eng. Chem. Res.*, vol. 55, no. 19, pp. 5514–5525, 2016.

[16]   M. S. Pétrissans and A. Zoulalian, "Influence of the pH on the Interactions between Nitrite and Sulfite Ions . Kinetic of the Reaction at pH 4 and 5," *Ind. Eng. Chem*, vol. 40, pp. 6068–6072, 2001.

[17]   M. Petrissans, A. Zoulalian, and H. Poincare, "Influence of the pH on the Interactions between Nitrite and Sulfite Ions . Kinetic of the Reaction at pH 4 and 5," pp. 6068–6072, 2001.

[18]   S. G. C. S.B. Oblath, S.S. Markowitz, T. Novakov, "KINETICS OF THE INITIAL REACTION OF NITRITE ION IN BISULFITE SOLUTIONS," 2011.

[19]   David Stokie, Piyush Verma "Reaction rate analysis of the liquid phase interaction between absorbed SOx and NOx in a pressurized oxy-combustion environment," *Ind. Eng. Chem. Res.(Submitted)*

[20]   A. Gopan, B. M. Kumfer, and R. L. Axelbaum, "Effect of operating pressure and fuel

moisture on net plant efficiency of a staged, pressurized oxy-combustion power plant,"
Int. J. Greenh. Gas Control, vol. 39, pp. 390–396, 2015.

[21]   N. M. C. J.L. Hudson, J. Erwin, "Kinetics of sulfur dioxide oxidation in aqueous
solution." p. 75, 1979.

[22]   S. B. Oblath, S. S. Markowitz, T. Novakov, and S. G. Chang, "Kinetics of the formation
of hydroxylamine disulfonate by reaction of nitrite with sulfites," *J. Phys. Chem.*, vol. 85,
no. 8, pp. 1017–1021, 1981.

Chapter 5. Pilot-scale testing of direct contact cooler for the removal of SOx and NOx from the flue gas of pressurized oxy-coal combustion and validation of the kinetic model.

5.1 Introduction

Pressurized oxy-fuel combustion of coal is a promising technology for carbon capture, utilization and sequestration (CCUS)[1], [2]. The primary motivation for pressurizing the combustion process is that it increases net plant efficiency, and by combusting fuel in oxygen, instead of air, the flue gas from the combustor is predominantly CO_2 and H_2O, leading to convenient separation of CO_2 for sequestration or use [3].   A second important advantage of the high-pressure flue gas is that it allows for a convenient co-removal of SO_x and NO_x. The CO_2 pipeline purity standards ($SO_x < 50$ ppm and $NO_x < 100$ ppm) for sequestration and/or enhanced oil recovery are stringent and hence an effective gas cleanup is required to achieve these standards [4], [5].

The concept of pressurized integrated pollution removal (P-IPR) for cost-effective and efficient scrubbing of SO_x and NO_x has been previously demonstrated for atmospheric oxy-combustion where the process requires flue gas compression [6]. White et al. [7] conducted experiments by initially cooling the atmospheric pressure flue gas to room temperature and condensing out the moisture, after which the flue gas was compressed and scrubbed, first at 15 bar, followed by further

compression and scrubbing at 30 bar. The results indicated 80% NO_x removal and 99% SO_x removal after the initial 15 bar scrubbing stage, with the remainder of NO_x removed in the 30-bar column. Shah et al. proposed a similar process, in which they compressed the flue gas between a pressure of 25 to 35 bar to remove more than 95% of both SO_x and NO_x [8]. While the process of integrated removal offers promise, a major challenge of this process for atmospheric pressure combustion is that the flue gas must be compressed before scrubbing. The presence of moist acid gases in the flue gas can lead to acid condensation and corrosion in the compressor (sour gas compression) if the flue gas moisture is not removed.

At atmospheric pressure, the rate of gas-phase oxidation of NO to NO_2 is limited by the low partial pressure of the reactants, restricting the use of co-removal technologies such as the DCC without employing additional catalyst or reagent. However, at elevated pressure, the partial pressures of NO and O_2 in the flue gas are high enough to oxidize a significant amount of NO to NO_2 in a reasonable residence time[9]. NO_2 has a significantly higher solubility than NO and dissolves into water to form HNO_2 and HNO_3. In the absence of NO_2, the absorption of SO_2 is limited by SO_2 water equilibrium, which, provided a limitation on the amount of water available to the absorption process, may not be enough to get the SO_2 concentration in the flue gas below the required concentration. However, NO_2, through the liquid phase reaction, can significantly shift the equilibrium by consuming the HSO_3^-, especially in acidic conditions[10]. Therefore, principally, reactive enhancement (RE) of SO_2 absorption in water occurs via the liquid phase reactions of HNO_2 – formed by the absorption of NO_2 in water – with HSO_3^- – formed by the absorption of SO_2.

Gopan et al. [2] proposed a reactive-absorption, counter-current, direct contact cooler (DCC) which uses cold water to scrub the SO_x and NO_x and act as the condenser for the flue gas moisture.

As shown in Figure 5.1, the moisture-laden flue gas, which is above the acid dew point temperature (> 200 °C), enters the column from the bottom and is cooled and scrubbed with water that enters from the top. The gas is cooled to around 55 °C, with a moisture content of < 1.5% v/v while the cooling water temperature increases from 42 °C to 165 °C. A critical objective of the process was to maximize the outlet temperature of the cooling water so that the heat integration has the highest exergy. Maximizing exergy enforces a major constraint on the DCC for the POC process, as compared to the atmospheric P-IPR process. The liquid to gas ratio, L/G, is limited to maximize the recoverable energy, which constricts the pH in the column (barring the use of an additional pH control). Depending on the moisture in the flue gas and the inlet water temperature, the L/G ratio can vary from 0.6 to 1.6 kg(l)/kg(g). Another unique aspect of this process is that the temperature of the cooling water increases significantly during the process, therefore an understanding of DCC scrubbing under variable high-temperature conditions is required.
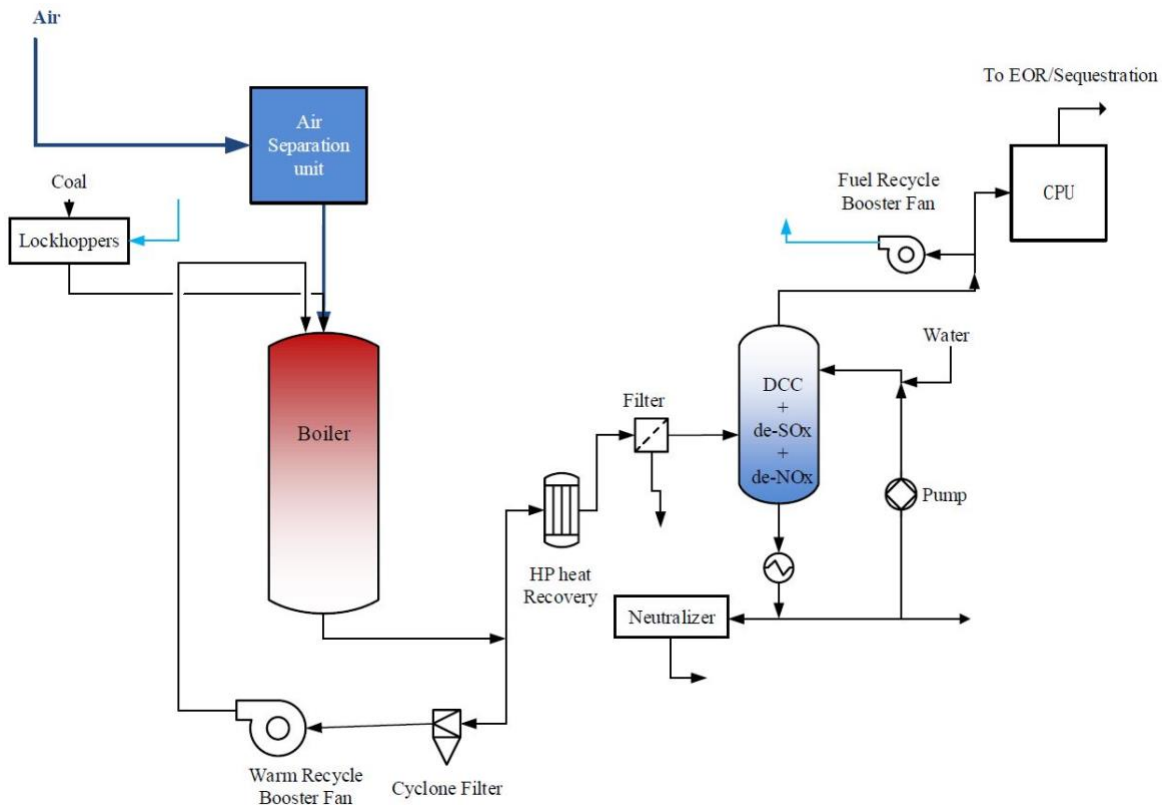
Figure 5.1. Schematic of a pressurized oxy-combustion process. The Direct Contact Cooler (DCC) is used to capture the latent heat of the moisture in the flue gas while simultaneously capturing SO_x and NO_x.

Since previous lab-scale studies have been conducted at close to room temperature and at high L/G ratios, there is a lack of experimental data available on high-temperature gas scrubbing. Thus, the focus of this chapter is to investigate the scrubbing efficiencies of SO_x and NO_x at conditions similar to the practical application of DCC in a POC process, as well as to identify and discuss the impact of sulfur to nitrogen ratio at different temperatures on the scrubbing efficiencies. With the growth of the oxy-combustion technologies, it is important to understand the role liquid phase reaction plays in SO_x removal under different conditions and the limiting parameters under these conditions. It is also important to validate the reaction kinetics to expand the understanding of functioning of the process. In this work, we analyze the impact of oxygen concentration, pressure (5 – 15 bar), temperature (22 – 215 ºC) L/G ratio (0.6 – 1.2) and SO_x/NO_x (0 – 1.15) ratio on the removal of SO_x and NO_x, with the objective to understand the RE of SO_2 absorption through the liquid phase reaction. A kinetic model developed in Aspen plus is validated against experimental results and is used to infer the influence of several operating parameters. The study also seeks to understand the interplay between the operating parameters, and how the process can be optimized in case of different process conditions. We believe that this work will advance the kinetic and operational understand of the DCC process, and will lead to the advancement of oxy-combustion technologies.

5.2 Reaction Chemistry

The reactions taking place in the DCC can be explained through four major physicochemical phenomena: 1) gas-phase NO reactions to produce water-soluble NO_x species, 2) dissolution of NO_x in water, 3) absorption of SO_2 and SO_3 in water and, 4) aqueous-phase reactions between oxides of sulfur and nitrogen-containing species. Figure 5.2 shows a simplification of the overall mechanism for the nitrogen and sulfur reactions and indicates the key gas-gas, gas-liquid and liquid-liquid reactions.
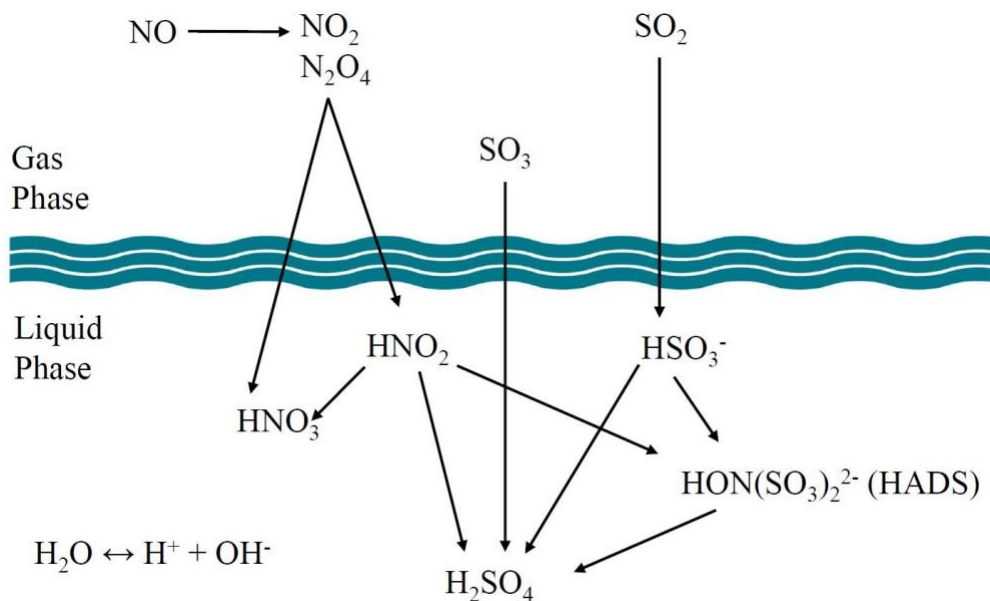
Figure 5.2 A simplified mechanism of NO_x and SO_x scrubbing [11].

Compared to liquid phase interaction between S and N containing species, the gas and interphase interactions are relatively well studied. Tsukahara et al. reviewed several studies on the gas-phase oxidation of NO to NO_2 and reported that NO oxidation is a third-order reaction, depending on NO and O_2 [12]. They also found that the kinetic constant for the reaction decreases slightly up to

a temperature of 500 °C and then increases at higher temperatures (k = $1200e^{\frac{530}{T}}\frac{L^2}{Mol^2.\,s}$). Since the DCC operates between gas temperatures of 20 to 200 °C, the dependency of the kinetic constant on temperature is significant to scrubbing NO.

NO$_2$ produced via

$$2NO(g) + O_2(g) \rightarrow 2NO_2(g) \tag{R1}$$

is readily absorbed in water to form HNO$_2$ and HNO$_3$ in a 1:1 ratio, according to Reaction 2.

$$2NO_2(g) + H_2O(aq) \rightarrow HNO_2(aq) + HNO_3(aq) \tag{R2}$$

This reaction has second-order kinetics with a rate constant of 10^8 M^{-1}s^{-1} at room temperature, when NO$_2$ reacts with liquid water at low partial pressure [13]. NO$_2$ can dimerize to form N$_2$O$_4$; however, the concentration of N$_2$O$_4$ has been reported to be low, with negligible impact on the kinetics of the scrubbing system [14].

Wang et al. used a radioactive tracer technique to study the kinetics of SO$_2$ absorption in water and reported a rate constant of 0.57×10^7 s^{-1} [15]. Due to this fast reaction rate,

$$SO_2(g) + H_2O(aq) \leftrightarrow HSO_3^-(aq) + H^+(aq) \tag{R3}$$

reaches equilibrium almost instantaneously, barring mass-transfer limitations.

Although experimental data on the liquid-phase chemistry is limited, several studies to model the scrubbing process have been conducted recently. Normann et al. [16] identified up to 33 individual gas and liquid reactions that may play a role in the gas, gas/liquid or liquid chemistry. The detailed mechanism is presented in Appendix A. They identified that a key role in the scrubbing chemistry is the complex interactions between HNO$_2$ and HSO$_3$, which are capable of enhancing the

oxidation rate to produce HNO₃ and H₂SO₄. They presented the Raschig mechanism to explain the interaction of HNO₂ and HSO₃⁻ in the liquid phase:

$$HNO_2(aq) + HSO_3^-(aq) \rightarrow NOSO_3^-(aq) + H_2O(aq) \tag{R4}$$

$$NOSO_3^-(aq) + H^+(+H_2O) \rightarrow HNO(aq) + H_2SO_4(aq) \tag{R5}$$

$$NOSO_3^-(aq) + HSO_3^-(aq) \rightarrow HNO(SO_3)_2^{2-}(aq) \tag{R6}$$

$$HNO(aq) + HNO(aq) \rightarrow N_2O(g) + H_2O(aq) \tag{R7}$$

$$HNO(SO_3)_2^{2-}(aq) + H^+(aq) \rightarrow HNOHSO_3^-(aq) + H^+(aq) + HSO_4^-(aq) \tag{R8}$$
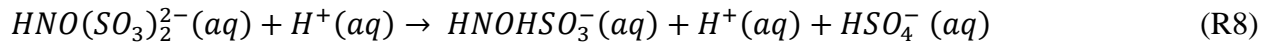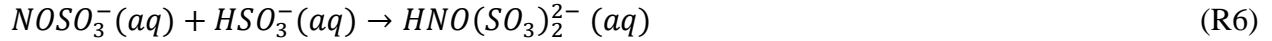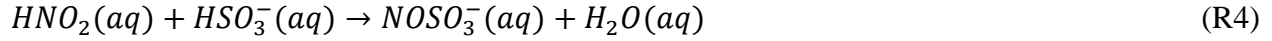
The model presented by Normann et al. is detailed but is also complicated by several intermediate species that are difficult to measure experimentally [16]. Importantly, this study concluded that further investigation into the interaction between the liquid ions, especially at pH less than 4, should be a priority.

Following a sensitivity analysis of the primary reactions, Ajdari et al. [14], [17] proposed a reduced mechanism of between 7 and 12 reactions based on the operational pH of the system, and concluded that the gas-phase reactions are limited by NO oxidation, whereas the liquid-phase interactions are predominantly pH controlled. They reduced the liquid-phase mechanism to two major reactions, Reaction 9 and 10, both of which are combinations of several unstable intermediaries to form a stable product. The reduced mechanism is presented in Appendix B. However, Ajdari et a. also recommended further investigation of the liquid-phase chemistry:

$$HNO_2 + HSO_3^- \rightarrow HSO_4^- + \frac{1}{2}N_2O + \frac{1}{2}H_2O \tag{R9}$$

$$HNO_2 + 2HSO_3^- \rightarrow HON(SO_3)_2^{2-}(HADS) + H_2O \quad . \tag{R10}$$
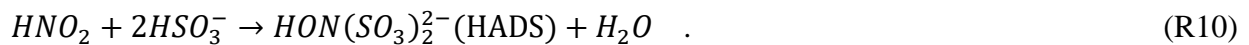
The reduced mechanism presented by Ajdari et al. is corroborated by the experimental work performed by Petrissans et al. [10] on liquid phase interaction between HSO_3^- and HNO_2 to ascertain the impact of pH on Reaction 9 and 10. They reported that Reaction 10 is the predominant reaction above the pH of 4 while Reaction 9 dominates below the pH of 2. Both the reactions take place between pH 2 and 4 to varying degrees.

Through an experimental and mathematical optimization of the model, Verma et al. [18] further reduced the mechanism to a total of 5 reactions (R1, R2, R3, R9, and R10) capable of characterizing the reaction system. They reported two main findings 1) the gaseous species such as N_2O_4 had a negligible impact on the kinetics, and 2) the dissociation of HNO_2 to HNO_3 and NO was not significant in DCC conditions. This mechanism is presented in Table 5.1 and used for modeling in this work.

Table 5.1 Reduced DCC Scrubbing Mechanism [18]

Reaction Number	Reaction	Type	Reference
R1	$2NO + O_2 \rightarrow 2NO_2$	Non-Equilibrium	[12]
R2	$2NO_2 + 2H_2O \leftrightarrow HNO_2 + NO_3^- + H_3O^+$	Equilibrium	Aspen
R3	$SO_2 + 2H_2O \leftrightarrow H_3O^+ + HSO_3^-$	Equilibrium	Aspen
R9	$HNO_2 + HSO_3^- \rightarrow \frac{1}{2}N_2O + HSO_4^- + \frac{1}{2}H_2O$	Non-Equilibrium	[19]
R10	$HNO_2 + 2HSO_3^- \rightarrow HADS + H_2O$	Non-Equilibrium	[14]

Several researchers have conducted lab-scale studies of the S-N reaction system at room temperature to understand the reaction mechanism and scrubbing efficiencies. Wall et al. [9] studied the oxidation of nitric oxide to nitrogen dioxide in the gas phase and its subsequent absorption in water in a bubble column from 1 to 30 bar pressure. They found that NO was readily

oxidized to water-soluble NO_2 at elevated pressures and that the process was kinetically controlled, according to Reaction 1. In a follow-up study, Wall et al. [20] introduced SO_2 in the gas phase and found that SO_2 caused a minor reduction in NO oxidation but did not have a significant effect on overall NO_x capture. Additionally, a reduction in residence time was found to reduce overall NO_x capture. Building on the study by Wall et al., White et al. [7] investigated the interdependence of NO_x and SO_x on the SO_x scrubbing efficiencies. They observed that NO_x reduction before scrubbing may be detrimental to the SO_x scrubbing potential. Although limited in scope, these lab-scale studies provide a relevant framework for the design and analysis of the study conducted in this work.

5.3 Material and Methodology

5.3.1. Experimental Methodology

Experiments were performed in the pilot-scale direct contact cooler (DCC) shown in Figures 5.3 and 5.4. The column was designed by Process Engineering Associates, LLC, with the vessel fabrication, piping and instrument assembly performed by Progressive Recovery, Inc. The DCC system was sized based on outlet conditions for a 100 kW_{th} pressurized oxy-combustion test furnace. It is a counter-current packed bed column with a 20.3 cm diameter and a 2.3 m packing height, consisting of 316 stainless steel saddle rings (Intalox) to create a high gas-liquid contact area, which enhances the absorption of gaseous pollutants in the liquid phase.

Synthetic flue gas was used for these experiments. Gas mixtures of SO_2 (3% SO_2/N_2 mix) and NO (10% NO/N_2 mix) (Praxair) were injected into the CO_2 line (Figure 3) which was heated with an electric in-line heater. To avoid oxidation of NO to NO_2 in the gas delivery system, oxygen was

added to the heated gas at the reactor inlet, so that the initial concentration of NO at the reactor inlet was well defined.

Temperature, pressure, flow rate and composition were varied to investigate their effect on NO_x and SO_2 scrubbing efficiency. The flue gas was fed at the bottom of the column while water was fed and distributed at the top. The water outlet from the experiment, which is acidic, was collected in the sump tank before leaving the column. The purified gas from the top of the column was analyzed using a PG-250 HORIBA gas analyzer.
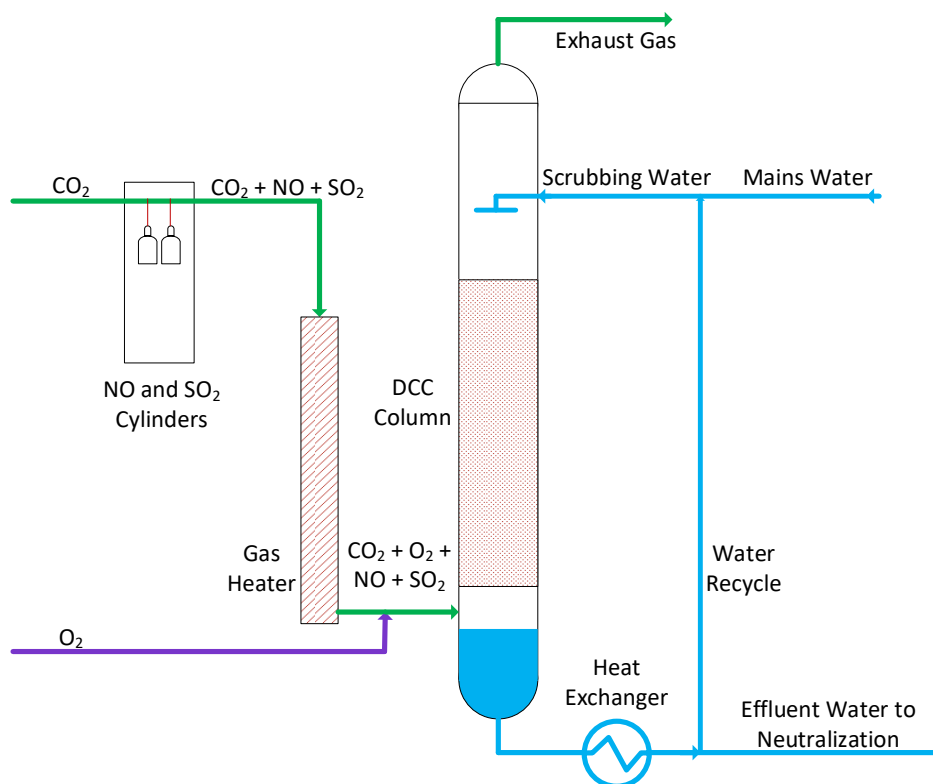
Figure 5.3. DCC Column Schematic.

In all experiments, fresh city water was supplied to the DCC with a pH ≈ 8. While the system is capable of water recycle to provide additional pH control, as shown in Figure 3, inlet pH was not a controlled parameter for the purposes of this study.
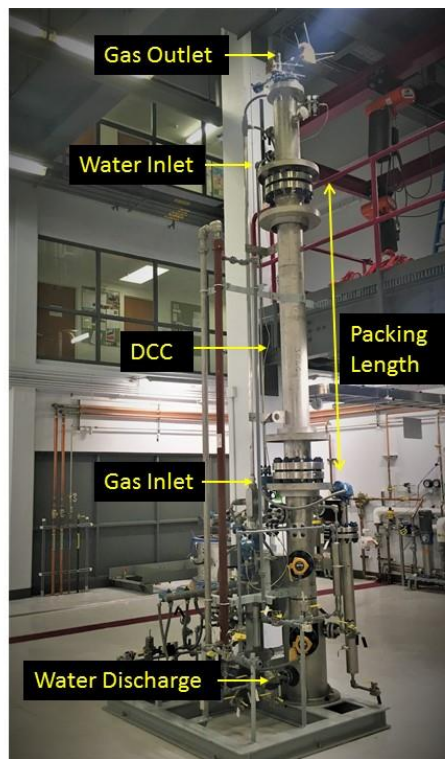
Figure 5.4 DCC scrubbing column in the pressurized oxy-combustion research facility at Washington University in St. Louis.

5.3.2 Modeling Methodology

The reactive absorption column was modeled using a rate-based formalism with a RadFrac unit in Aspen plus V9 with the dimensions and internals of the DCC column. Since the DCC experiments are constrained by reaction time, the rate-based model provides a framework to analyze the column with non-equilibrium reactions. The ionic interaction in the liquid phase requires the use of an electrolytic equation of state for the thermodynamic properties of the components. Hence,

ELECNRTL was used as the property method because of its compatibility with the system in both the liquid and gas phases. For the numerical calculations, the column was divided into ten stages with the gas being introduced into the column below the bottom-most stage and the water above the top stage. The analysis found no relevant increase in accuracy with more than 10 stages. For high-temperature gas and liquid interaction, the column was assumed to be adiabatic, with no heat loss to the surroundings. The process design of the model followed the same pattern as the experimental system, with the gas being mixed together and then heated in the gas heater before entering the column. The inlet parameters of the model were updated according to the experimental parameters for each analysis. The reactions used for the simulation are described in Table 1, with the reactions in equilibrium handled directly through Aspen. For the kinetic reactions, Reaction 1 was supplied through a kinetic sub-routine written separately, and kinetic parameters for Reactions 9 and 10 were provided in the form of power-law expressions in Aspen. Because of their comparatively fast reaction rates, Reactions 2 and 3 were treated as equilibrium reactions in Aspen.

5.4 Results and Discussion

For the base-case, a total gas flow rate of 800 SLPM at 15 bar and 22°C was used, which corresponds to a residence time of 130 seconds. The composition of the simulated dry flue gas is presented in Table 5.2. To be relevant to the Staged, Pressurized Oxy-Combustion (SPOC) process [2] an L/G of 0.95 ($kg_{(l)}/kg_{(g)}$) was maintained for the experiment. As pollutant concentrations are dependent on coal composition and burner design, 500 ppm for both NO and SO_2 were chosen, based on approximate pollutant concentrations typically encountered during oxy-combustion of low sulfur coals [7]. As will be presented in the subsequent sections, for this base-case scenario,

we find that the SO_2 scrubbing efficiency approached 100% and the NO scrubbing efficiency was just above 90% at steady state, which is a promising result for SO_x and NO_x removal.

Table 5.2. Base-Case Gas Inlet Composition

Species	*Volume*
O_2	3%
CO_2	95%
N_2	2%
SO_2	500 ppm
NO	500 ppm

5.4.1 Investigation of NO oxidation in the column

The oxidation of NO to NO_2 is a third-order gas-phase reaction, where the rate depends on the concentration of NO and O_2. In previous modelling studies, this reaction was found to be the slowest, however, this finding has not been demonstrated in a pilot-scale experimental system [14]. To ascertain the impact of NO oxidation on the scrubbing of NO_x, experiments were conducted at 13.5 bar(a) and the oxygen concentration in the synthetic flue gas was varied from 0 to 4 % v/v. The oxygen concentrations used for the experiments are consistent with those typically found in pulverized coal boiler flue gas. The operating conditions for this experiment are provided in Table 5.3. The measured instantaneous outlet concentration of NO as a function of the inlet oxygen concentration are shown in Figure 5.5. At steady state, the minimum outlet NO concentration was 55 ppm, which corresponds to a capture efficiency of 92%. Results indicate that NO to NO_2 conversion is very sensitive to oxygen partial pressure in the range of 0 to 0.15 bar, but approaches a constant value at higher oxygen levels. It is important to note that for a DCC operating at 15 bar, a partial pressure of 0.15 bar corresponds to excess oxygen of 1% in the flue gas. Therefore, a

reduction of excess oxygen in the flue gas from 3% to 1% would not have a significant impact on NO oxidation. However, it would lead to a significant reduction in energy consumption in the air separation unit of a POC power plant and the downstream Gas Purification Unit, and thus reduce the cost of electricity.

Assuming instantaneous NO_2 absorption into the liquid phase (relative to the formation of NO_2), a comparison can be made between the results of the NO oxidation model and the measured NO outlet concentrations. Based on the inlet oxygen concentration of the experiment, and the pressure and residence time of the gas in the column, the NO oxidation rate was calculated using Reaction 1 in Table 5.1. The results suggest that the scrubbing of NO_x can be very closely predicted by the rate of oxidation from the model. This result is corroborated by lab-scale studies by Wall et al. [9] predicting that NO oxidation is the controlling step in the scrubbing of NO_x from the flue gas at low temperature.
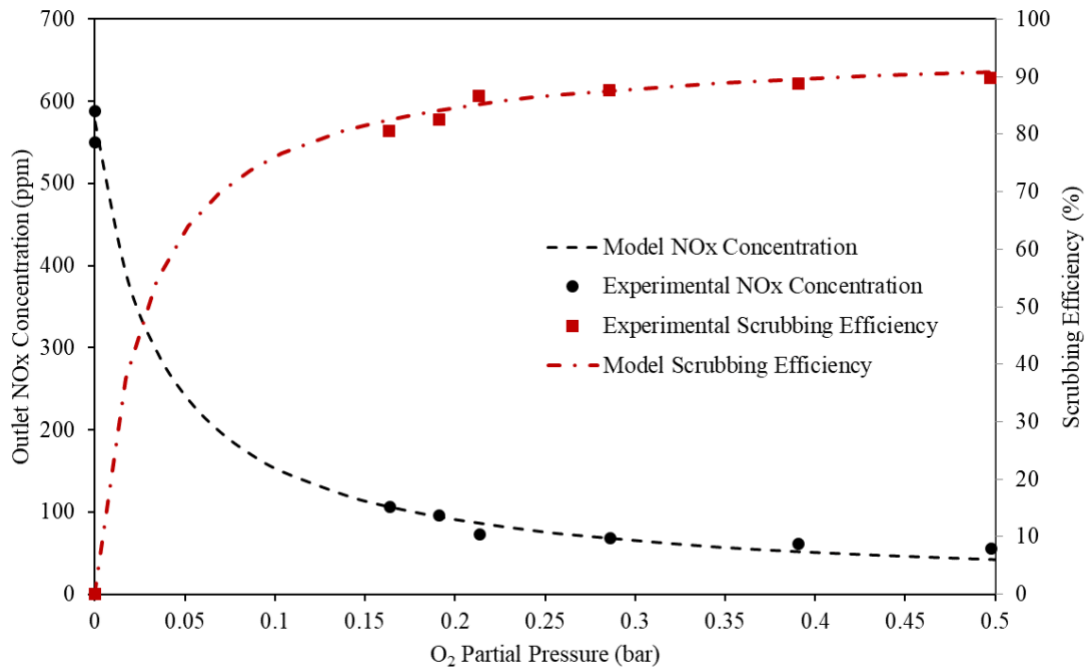
Figure 5.5. Change in NO_x outlet concentrations with oxygen partial pressure.

Table 5.3. Operating conditions corresponding to Figure 5.5.

Parameters	
Pressure	13.5 bar(a)
Temperature	24°C
Oxygen Concentration	0 – 4 % v/v
Gas Flowrate	777 SLPM
L/G Ratio	0.94 $kg_{(l)}/kg_{(g)}$
Gas Residence Time	120 seconds
NO Inlet Concentration	566 ppm
SO_2 Inlet Concentration	421 ppm

5.4.2 The influence of oxygen partial pressure on NO_x and SO_2 capture

As NO oxidation is shown to be the controlling step, the effects of total pressure, oxygen partial pressure, and residence time on NO and SO_2 scrubbing were experimentally investigated in more detail to determine optimal operating conditions. The range of operating conditions for this study is presented in Table 5.4. When varying the operating pressure, the mass flow rate of the gas was held constant. Figure 5.6 shows the change in NO capture as a function of O_2 partial pressure at four different pressures and was obtained by increasing the oxygen concentration from zero to the maximum and then decreasing back to zero to capture any hysteresis effect. Each data point was collected with a resolution of 1 second.

Figure 7 shows that the impact of pressure on NO scrubbing is enhanced for O_2 partial pressure below 0.25 bar, with the reduction in pressure from 15 bar (130 seconds residence time) to 11 bar (95 seconds) resulting in approximately 10% decrease in NO scrubbing efficiency. At higher O_2 partial pressures, the decrease in scrubbing efficiency with pressure is even less, and NO capture approaches 90% within the range of gas residence times. However, when pressure is further

reduced to 9 bar (residence time = 78 seconds), the NO scrubbing is more severely affected. From Figure 7, the results indicate that the minimum residence time for NO scrubbing in this system should be approximately 95 seconds. This also drives home a larger point that for a full-scale system, the extent of NO removal will be a combined function of residence time and oxygen concentration, varying non-linearly with different combinations of the two.

Throughout the experiments described above, a high SO_2 scrubbing efficiency in the range of 93 to 100 % was consistently observed. Importantly, a scrubbing efficiency of less than 100% was only observed in cases when the oxygen concentration in the column was effectively zero. The scrubbing of SO_2 is discussed in more detail in the following sections.
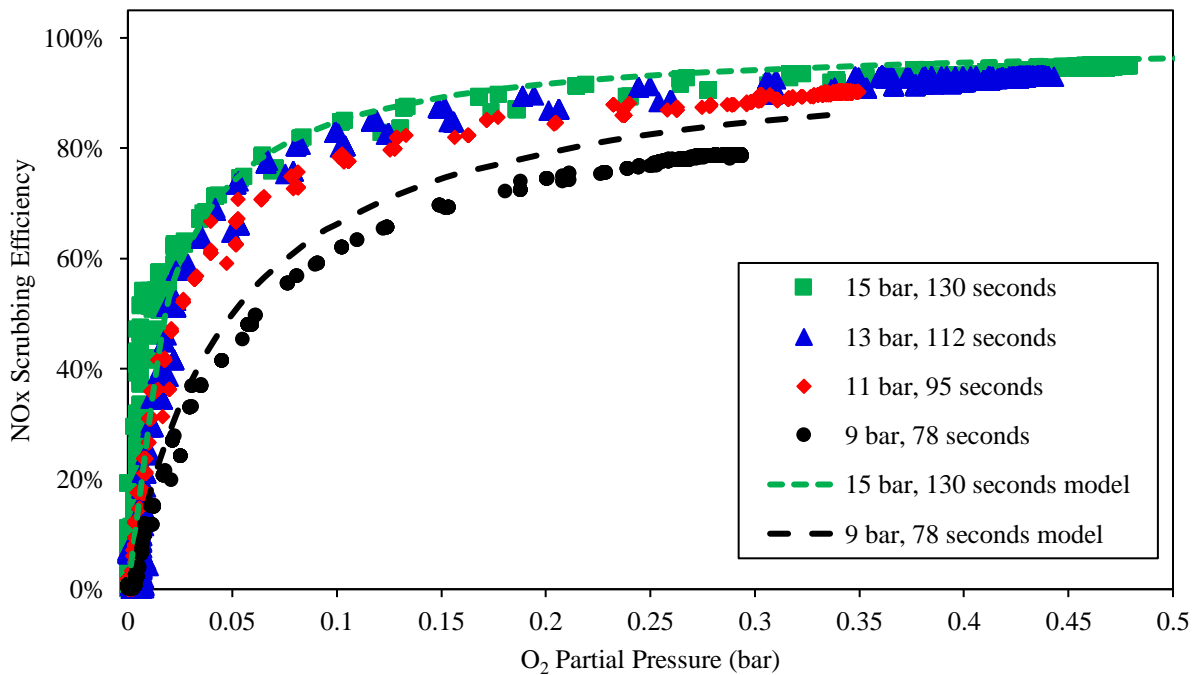
Figure 5.6 The effect of residence time and oxygen partial pressure on NO_x conversion.

Table 5.4 Operating conditions corresponding to Figure 5.6

Parameters

Pressure	9 -15 bar(a)
Temperature	23°C
Oxygen Concentration	0 – 3.1 %
Gas Flowrate	801 SLPM
L/G Ratio	0.97 $kg_{(l)}/kg_{(g)}$
Gas Residence Time	130 – 78 seconds
NO Inlet Concentration	530 ppm
SO_2 Inlet Concentration	530 ppm

5.4.3 Impact of pressure on NO and SO_2 removal

There were two main objectives while studying the impact of pressure on the removal of SO_x and NO_x: 1) To understand the absolute scrubbing efficiencies of SO_x and NO_x and 2) To contrast the impact of pressure with an increase in NO/SO_2 ratio. All the experiments were carried out with an oxygen concentration of 3% v/v and with a constant residence time and L/G ratio. The detailed parameters for these experiments can be found Table 5.5. The results presented in Fig. 5.7 suggest a significant impact of pressure on both NO and SO_2 scrubbing efficiency, with higher pressure resulting in higher scrubbing efficiencies. The decrease in NO scrubbing efficiency at lower pressures is the result of reduced partial pressure of NO and O_2 in the gas phase, leading to a lower reaction rate and consequently decreasing the conversion to NO_2 via Reaction 1. Moreover, the absolute scrubbing efficiency is close to 10% higher for an inlet NO concentration of 535 ppm compared to the inlet NO concentration of 263 ppm at all pressures. This is mainly because for a constant residence time, the initial reaction rate for NO is higher when the concentration is high, resulting in an outlet concentration that is not significantly different (72 ppm and 61 ppm at 15 bar), however has a much higher scrubbing efficiency since the base value is different. This has an important implication for designing the DCC, mainly since the pipeline guidelines are based on

96

absolute concentrations, a higher inlet NO concentration may not require longer residence time to stay within limits, however, it would result in significantly high liquid phase concentrations of HNO_2 and consequently higher SO_2 removal.

The absorption of SO_2 also increases with increase in pressure both because of higher direct absorption and more RE, via the liquid phase interaction with HNO_2. It remains above 90% for 10 and 15 bar at the NO/SO_2 of both 0.57 and 1.15. At 5 bar, there is a significant decrease in SO_2 scrubbing efficiency, especially at the NO/SO_2 ratio of 0.57 (Fig. 5.7 (a)), where the scrubbing efficiency drops to 71% compared to 87% for the NO/SO_2 ratio of 1.15(Fig. 5.7 (b)). This is mainly because at 5 bar, the amount of NO converted to NO_2 is low when the inlet concentration of NO is lower. This results in lower HNO_2 concentration in the liquid phase which results in a lower rate of liquid phase reaction between HNO_2 and HSO_3^-, resulting in lower scrubbing of SO_2. It is important to note that the reduction in SO_2 absorption because of reduced pressure can be compensated with higher NO concentration at the inlet. A tradeoff between the NO/SO_2 ratio and the operating pressure exists depending on the type of fuel.

Table 5.5 Experimental parameters for Figure 5.7

Parameter	Value
Temperature	22°C
Pressure	5 bar; 10 bar; 15 bar
SO_2 concentration	465 ppm
NO concentration	263 ppm (NO/SO_2 = 0.57); 535 ppm (NO/SO_2 = 1.15)
CO_2 concentration	96% (v/v)
O_2 concentration	3% (v/v)
L/G ratio (mass/mass)	0.86
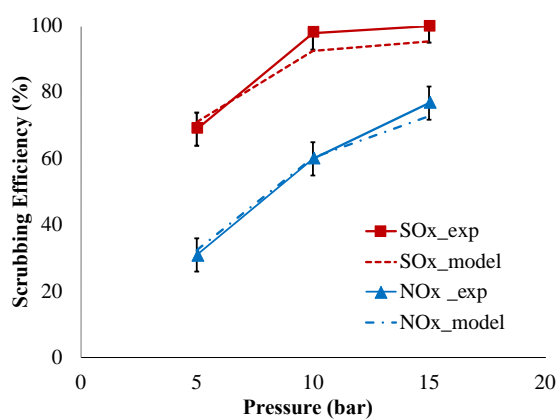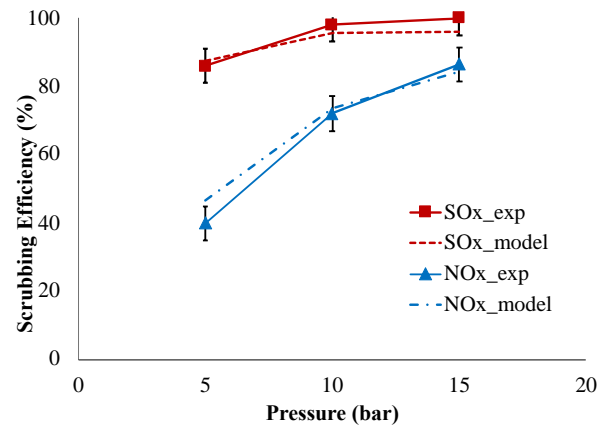
(a) NO/SO$_2$ = 0.57   (b) NO/SO$_2$ = 1.15

Figure 5.7 Impact of pressure on SO$_2$ and NO scrubbing efficiency at different NO/SO$_2$ ratio.

5.4.5 Impact of inlet gas temperature and NO/SO$_2$ ratio

The inlet temperature of the flue gas going to the DCC is determined by the acid dew point temperature in a POC power plant. A higher SO$_3$ content in the flue gas can result in the flue gas entering the DCC at higher temperature, therefore it is important to understand the impact on temperature on the RE and the overall scrubbing of SO$_2$ and NO. The experiments were carried out at 10 bar and 3% v/v inlet O$_2$ concentration. The concentration of SO$_2$ was kept constant at 465 ppm and the NO concentration was varied to understand the impact of NO/SO$_2$ ratio. A detailed set of parameters is presented in Table 5.6. At first, the NO concentration entering in the column was kept zero, which signifies that the removal of SO$_2$ is only due to the absorption in the column. The concentration of NO is then increased at the ratios of NO/SO$_2$=0.57 and 1.15. The same experiments are performed at three different temperatures of 22 ℃, 113 ℃, and 215 ℃, to study temperature impact. The presence of NO in the flue gas enhances the removal of SO as per

reactions R4 and R5. The measure of this impact was studied at varying temperature and different NO concentrations.

Table 5.6 Experimental parameters for Figure 5.8

Parameter	Value
Temperature	24˚C; 115˚C; 213˚C
Pressure	10 bar
SO_2 concentration	465 ppm
NO concentration	263 ppm for $NO/SO_2 = 0.57$ 535 ppm for $NO/SO_2 = 1.15$
CO_2 concentration	96% (v/v)
O_2 concentration	~3% (v/v)
Water flow rate	0.26 ± 0.01 gpm
L/G ratio (mass/mass)	0.86

Figure 5.8 (a) shows the increase in scrubbing efficiencies with the increase in NO inlet concentration in the inlet flue gas (or NO/SO_2 ratio). As mentioned earlier, it was assumed that, Overall SO_x removal is just the summation of removal due to absorption plus the removal due to reaction enhancement (RE). At any constant temperature, the share of SO_x removal due to absorption remains constant, however with the NO increase, reaction enhancement share goes up. This is mainly because, with the increase in the NO inlet concentration there is higher NO_x oxidation in the column for the same gas residence time. This results in a higher concentration of HNO_2 in the liquid phase, which increase the rate of reaction R9 and R10, and consequently higher consumption of HSO_3^- ion. This causes the equilibrium of R3 to shift in forward direction leading to more removal of SO_x. This is mainly why a higher NO inlet concentration is preferred for systems with higher SO_2 concentration. Impact of temperature on overall SO_2 removal along with the impact on individual contributing factors is presented in Fig. 5.8 (b), which shows the decrease in scrubbing efficiency of SO_2 with increase in temperature at any constant NO/SO_2 ratio. As the

99

temperature increases from 22˚C to 215˚C, the removal due to absorption decreases, however the reaction enhancement is seen to increase. The overall removal of SO_2 decreases as the increase due to liquid phase reactions is not sufficient enough to counter the decrease due to direct absorption. At higher temperature, R9 and R10 have higher reaction rates causing more removal due to liquid phase reactions.

(a) Constant T = 215 ºC   (a) Constant NO/SO_2 = 1.15
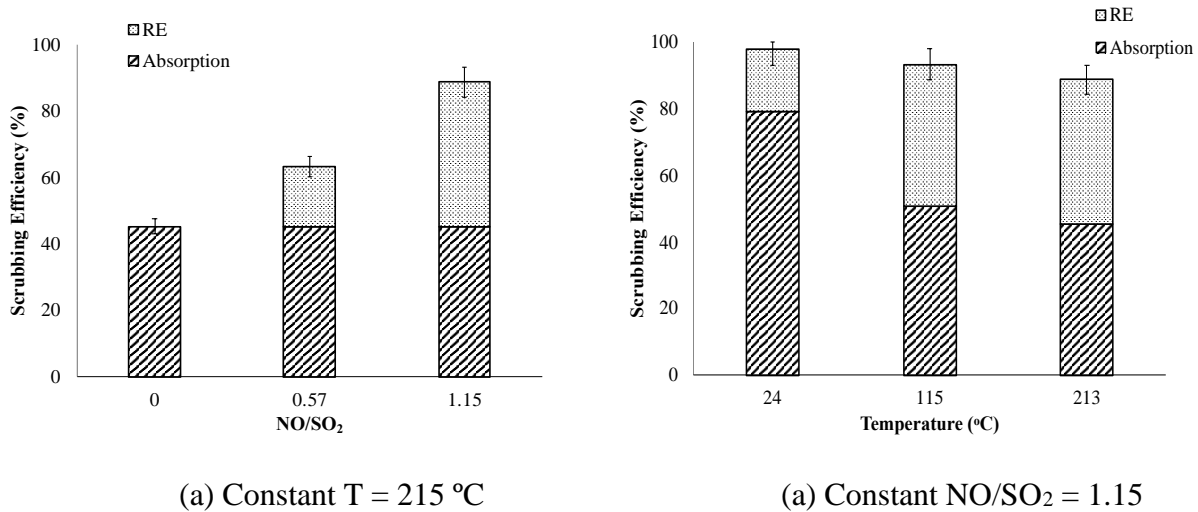
Figure 5.8 SO_2 removal with varying temperature and NO/SO_2 ratio

5.4.6 Impact of L/G ratio on NO and SO₂ scrubbing efficiency

The amount of water required to recover the latent heat from POC flue gas with minimum exergy loss depends upon the inlet temperature of the flue gas and its moisture content. Depending on the moisture in the coal and the type of recycle, the range of required L/G ratio can vary significantly. Therefore, in the following set of experiments L/G ratio was varied between 0.6 – 1.17 kg(l)/kg(g), to understand its impact of on the scrubbing efficiency of SO_x and NO_x. Apart from the cooling water flow rate, all other inlet parameters were kept constant. The gas inlet temperature was maintained at 215 ˚C. Each set of experiments were first run without NO in the flue gas to collect

the SO₂ absorption data, followed the introduction of NO to understand the impact of NO on SO₂

absorption. The condition used in the experiments are presented in Table 5.7.

Table 5.7 Experimental parameters for impact of L/G ratio

Parameter	Value
Temperature	215°C
Pressure	10 bar
SO_2 concentration	465 ppm
NO concentration	535 ppm
CO_2 concentration	96% (v/v)
O_2 concentration	~3% (v/v)
L/G ratio (mass/mass)	0.6; 0.73; 0.86; 1.17 kg(l)/kg(g)

(a)   (b)
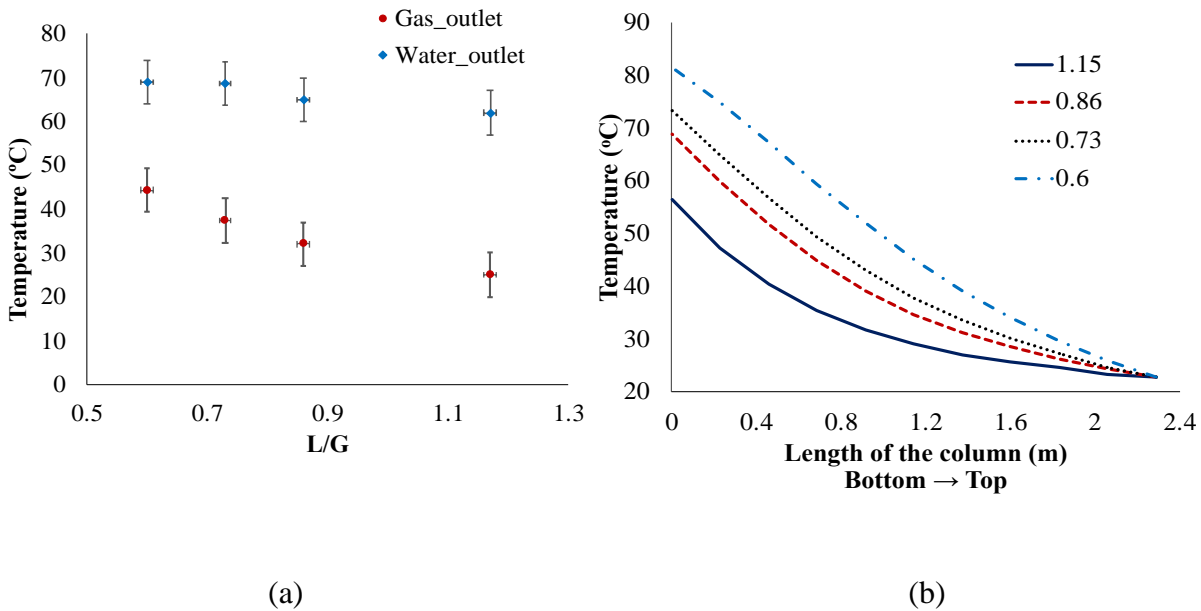
Figure 5.9 (a) Experimental outlet temperature of gas and liquid at different L/G ratio; (b) Model prediction of water temperature at different L/G ratio along the length of the column.

Primarily, at high L/G ratios the gas cools faster in the column, which decreases the gas volume

and increases its residence time. The simulated temperature profile from the model at different

101

L/G condition can be seen in Fig. 5.9(b). Additionally, the temperature of the gas and liquid outlet also increases with a decrease in L/G ratio, since more sensible heat from the gas is added to the successively reduced water flow. The gas and liquid outlet temperatures from the experiment are presented in Fig 5.9 (a). We found a small but significant discrepancy between experimental and modeling results for the water outlet temperature. A probable reason is the heat loss from the uninsulated sump where the water temperature is being measured, whereas the simulated model is considered to be adiabatic.

(a)   (b)
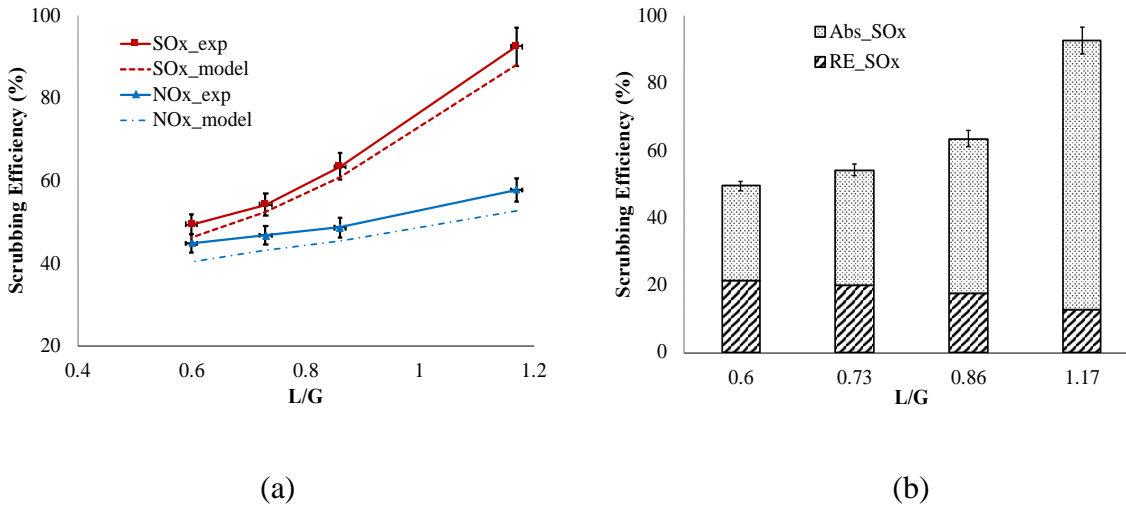
Figure 5.10 Impact of L/G ratio on SOx and NOx removal

The influence of L/G ratio on the overall of SO_2 and NO is presented in Fig. 5.10. The SO_2 removal increases sharply, around 50% points, with the increase in L/G ratio, compared to NO which only increases around 10% points. The small increase in NO_x removal is both, a function of increased residence time with gas cooling faster at higher L/G ratios, and the increase in kinetic constant for NO oxidation which is higher at lower temperatures. Since, NO_x removal is mainly controlled by gas phase oxidation of NO, the reduction in water flow rate doesn't directly impact the removal of

NO. However, this is not true of SO_2 removal which increases sharply with the increase in water flow. The breakdown of SO_2 absorption with and without NO_x is presented in Figure xx. At an L/G ratio of 1.17, where most of the SO_2 is removed, the majority of the removal is possible without NO_x, which only accounts for around 12% increase in the RE. With decreasing L/G ratio, although the overall removal of SO_2 decreases, the fraction removed through RE increases. At the L/G ratio of 0.6, the fraction of SO_2 removed by liquid phase RE is close to 45%. There are a several counteracting factors that results in this trend. Increase in liquid temperature at low L/G ratios, results in direct reduction of SO_2 absorption, and consequently reduced HSO_3^- concentration. Taken on its own, this is a deterrent to the liquid phase reaction rate. Additionally, looking at the removal of NO_x, it can be assumed the HNO_2 concentration also decreases slightly with the decrease in L/G ratio. However, with reduced L/G ratio there is an increase in water temperature, which increases the kinetic constant of the liquid phase reaction (R9 and R10). Additionally, there is also an increase in the liquid residence time which gives dissolved HSO_3^- and HNO_2 more time to react. The latter two factors compensate for the reduced concentration while increase the fraction of SO_2 removed through the liquid phase reaction at higher liquid temperature and low L/G ratio. The model generally under predicts the removal of both SO_x and NO_x in all cases, which is mainly because of heat loss from the column, which results in lower liquid temperature and consequently, higher removal compared to an adiabatic column assumption.

5.5 Conclusions

A key step towards the commercialization of pressurized oxy-combustion technology is the demonstration and parametric testing of a pilot-scale direct contact column for latent heat recovery and pollutant removal. This study represents the first efforts in this direction. For the majority of experiments conducted in this study, the SO_2 capture approached 100%, making NO_x capture the primary metric of performance. This study confirms that NO oxidation is the controlling reaction in the overall scrubbing of SO_x and NO_x at temperatures up to 200°C, with a small variation in NO_x removal at a higher temperature, which requires further investigation. Moreover, an NO_x capture efficiency of 80% can be achieved with a modest residence time of 95 seconds and pressure of 11 bar, with further improvement (>90%) achieved by increasing the residence time and/or pressure. The NO_x capture efficiency is found to be rather insensitive to oxygen partial pressure until the pressure is less than 0.1 bar, which implies that the excess oxygen in the flue gas of a POC power plant can be as low as 1%, without affecting scrubbing efficiency. This is important because lower excess would allow for higher net plant efficiency.

The impact of pressure is mainly apparent through the enhanced gas phase oxidation of NO. At higher pressure higher NO oxidation results in higher NO removal and consequently higher SO_2 removal. The importance of NO_2 on SO_2 scrubbing was also confirmed. A low NO concentration in the flue gas leads to a significant reduction in SO_2 scrubbing, especially at high temperature where the solubility of SO_2 is decreased. This discourages the employment of other NO removal technologies before the DCC. The optimal value of N/S will depend on temperature, pressure and the pH of the system, and a system-dependent optimization will be required to establish this value.

The impact of L/G ratio was studied, which makes it clear that even though reaction enhancement increases at lower L/G ratio, the overall reduction in SO_x removal is significant, compared to reduction in NO removal.

Finally, the simple 5-step model presented in the study is able to predict the SO_x and NO_x scrubbing efficiency with reasonable accuracy. It can be improved with the availability of more data at high temperature but at present can assist in the design and optimization of a full-scale DCC for a POC power plant.

5.6 References

[1]   H. Hagi, M. Nemer, Y. Le Moullec, C. Bouallou, Towards second generation oxy-pulverized coal power plants: Energy penalty reduction potential of pressurized oxy-combustion systems, Energy Procedia. 63 (2014) 431–439.

[2]   A. Gopan, B.M. Kumfer, J. Phillips, D. Thimsen, R. Smith, R.L. Axelbaum, Process design and performance analysis of a Staged, Pressurized Oxy-Combustion (SPOC) power plant for carbon capture, Appl. Energy. 125 (2014) 179–188.

[3]   A. Gopan, B.M. Kumfer, R.L. Axelbaum, Effect of operating pressure and fuel moisture on net plant efficiency of a staged, pressurized oxy-combustion power plant, Int. J. Greenh. Gas Control. 39 (2015) 390–396.

[4]   E. de Visser, C. Hendriks, M. Barrio, M.J. Mølnvik, G. de Koeijer, S. Liljemark, Y. Le Gallo, Dynamis CO_2 quality recommendations, Int. J. Greenh. Gas Control. 2 (2008) 478–484.

[5]   A. Dugstad, M. Halseid, B. Morland, Effect of SO_2 and NO_2 on corrosion and solid formation in dense phase CO_2 pipelines, Energy Procedia. 37 (2013) 2877–2887.

[6]   T. Zelalem Tumsa, S. Hoon Lee, F. Normann, K. Andersson, S. Ajdari, W. Yang, In Press, Concomitant removal of NOx and SOx from a pressurized oxy-fuel combustion process using a direct contact column, Chem. Eng. Res. Des. (2017).

[7]   V. White, A. Wright, S. Tappe, J. Yan, The Air Products Vattenfall oxyfuel CO_2compression and purification pilot plant at schwarze pumpe, Energy Procedia. 37 (2013) 1490–1499.

[8]   M. Shah, N. Degenstein, M. Zanfir, R. Kumar, J. Bugayong, K. Burgers, Near zero emissions oxy-combustion CO_2purification technology, Energy Procedia. 4 (2011) 988–995.

[9]   A. Gopan, P. Verma, Z. Wang, R. Axelbaum, Quantitative analysis of the impact of flue gas recirculation on the efficiency of oxy-coal power plants, Int. J. Greenh. Gas Control. (2019).

[10] S.B. Oblath, S.S. Markowitz, T. Novakov, S.G. Chang, Kinetics of the formation of hydroxylamine disulfonate by reaction of nitrite with sulfites, J. Phys. Chem. 85 (1981) 1017–1021.

[11] H. Tsukahara, T. Ishida, M. Mayumi, Gas-phase oxidation of nitric oxide: Chemical kinetics and rate constant, Nitric Oxide - Biol. Chem. 3 (1999) 191–198.

[12] Y.N. Lee, S.E. Schwartz, Reaction kinetics of nitrogen dioxide with liquid water at low partial pressure, J. Phys. Chem. 85 (1981) 840–848.

[13] S. Ajdari, F. Normann, K. Andersson, F. Johnsson, Reduced Mechanism for Nitrogen and Sulfur Chemistry in Pressurized Flue Gas Systems, Ind. Eng. Chem. Res. 55 (2016) 5514–5525.

[14] A. Solution, R. Tracers, Kinetic Study of Sulfur Dioxide in, (1964) 574–580.

[15] F. Normann, E. Jansson, T. Petersson, K. Andersson, Nitrogen and sulphur chemistry in pressurised flue gas systems: A comparison of modelling and experiments, Int. J. Greenh. Gas Control. 12 (2013) 26–34.

[16] S. Ajdari, F. Normann, K. Andersson, F. Johnsson, Gas phase oxidation of SO2 by NO2 in pressurized flue gas systems - an experimental investigation, Energy Procedia. 46 (2013) 2011–2013.

[17] M.S. Pétrissans, A. Zoulalian, Influence of the pH on the Interactions between Nitrite and Sulfite Ions . Kinetic of the Reaction at pH 4 and 5, Ind. Eng. Chem. 40 (2001) 6068–6072.

[18] P. Verma, Z. Gromotka, G. Yablonsky, D. Stokie, D. Constales, B. Kumfer, R.L. Axelbaum, Optimizing complexity in the kinetic modelling of integrated flue gas purification for pressurized oxy-combustion, Chem. Eng. J. (2020).

[19] S.B. Oblath, S.S. Markowltz, T. Novakov, S.G. Chang, Kinetics of the initial reaction of nitrite ion in bisulfite solutions, J. Phys. Chem. 86 (1982) 4853–4857.

[20] T. Ting, R. Stanger, T. Wall, Laboratory investigation of high pressure NO oxidation to NO2and capture with liquid and gaseous water under oxy-fuel CO2compression conditions, Int. J. Greenh. Gas Control. 18 (2013) 15–22.

[21] R. Stanger, T. Ting, C. Spero, T. Wall, Oxyfuel derived CO2 compression experiments with NOx, SOx and mercury removal-Experiments involving compression of slip-streams from the Callide Oxyfuel Project (COP), Int. J. Greenh. Gas Control. 41 (2015) 50–59.

[22] Ö. Yildirim, A.A. Kiss, N. Hüser, K. Leßmann, E.Y. Kenig, Reactive absorption in chemical process industry: A review on current activities, Chem. Eng. J. 213 (2012) 371–391.

[23] J.W. Armitage, Studies of the Reaction Between Nitrogen Dioxide and Sulfur Dioxide, 130 (1971) 125–130.

Chapter 6.   A direct contact cooler design for simultaneously recovering latent heat and capturing SOx and NOx from pressurized flue gas

6.1 Introduction

The goal of rapidly decarbonizing the electricity grid while maintaining its reliability has led to significant interest in carbon capture, utilization, and storage (CCUS) technologies for power plants [1,2]. Pressurized oxy-combustion (POC), where fuel is burned at elevated pressure in the presence of oxygen and recycled flue gas, has emerged as a promising lower-cost technology for the implementation of CCUS [3]. The combustion products from solid-fuel-based POC processes consist primarily of CO_2 and H_2O, with small amounts of sulfur and nitrogen oxides. The principal motivation for high-pressure combustion is the benefit of condensing the flue gas moisture at a higher temperature compared to atmospheric pressure combustion [3,4]. The latent heat recovered

from the flue gas at higher temperature can be integrated into the steam cycle to increase plant efficiency. In a POC process operating at 15 bar, the integration of moisture latent heat can lead to a potential increase of 1.5 – 2.5 percentage points in net plant efficiency [5]. Since the CO_2 product needs to be compressed downstream for transportation and storage, and the cost of compressing oxygen is comparable to that of compressing CO_2, there is no additional cost for pressurizing the upstream combustion process.

The second significant benefit of high pressure is the potential to remove SO_x and NO_x simultaneously and economically in a reactive-absorption column. The SO_x and NO_x in the flue gas are major pollutants formed during coal and biomass combustion that also have the potential to corrode plant equipment [6]. In conventional atmospheric pressure combustion processes, the removal of SO_x and NO_x is achieved in two steps - a selective catalytic reduction (SCR) unit to remove NO_x and a flue gas desulfurization (FGD) unit to remove SO_x [7,8]. In a POC process, the partial pressure of O_2 is higher in the flue gas because of the higher total pressure. This helps to more rapidly oxidize NO into water-soluble NO_2, making it easily removable in an absorption column [9]. The solution-based reactions between nitrogen and sulfur species further enhance removal of NO_x and SO_x, such that POC has brought the opportunity for the integrated pollutant removal (IPR), where NO_x and SO_x are simultaneously scrubbed in a pressurized water-wash column, i.e., direct contact cooler (DCC). A cost reduction of about 70% has been reported for this technology, compared with conventional cleaning technologies using SCR and FGD [10].

Previous work on simultaneous removal of SO_x and NO_x focused on flue gas from atmospheric pressure oxy-combustion of coal. White et al. used a slipstream from an atmospheric-pressure, 160 kW_{th} oxyfuel combustor to evaluate SO_x and NO_x removal [11]. The flue gas was cooled to room temperature such that the majority of the moisture was removed before compressing to 5 – 15 bar to prevent acid condensation in the compressors. They concluded that it was possible to remove SO_x and NO_x components from oxy-fuel-derived CO_2 without employing FGD or SCR technologies. Murciano et al. performed lab-scale experiments on dry synthetic flue gas to understand the effect of pressure and residence time on NO_x and SO_x scrubbing [12]. They reported that NO is readily oxidized to NO_2 at high pressure in the presence of oxygen. However, SO_2 was not oxidized to SO_3. They also noted an interaction between SO_2 and NO_2 in the presence of water vapor, however, the analysis was complicated by the formation of acid droplets. A similar study by White et al. on an atmospheric oxy-combustion slipstream analyzed SOx and NOx removal in a two-stage system of 15 and 30 bar [13]. They reported that NO reduction was a function of residence time and pressure, while SO_2 removal was affected by both residence time and make-up water flow rate. These studies confirmed that SO_x and NO_x removal at high pressure, low temperature, and high liquid-to-gas ratio(L/G) was possible, without the objective to recover the latent heat of moisture. C.IIoeje et al. and Tumsa et al. modeled and parametrically analyzed similar DCC processes, both of which established the possibility of pressurizing the flue gas and then removing SO_x and NO_x using a water contact column. They suggested pressurizing the gas to 30 bar for greater NO_x removal [14,15]. Similar to the experimental system, these models did not consider recovering the latent heat from the flue gas. The moisture in the flue gas was removed in a cooler before compression, and cold flue gas was fed into the column at high L/G ratios.

Although these studies confirm the possibility of removing SO_x and NO_x at high pressure, a detailed analysis is required for POC systems where the flue gas is already at high pressure and temperature. As proposed by Gopan et al., the recovery of latent and sensible heat, along with the removal of SO_x and NO_x in one single column, will further reduce the complexity and cost of the POC power plant [3]. In this case, the DCC can act both as a heat exchanger to recover latent and sensible heat from the flue gas and an absorber for SO_x and NO_x. Moreover, to maximize plant efficiency, the water temperature exiting the DCC must be maintained at a relatively high temperature, which is accomplished by constraining the L/G ratio, making scrubbing a high-temperature process [4,5]. The performance of SO_x and NO_x removal in a DCC at high water temperature and low L/G ratio has received little attention.

In this work, we propose a novel design for a DCC operated at 15 bar for a 550 MWe pressurized oxy-combustion power plant, and we use a validated model for performance evaluation. The conventional DCC design typically contains a counter-current absorber with one water inlet at the top and one gas inlet at the bottom of the column. The design proposed in this work allows for multiple water inlets. A model is used to optimize the number of inlets and the water flow rate for each inlet to maximize the NO_x and SO_x removal. The reaction kinetics used in the model are validated against results from a 100 kW_{th} pilot-scale DCC experiment. We compare the temperature and volumetric flow profiles for gas and liquid in the conventional and new designs and discuss the effect of moisture condensation on the residence time and gas and liquid reaction kinetics. Finally, a comparison and analysis of the differences in SO_x and NO_x removal efficiency are presented. This work is the first effort to model and optimize a single DCC column that integrates heat recovery and SO_x and NO_x removal.

6.2. Methodology

6.2.1 Modeling Methodology

The design of the DCC is based on flue gas from a 550 MWe pressurized oxy-combustion plant

using Montana PRB coal [16]. The flue gas conditions and composition are presented in Table 6.1.

The 1.2% oxygen concentration in the flue gas is based on the work of Zhiwei et al., which showed

that complete combustion of coal particles could be achieved in oxy-combustion with an excess

oxygen concentration of just 1% when operating at 15 bar [17]. The inlet concentration of NO_x

and SO_x to the DCC depends on the amount of sulfur and nitrogen in the coal. Inlet concentrations

of 900 ppm SO_2 and 900 ppm NO are assumed for this analysis, which is in the same range as the

values assumed by Ajdari et al. and IIoeje et al. for similar analyses [15,18]. The trace elements,

such as chlorine and mercury, are not considered in the model since they are in small quantities

and do not affect the chemistry of the process.

The DCC was modeled as a rate-based reactive absorption column using a RadFrac unit in Aspen

plus V9, as a rate-based model is required to analyze residence time constraints. The ionic

interaction in the liquid phase requires the use of an electrolytic equation of state for the

thermodynamic properties of the components. Hence, ELECNRTL was used as the property

method because of its compatibility with the system in both the liquid and gas phases. The column

was modeled as a ten-stage column, with gas introduced below the bottom-most stage. For the

conventional DCC design, water is introduced above the top stage. For the modified DCC design

with multiple water inlets, water can be introduced above each stage. The analysis found no

relevant increase in accuracy with more than ten stages. The results are presented with the bottom-most stage numbered as Stage 1. The column was assumed to be adiabatic, with no heat loss to the surroundings.

Table 6.1 Inlet modeling parameters

Parameter	Value
DCC pressure (bar)	15
Inlet gas flowrate (kg/s)	205.3
Inlet gas temperature (°C)	200
Inlet water flowrate (kg/s)	212.5
Inlet water temperature (°C)	24
Inlet gas composition	(% v/v)
CO_2	55.4
H_2O	40.2
O_2	1.2
NO	0.09
NO_2	0.01
SO_2	0.09
SO_3	0.01

6.2.2   Column Design

A conventional design, presented in Fig. 6.1(a), is a counter-current packed column with water coming from the top and gas from the bottom. For this study, the L/G ratio was determined by fixing the moisture content of the outlet flue gas to be 1.5 % v/v and maximizing water outlet temperature. The resulting L/G ratio was close to 1.03 kg/kg, and the corresponding outlet water temperature was around 160 °C. Based on this L/G ratio, the column diameter was sized for a 75% approach to the flooding velocity for optimum mass transfer, which comes out to be 5.6 m. The height of the conventional column was determined based on the targeted outlet concentration of

SO$_x$ (< 50 ppm). The packing material selected was 80 mm Raschig rings since this provides good mass transfer with a reasonable pressure drop in the column.
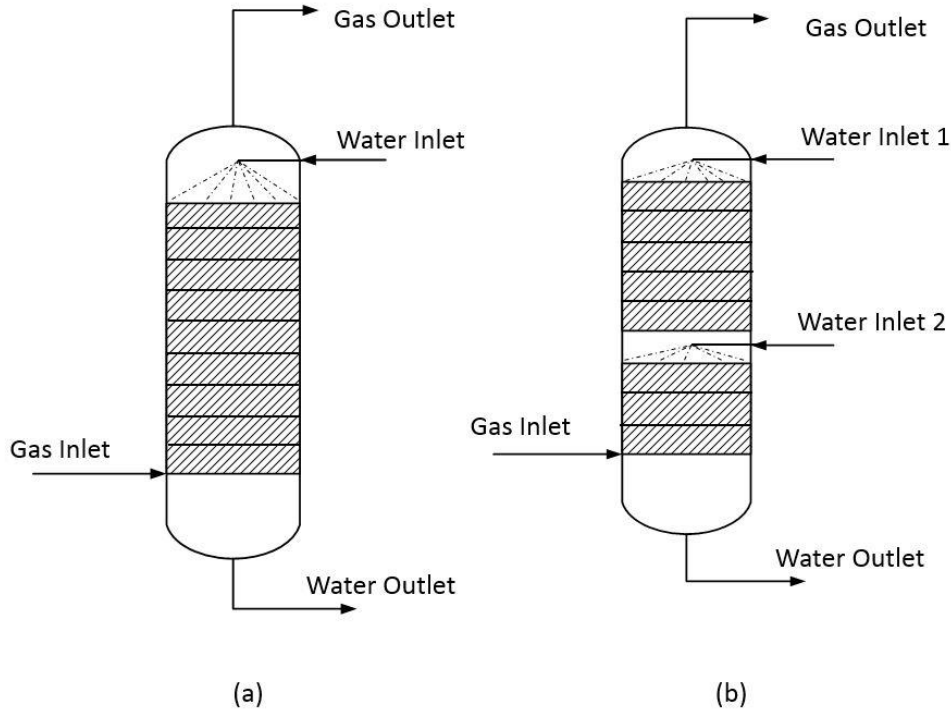
Figure 6.1 (a) Conventional and (b) Proposed multi-water-inlet column design.

The proposed column, shown in Fig. 6.1(b), uses the same dimension and packing material as those of the conventional column in Fig. 6.1(a). To ascertain the inlet water flow rate at each stage in an optimized design, ten water inlets, one above each stage, were introduced in the column. Two parameters were applied as constraints – the total water flow rate and the outlet gas moisture concentration (< 1.5 % v/v). The multivariate optimization tool in Aspen Plus was used to minimize the two objective variables – the outlet NO$_x$ and SO$_x$ concentration, by varying the water flow to each stage. The optimization results suggested that a simple design with only two water inlets provides the best removal efficiency, one stream at the top with 23.5% of the total flow and

the remaining entering above the 4th stage. The outlet SO_x concentration and NO_x concentration in the optimized design were achieved below 50 ppm and 100 ppm, respectively. The required outlet concentrations are based on the CO_2 transport pipeline quality guidelines [19,20]. These split ratios and injection locations could vary with the total moisture content in the flue gas, inlet gas and liquid temperature, and the inlet SO_x and NO_x concentration. Hence, for a different coal and combustion design, further optimization would be needed.

6.2.3 Chemical Kinetics and Model Validation

In addition to the thermophysical water condensation process, several gas- and liquid-phase reactions occur inside the DCC. The most important reaction for NO_x removal is the oxidation of NO to NO_2. Tsukahara et al. reviewed several studies on the gas-phase oxidation of NO to NO_2 and reported that NO oxidation is a third-order reaction, depending on the partial pressure of NO and O_2 [21]. They reported that the kinetic constant for the reaction decreases slightly up to a temperature of 500 °C and then increases at higher temperatures. Since the DCC is designed to operate between gas temperatures of 20 to 200 °C, it is important to consider the dependency of the kinetic constant on temperature. Ting et al. [9] also reported similar reaction kinetics with rate constants relevant for high-pressure operations.

In the DCC column, NO_2 produced via,
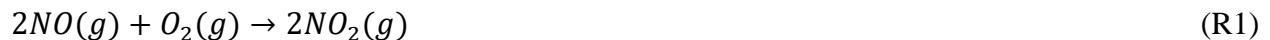
$$2NO(g) + O_2(g) \rightarrow 2NO_2(g) \tag{R1}$$

is readily absorbed in water to form HNO_2 and HNO_3 in a 1:1 ratio, according to

$$2NO_2(g) + H_2O(aq) \rightarrow HNO_2(aq) + HNO_3(aq) \,. \tag{R2}$$
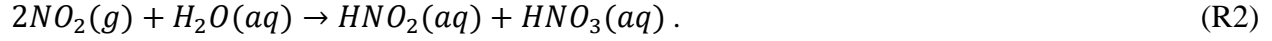
The SO_2 in the gas is absorbed in water to form HSO^-_3, according to

$$SO_2(g) + H_2O(aq) \leftrightarrow HSO_3^-(aq) + H^+(aq) \,. \tag{R3}$$

Both Reaction 2 and 3 are instantaneous and are treated as equilibrium reactions in the kinetic model [22, 23]. Similarly, SO_3 dissolves instantaneously in water to form H_2SO_4 according to Reaction 4 and is also treated as an equilibrium reaction.

$$SO_3(g) + H_2O(aq) \leftrightarrow HSO_4^-(aq) + H^+(aq) \tag{R4}$$
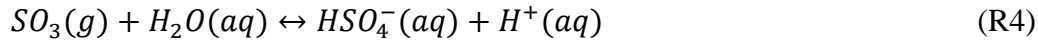
Although the liquid-phase interactions have received less attention, Normann et al. [24] found that complex interactions between HNO_2 and HSO^-_3, which are capable of enhancing the oxidation rate to produce HNO_3 and H_2SO_4, play an important role in the scrubbing chemistry. They presented the Raschig mechanism to explain the interaction of HNO_2 and HSO_3^- in the liquid phase:

$$HNO_2(aq) + HSO_3^-(aq) \rightarrow NOSO_3^-(aq) + H_2O(aq) \tag{R5}$$

$$NOSO_3^-(aq) + H^+(+H_2O) \rightarrow HNO(aq) + H_2SO_4(aq) \tag{R6}$$

$$NOSO_3^-(aq) + HSO_3^-(aq) \rightarrow HNO(SO_3)_2^{2-}(aq) \tag{R7}$$

$$HNO(aq) + HNO(aq) \rightarrow N_2O(g) + H_2O(aq) \tag{R8}$$

$$HNO(SO_3)_2^{2-}(aq) + H^+(aq) \rightarrow HNOHSO_3^-(aq) + H^+(aq) + HSO_4^-(aq) \,. \tag{R9}$$
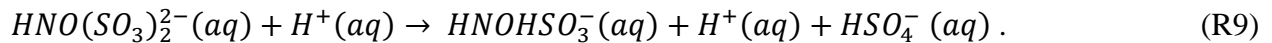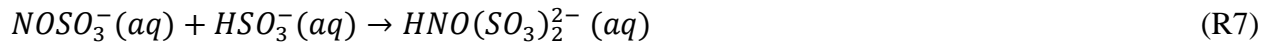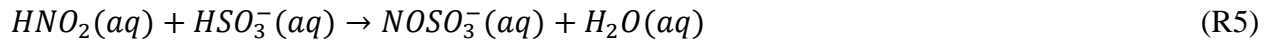
They concluded that the liquid phase interaction between HNO_3^- and HNO_2 should be further investigated in the range of pH relevant to DCC. Based on a sensitivity analysis of the primary reactions, Ajdari et al. [18, 25] proposed a reduced mechanism of between 7 to12 reactions for the

relevant pH range. They concluded that the gas-phase reactions are limited by NO oxidation, whereas the liquid-phase interactions are predominantly pH controlled. They reduced the liquid-phase mechanism to two major reactions, Reaction 10 and 11:

$$HNO_2 + HSO_3^- \rightarrow HSO_4^- + \frac{1}{2}N_2O + \frac{1}{2}H_2O \qquad (R10)$$

$$HNO_2 + 2HSO_3^- \rightarrow HON(SO_3)_2^{2-}(\text{HADS}) + H_2O \qquad (R11)$$
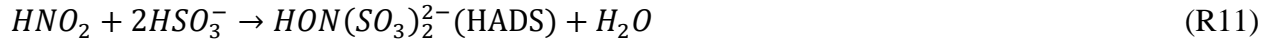
In our previous work [26], we further reduced the entire mechanism to a total of 5 reactions (R1, R2, R3, R10, and R11) through an experimental and mathematical optimization of the model, as shown in Table 6.2. Two main findings were reported in this work: 1) the gaseous species such as N_2O_4 have a negligible impact on the kinetics, and 2) the dissociation of HNO_2 to HNO_3 and NO is not significant in DCC conditions. The SO_3 absorption reaction is not considered in the kinetic models discussed above because SO_3 is highly soluble in water and is removed at the entrance to the column, hence it does require a kinetic analysis. However, it was included in the Aspen model presented in this work.

Table 6.2 Reduced reaction mechanism used in the modeling

	Reaction	Type
1	$2NO + O_2 \rightarrow 2NO_2$	Kinetic [9]
2	$2NO_2 + H_2O \rightarrow HNO_2 + HNO_3$	Equilibrium
3	$SO_2 + H_2O \leftrightarrow HSO_3^- + H^+$	Equilibrium
4	$SO_3 + H_2O \rightarrow HSO_4^- + H^+$	Equilibrium
5	$HNO_2 + HSO_3^- \rightarrow HSO_4^- + \frac{1}{2}N_2O + 0.5\ H_2O$	Kinetic [28]
6	$HNO_2 + 2HSO_3^- \rightarrow HNO(SO_3)_2^{2-} + H_2O$	Kinetic [28]

This proposed kinetic model was validated in a small pilot-scale DCC by Stokie et al. [27]. The experiments were performed in a counter-current packed bed with an 0.2 m diameter and 2.3 m of packing. Several parametric studies were performed at 15 bar pressure and inlet gas temperatures of 24 and 202 °C using synthetic flue gas containing SO_2, NO, O_2 and CO_2. Experimental and model results for 15 bar pressure and 24 °C inlet gas temperature are presented in Fig. 6.2. In this experiment, the NO concentration was varied from 0 to 1000 ppm with SO_2 and O_2 concentrations fixed at 500 ppm and 3%, respectively. The residence time of the gas in the column was maintained at 120 seconds for each condition. For these conditions, the NO removal increased with increasing inlet NO concentration, and SO_2 removal was higher than 95% for each case. The kinetic model presented in Table 6.2 was capable of accurately predicting the outlet concentration of NO and SO_2. Experimental system details and additional results can be found in the study by Stokie et al. [27].
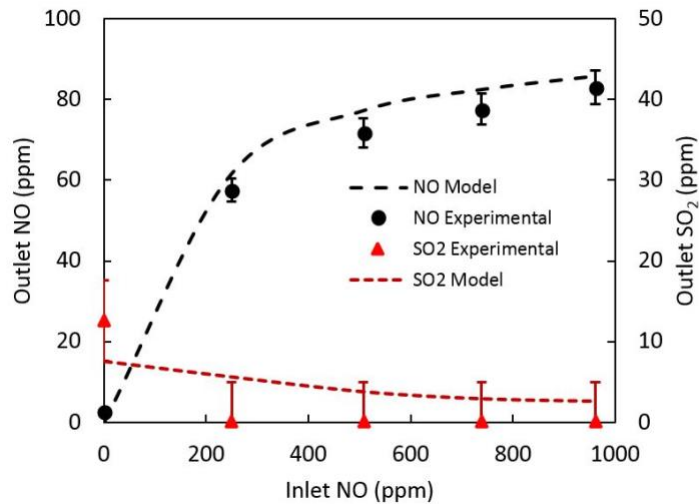
Figure 6.2 Kinetic model validation

6.3 Result and Discussion

For the base case analysis, a conventional column with one water inlet at an L/G ratio of 1 was simulated for the targeted outlet moisture and SO_x concentration. An analysis of the time scales for heat and mass transfer and the rate of chemical reaction revealed that the removal of SO_x and NO_x in the column is limited by the oxidation of NO to NO_2. This result was also observed in the experiments by Stokie et al. [27] and Stanger et al. [29]. Since the L/G ratio and the flue-gas oxygen content are both fixed, the removal of NO and SO_2 depends on the residence time and temperature profile in the column. The residence time enhances the overall reaction time for NO oxidation, while the temperature profile impacts the local kinetic constant of both gas- and liquid-phase reactions. The proposed new column design, with the same column height, diameter, and packing, was modeled and operated to achieve a similar moisture outlet concentration and NO_x (< 100 ppm) and SO_x (< 50 ppm) concentrations less than the target.

6.3.1. Gas temperature profile comparison

The Aspen results indicate that in a conventional column, it is possible to remove SO_x and NO_x to the required standards. These results also reveal that only a small fraction of this residence time is required for cooling and condensing the moisture in the gas, owing to a faster time constant for heat transfer compared to NO oxidation. A majority of the cooling and condensation is achieved in about 40% of the column height with the specified L/G ratio. In the conventional column, most of the cooling and condensation occurs in the top section of the column due to the counter-current, one-water-inlet design.

In Fig. 6.3, a comparison between the gas temperature profile in the conventional column and the optimized column is presented. In the optimized column, most of the water (76%) is fed above the 4th stage, which is a sufficient height for the majority of heat transfer. This modification leads to a faster temperature drop in the bottom part (below the lower water inlet) of the optimized column. The gas outlet temperature is slightly higher than that of the conventional design because a smaller L/G ratio in the upper section leads to a reduced surface area of contact. A different packing in the upper column could yield better heat transfer.
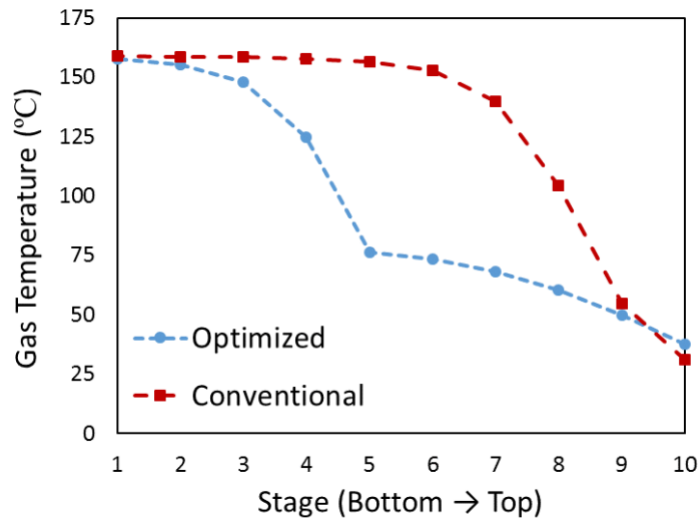
Figure 6.3 Gas temperature profile in the two designs

The kinetics for NO oxidation is significantly affected by the gas temperature profile. In Fig. 6.4, the rate constant for the NO oxidation reaction for the optimized column is compared to that of the conventional DCC for each stage. Except for the top stage (Stage 10), the rate constant ratio ($k_{optimized}/k_{conventional}$) is higher than unity throughout the length of the column because the flue gas temperature is lower in the optimized design than in the conventional design. The highest ratio is in Stages 5 through 7, where the rate constant is 35% higher in the optimized column, as this is where the gas temperature difference between the two columns is greatest. On average, over the

121

entire column, there is a 13.2 % increase in the rate constant for NO oxidation. This increased NO oxidation rate is one factor that contributes to the higher removal of NO_x in the optimized design.
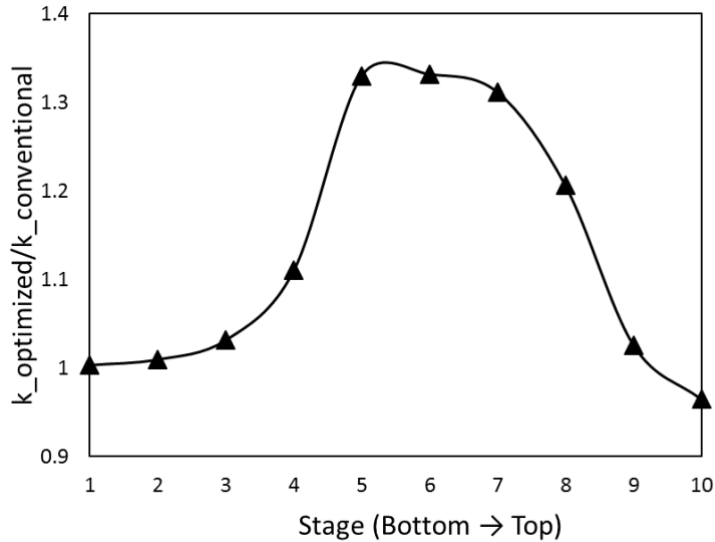
Figure 6.4 Comparison of the rate constants for NO oxidation for each stage of the two designs

6.3.2. Change in Volumetric Flow Rate and Residence Time

As seen in Fig. 6.5a, the total volumetric gas flow rate in the optimized design decreases significantly faster in the lower section. This is due to earlier condensation of moisture and faster cooling of the gas, both of which reduce volumetric flow rate. In the conventional design, most of the cooling and condensation occurs in the upper section of the column. In contrast, in the optimized design, they are largely completed by Stage 5, leading to a much lower flow rate in the remaining part of the column. It should be noted that the inlet flue gas for this study contains close to 40% moisture, which leads to a sharp drop in volumetric flow rate when condensation occurs. Depending on the amount of moisture in the flue gas, the design can be modified to optimize the water inlet for fast condensation. On the conventional column, the volumetric flow rate drops close

to 60% in the entire length of the column, from 15 m³/s to close to 6 m³/s. However, in the optimized column, most of this drop is accomplished by Stage 5.

(a)   (b)
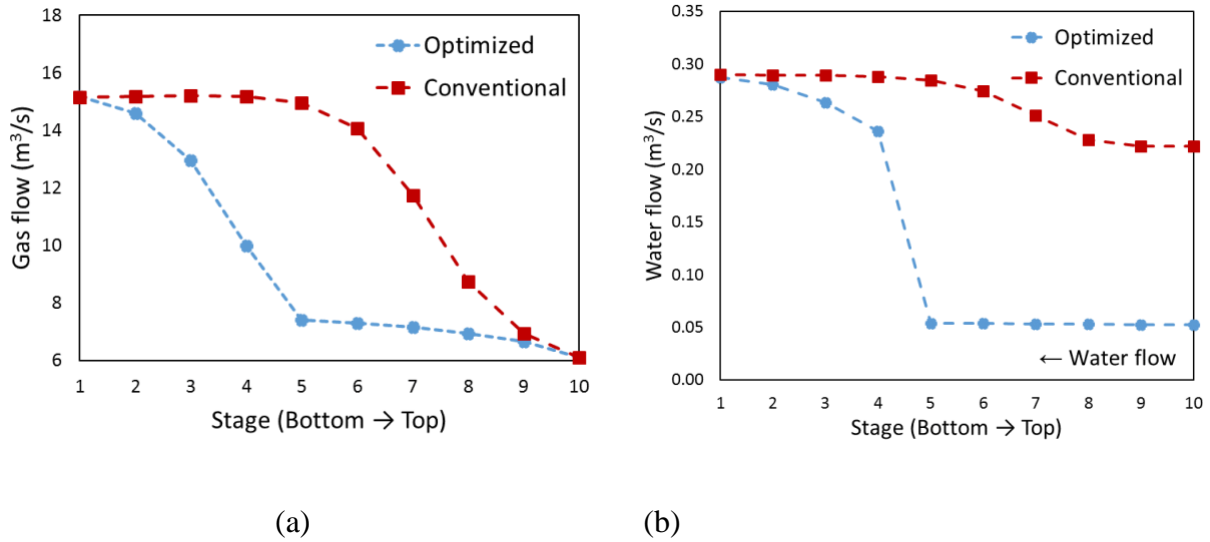
Figure 6.5 Comparison of volumetric flow profile of a) gas and b) water in the conventional and optimized design

Figure. 6.5(b) presents the total water flow rate at each stage. It should be noted that the water flow is from Stage 10 to Stage 1. The total water at the outlet(Stage 10) increases from 0.22 m³/s to 0.28 m³/s due to water condensation from the flue gas in both columns. For the conventional column, the increase in the flow occurs between Stages 6 and 9, while in the optimized design, the addition of water due to moisture condensation is completed before the second water inlet (between Stages 1 to 4). The optimized design exploits the fact that heat transfer is a fast process compared to reaction kinetics. A column with the sole objective of recovering the latent heat would require about 40% of the total length of the design presented in this work.

The different gas flow rates over the ten stages lead to different cumulative gas residence times in the two columns, as shown in Fig. 6.6. The total residence time in the optimized column is

123

39 seconds longer (or 34% larger) than that in the conventional column. The relative increase in the residence time is apparent above Stage 4. Since the removal of NO_x, and consequently SO_x, is limited by the NO oxidation rate, a longer residence time increases the total amount of NO converted to NO_2. This results in higher NO_x removal and, consequently, higher SO_x removal because of the liquid phase interactions.
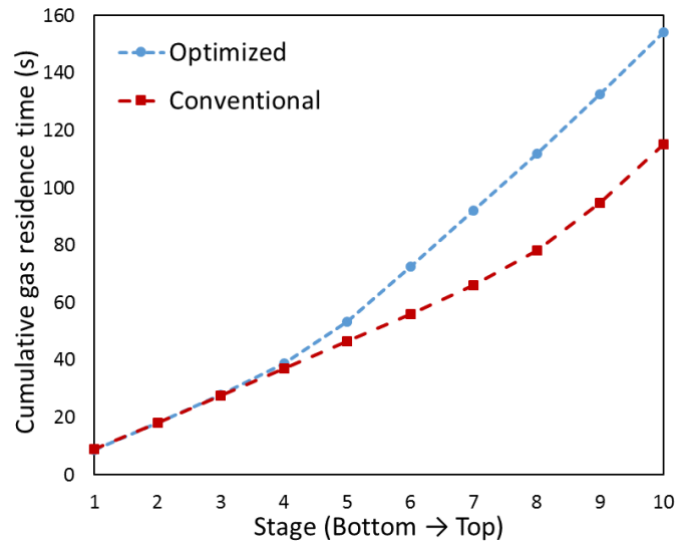
Figure 6.6 Comparison of gas residence time in the conventional and optimized design

6.3.3   Impact on NO_x and SO_x Reaction

There are three factors that affect the greater NO to NO_2 oxidation in the optimized column, and thus the larger NO removal. These factors are 1) an increased rate constant due to the sharper drop in gas temperature in the optimized design, 2) an increase in gas residence time due to the faster cooling and moisture condensation in the flue gas, and 3) an increase in partial pressure of the reactants due to the reduced gas volume. The molar flow rate of NO and the comparison of total NO to NO_2 conversion over the ten stages are presented in Fig. 6.7(a) and 6.7(b), respectively. As seen in Fig. 6.7(b), between Stages 4 and 6, the total NO converted to NO_2 in the optimized column

124

is 2 – 4 times higher than the conversion in the conventional column. As discussed in relation to Fig. 4, the ratio of the rate constants also peaks between Stages 4 to 7. The overall impact of the increase in the rate constant, residence time, and NO partial pressure in these stages makes the NO removal high. Even though the residence time is higher in the upper stages, the NO concentration in the optimized column has been reduced to a smaller value, and hence the overall rate becomes slightly smaller than the conventional column for Stage 7 and beyond. It should be noted that the benefit of the optimized design is not limited to the pressurized oxy-combustion processes and should be applicable to other removal technologies having similar kinetic and heat removal constraints.

| (a) | (b) |
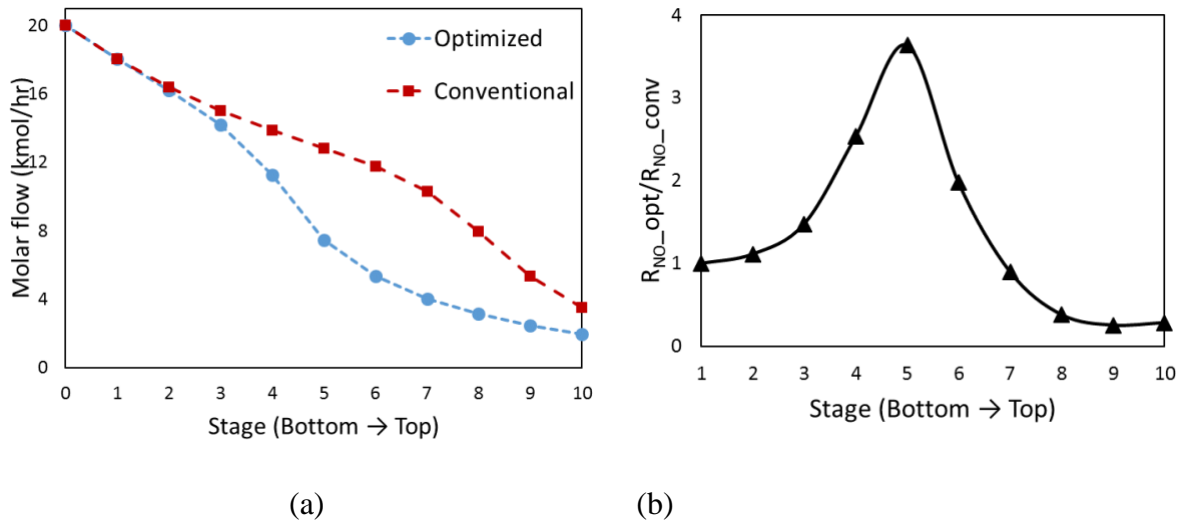
Figure 6.7 (a) molar flow rate of NO and (b) the ratio of NO consumption between optimized and conventional column (Stage '0' in Figure 7(a) represents the inlet conditions.)

SO_2 removal depends upon the interaction between absorbed NO_2 (through HNO_2) and absorbed SO_2 (through HSO_3^-). The liquid phase reaction is first order in both HNO_2 and HSO_3^-, hence an increase in the concentration of either reactant increases the reaction rate. Figure 6.8 demonstrates the comparison of SO_2 flow in the two designs. For the conventional column, SO_2 is removed

slowly and almost linearly in the bottom stages but rapidly in Stages 7–10. However, in the optimized column, SO_2 reduction is rapidly in the first five stages. This is due to two reasons. First, in the conventional design, the NO oxidation rate is high in the top section, which results in higher HNO_2 concentration in the liquid phase in Stages 7–10, and a higher liquid phase reaction rate. In the optimized design, the NO oxidation is high between Stages 3 – 6, resulting in high HNO_2 concentration and higher reaction rate in the bottom stages. Also, since most of the SO_2 is already consumed in the bottom stages, the unreacted HNO_2 from the top stages flows down and reacts with HSO_3^- leading to higher removal rates. The second reason for rapid SO_2 reduction in the first five stages is that SO_2 absorption is a function of SO_2 partial pressure and liquid temperature. Due to the faster moisture condensation in the bottom stages of the optimized design, the partial pressure of SO_2 increases sharply compared to conventional design, resulting in higher absorption of SO_2 in the bottom stages and, consequently, a faster liquid-phase reaction. The water temperature also drops rapidly in the optimized design (Figure 6.3), which results in higher absorption of SO_2 in lower stages of the optimized design compared to conventional design. The overall impact of these factors results in enhanced removal of SO_2 in the optimized column.

It should be noted that almost all the SO_2 is removed in the process for the conditions specified, and it would be possible to remove an even greater amount of SO_2 if more were supplied at the inlet. The removal is only limited by the amount of NO in the system. However, the SO_2 removal is also very sensitive to the amount of NO_x in the inlet; therefore, with a reduced N/S ratio, the SO_2 removal may decline. An enhanced pressure or a modified L/G ratio can be employed to achieve similar objectives in such cases.
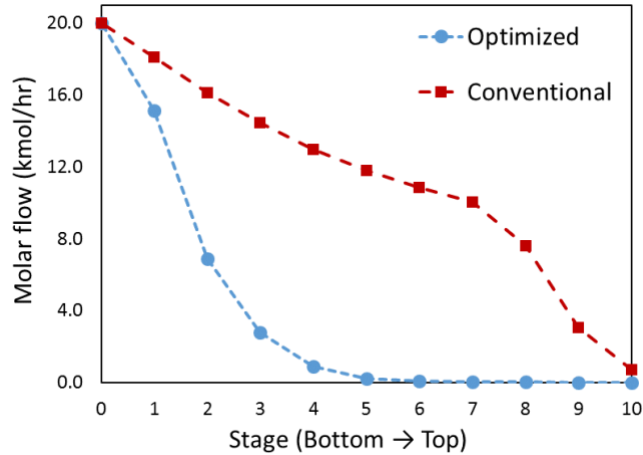
Figure 6.8 SO$_2$ mole flow over 10 stages in the conventional and optimized design

6.3.4   Comparison of NO$_x$ and SO$_x$ removal efficiencies

Figure 6.9 summarizes the scrubbing efficiency of SO$_x$ and NO$_x$ for both designs. The increase in gas residence time and rate constant of the NO oxidation reaction in the optimized design enhances the scrubbing of NO by almost nine percentage points compared to the conventional design. Consequently, the increased formation and subsequent absorption of NO$_2$ and the reduced temperature and increased partial pressure (due to faster moisture condensation) enhances the liquid phase reaction with HSO$^-_3$, resulting in faster and greater absorption of SO$_2$ in water. The scrubbing efficiency of SO$_x$ increases by almost three percentage points to 99.98%. The optimized two-water-inlet design is much more efficient and, consequently, more economical than the conventional counter-current design.
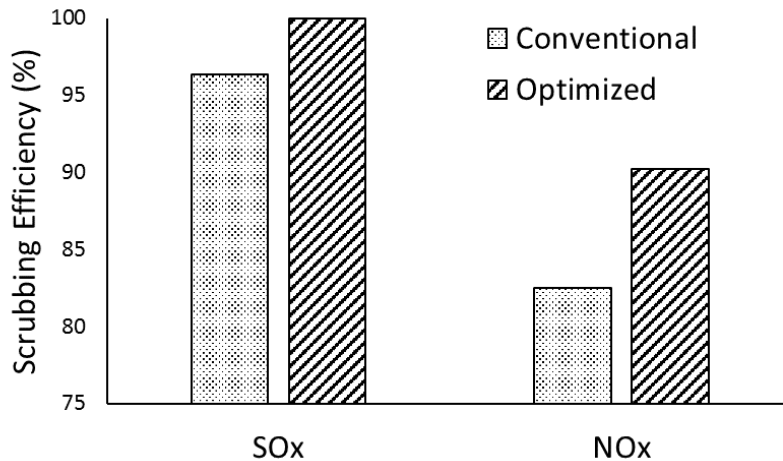
Figure 6.9 Comparison of NO_x and SO_x removal in the conventional and optimized designs.

6.4 Conclusion

A direct contact cooler that simultaneously recovers flue gas heat and removes SOx and NOx can significantly reduce the cost of pollutant removal in pressurized oxy-combustion systems. This study modeled and optimized this type of direct contact cooler using a reaction mechanism and kinetic data validated by pilot-scale experiment results. A time scale analysis of the heat and mass transfer and chemical reactions indicates that the NO removal is limited by the NO oxidation reaction.

A conventional column design was compared with a novel optimized design. In the conventional column, gas is fed from the bottom and water from the top. The gas temperature remains high until the upper section, where most of the moisture condensation and gas temperature reduction occur. To optimize the design, the water supply to the column is split into multiple streams, one for each of the column stages, and then the flow rates for each water stream is optimized to maximize the

128

SO$_x$ and NO$_x$ removal efficiency. The optimal design for the system studied has only two water streams, with 23.5% of the water fed from the top and the remaining fed from Stage 4th. The optimized design proved to be significantly better in terms of SO$_x$ and NO$_x$ scrubbing efficiency. In this design, the heat transfer in the lower sections is enhanced, leading to faster temperature drop and earlier moisture condensation. The lower temperature and moisture content both contribute to a lower volumetric gas flow rate and hence a longer residence time (34% longer). Since the NO oxidation reaction occurs faster at lower temperatures, the optimized column has a higher NO oxidation rate, in addition to a longer residence time for NO to oxidize, leading to significantly higher NO$_x$ and SO$_x$ removal efficiencies.

6.5 References

[1]   Guo JX, Huang C. Feasible roadmap for CCS retrofit of coal-based power plants to reduce Chinese carbon emissions by 2050. Appl Energy 2020;259:114112. https://doi.org/10.1016/j.apenergy.2019.114112.

[2]   Rissman J, Bataille C, Masanet E, Aden N, Morrow WR, Zhou N, et al. Technologies and policies to decarbonize global industry: Review and assessment of mitigation drivers through 2070. Appl Energy 2020;266:114848. https://doi.org/10.1016/j.apenergy.2020.114848.

[3]   Gopan A, Kumfer BM, Phillips J, Thimsen D, Smith R, Axelbaum RL. Process design and performance analysis of a Staged, Pressurized Oxy-Combustion (SPOC) power plant for carbon capture. Appl Energy 2014;125:179–88. https://doi.org/10.1016/j.apenergy.2014.03.032.

[4]   Gopan A, Kumfer BM, Axelbaum RL. Effect of operating pressure and fuel moisture on net plant efficiency of a staged, pressurized oxy-combustion power plant. Int J Greenh Gas Control 2015;39:390–6. https://doi.org/10.1016/j.ijggc.2015.05.014.

[5]   Gopan A, Verma P, Wang Z, Axelbaum R. Quantitative analysis of the impact of flue gas recirculation on the efficiency of oxy-coal power plants. Int J Greenh Gas Control 2019.

[6]   Vannerberg NG, Sydberger T. Reaction between SO2 and wet metal surfaces. Corros Sci 1970;10:43–9. https://doi.org/10.1016/S0010-938X(70)80096-8.

[7]   Radojevic M. Reduction of nitrogen oxides in flue gases. Elsevier Ltd; 1998. https://doi.org/10.1016/b978-0-08-043201-4.50097-6.

[8]   Srivastava RK, Jozewicz W. Flue gas desulfurization: The state of the art. J Air Waste Manag Assoc 2001;51:1676–88. https://doi.org/10.1080/10473289.2001.10464387.

[9]   Ting T, Stanger R, Wall T. Laboratory investigation of high pressure NO oxidation to NO2and capture with liquid and gaseous water under oxy-fuel CO2compression conditions. Int J Greenh Gas Control 2013;18:15–22. https://doi.org/10.1016/j.ijggc.2013.06.016.

[10]   Hume S. Enabling Staged Pressurized Oxy-Combustion: Improving Flexibility and Performance at Reduced Cost. 2019.

[11]   White V, Torrente-Murciano L, Sturgeon D, Chadwick D. Purification of oxyfuel-derived CO2. Energy Procedia 2009;1:399–406. https://doi.org/10.1016/j.egypro.2009.01.054.

[12]   Murciano LT, White V, Petrocelli F, Chadwick D. Sour compression process for the removal of SOx and NOx from oxyfuel-derived CO2. Energy Procedia 2011;4:908–16.

https://doi.org/10.1016/j.egypro.2011.01.136.

[13] White V, Wright A, Tappe S, Yan J. The Air Products Vattenfall oxyfuel CO2compression and purification pilot plant at schwarze pumpe. Energy Procedia 2013;37:1490–9. https://doi.org/10.1016/j.egypro.2013.06.024.

[14] Tumsa TZ, Lee SH, Normann F, Andersson K, Ajdari S, Yang W. Concomitant removal of NOx and SOx from a pressurized oxy-fuel combustion process using a direct contact column. Chem Eng Res Des 2018;131:626–34.

[15] Iloeje C, Field R, Ghoniem AF. Modeling and parametric analysis of nitrogen and sulfur oxide removal from oxy-combustion flue gas using a single column absorber. Fuel 2015;160:178–88. https://doi.org/10.1016/j.fuel.2015.07.057.

[16] Hume S, Yang Z, Kumfer B, Axelbaum R, Dhungel B, Slater JD, et al. Improving Flexibility and Performance of Staged Pressurized Oxy-Combustion. 14th Greenh. Gas Control Technol. Conf. Melb., 2018, p. 21–6.

[17] Yang Z, Khatri D, Verma P, Li T, Adeosun A, Kumfer BM, et al. Experimental study and demonstration of pilot-scale, dry feed, oxy-coal combustion under pressure. Appl Energy 2021;285:116367. https://doi.org/10.1016/j.apenergy.2020.116367.

[18] Ajdari S, Normann F, Andersson K, Johnsson F. Reduced Mechanism for Nitrogen and Sulfur Chemistry in Pressurized Flue Gas Systems. Ind Eng Chem Res 2016;55:5514–25. https://doi.org/10.1021/acs.iecr.5b04670.

[19] de Visser E, Hendriks C, Barrio M, Mølnvik MJ, de Koeijer G, Liljemark S, et al. Dynamis CO2 quality recommendations. Int J Greenh Gas Control 2008;2:478–84.

https://doi.org/10.1016/j.ijggc.2008.04.006.

[20]   Wetenhall B, Race JM, Downie MJ. The Effect of CO2 Purity on the Development of
       Pipeline Networks for Carbon Capture and Storage Schemes. Int J Greenh Gas Control
       2014;30:197–211. https://doi.org/10.1016/j.ijggc.2014.09.016.

[21]   Tsukahara H, Ishida T, Mayumi M. Gas-phase oxidation of nitric oxide: Chemical kinetics
       and rate constant. Nitric Oxide - Biol Chem 1999;3:191–8.
       https://doi.org/10.1006/niox.1999.0232.

[22]   Lee YN, Schwartz SE. Reaction kinetics of nitrogen dioxide with liquid water at low
       partial pressure. J Phys Chem 1981;85:840–8. https://doi.org/10.1021/j150607a022.

[23]   Wang J., Himmelblau DM. Kinetic Study of Sulfur Dioxide in aqueous solution with
       radioactive tracers. AICHE J 1964:574–80.

[24]   Normann F, Jansson E, Petersson T, Andersson K. Nitrogen and sulphur chemistry in
       pressurised flue gas systems: A comparison of modelling and experiments. Int J Greenh
       Gas Control 2013;12:26–34. https://doi.org/10.1016/j.ijggc.2012.11.012.

[25]   Ajdari S, Normann F, Andersson K, Johnsson F. Gas phase oxidation of SO2 by NO2 in
       pressurized flue gas systems - an experimental investigation. Energy Procedia
       2013;46:2011–3.

[26]   Verma P, Gromotka Z, Yablonsky G, Stokie D, Constales D, Kumfer B, et al. Optimizing
       complexity in the kinetic modelling of integrated flue gas purification for pressurized oxy-
       combustion. Chem Eng J 2020. https://doi.org/10.1016/j.cej.2019.122875.

[27]   Stokie D, Verma P, Kumfer BM, Yablonsky G, Suresh AK, Axelbaum RL. Pilot-scale

testing of direct contact cooler for the removal of SOx and NOx from the flue gas of pressurized oxy-coal combustion. Chem Eng J 2021;414:128757. https://doi.org/10.1016/j.cej.2021.128757.

[28] Axelbaum R, Stokie D, Verma P, Kumfer B, Min Y, Zhu Y, et al. Integrated Flue Gas Purification and Latent Heat Recovery for Pressurized Oxy-Combustion. 2019.

[29] Stanger R, Ting T, Spero C, Wall T. Oxyfuel derived CO2 compression experiments with NOx, SOx and mercury removal-Experiments involving compression of slip-streams from the Callide Oxyfuel Project (COP). Int J Greenh Gas Control 2015;41:50–9. https://doi.org/10.1016/j.ijggc.2015.06.022.

Chapter 7. Quantitative analysis of the impact of flue gas recirculation on the efficiency of oxy-coal power plants.

7.1 Introduction

Fossil fuels are abundant, widely-distributed, and reliable, yielding an uninterrupted supply of energy worldwide. However, they produce large quantities of anthropogenically-derived carbon dioxide (CO_2) [1]. Most agencies that evaluate and project future world energy scenarios have identified the need for the continued use of fossil fuels, but with a means to capture the carbon dioxide produced from its combustion [1,2]. Carbon capture, utilization, and sequestration (CCUS) has been demonstrated as a viable means of mitigating the impact of climate change, in both pilot and full-scale power plants [3,4].

Among the different methods of capturing carbon dioxide from coal-fired power plants, oxy-coal combustion is considered as one of the most promising [5]. In oxy-combustion, the fuel is combusted with a mixture of oxygen and recycled flue gas (RFG). Typically, 60–70% of the flue gas is recycled back to the combustor [4,6,7]. This large amount of flue gas recycle (FGR) is typically required to control the flame temperature in the combustor, and thereby maintain heat flux profiles to the steam tubes that are similar to those in conventional, air-fired power plants [8]. After condensing the moisture in the flue gas, the product stream from oxy-combustion is a concentrated stream of CO_2, which can be purified and compressed for utilization or sequestration. Although first-generation oxy-combustion power plants—with carbon capture—have been shown

to be promising and technically feasible, their net plant efficiencies are up to 10 percentage points lower (25% relative) than traditional air-fired combustion without carbon capture [9]. This large energy penalty leads to an increase in the cost of electricity [10], hindering broad acceptance of the technology. The reduction in efficiency is due to the parasitic energy requirements of 1) the air separation unit (ASU) used to produce oxygen, 2) the gas processing unit (GPU) for CO_2 purification and compression, and 3) the recycle of flue gas to control heat flux.

Recognizing that the energy required to compress CO_2 downstream of the boiler is comparable to the energy required to compress the O_2 feedstock upstream, in recent years pressurized oxy-combustion (POC) has been developed as an advanced oxy-combustion technology [11–13]. Since the CO_2 produced during oxy-coal combustion is ultimately compressed to ~ 150 bar for utilization or sequestration, pressurizing the combustion process has no additional energy cost. At the same time, pressurizing the combustion process has several advantages [12]. One of the major advantages is that at higher pressure, the moisture in the flue gas condenses at a higher temperature. Thus, the latent heat of condensation can be recovered and integrated to the steam cycle, resulting in an increase in plant efficiency [14]. Studies have shown that by increasing the operating pressure of the boiler to around 10 bar and recovering the latent heat of the moisture in the flue gas, the plant efficiency can be increased by around 3 percentage points [11,14,15]. Further increases in operating pressure have limited impact on plant efficiency [15].

While pressurization of the combustion process holds promise for increasing the efficiency of the oxy-combustion power plant, additional improvements are needed to ensure broad implementation of the POC technology. For both atmospheric and pressurized oxy-combustion, the ASU and

135

GPU are fundamental requirements, however, the large amount of FGR is not. Rather, FGR is merely a convenient method to control wall temperature and heat flux. Several groups have focused on the attractiveness of oxy-fuel pulverized coal power plants, in terms of their similarity to air fired plant and commercially available component. The aim to remain operationally close to air-fired plant ensures that a high amount of FGR is employed to control the heat flux and heat flux profiles to be similar to air-fired units [16,17]. The use of flue gas recycle, primary recycle for fuel delivery, and secondary recycle—constituting the majority—for controlling the heat flux has been employed for various types of oxy-fuel plants, including pulverized coal fired and circulating fluidized bed systems [18]. However, a fundamental thermodynamic study on the impact of designing such a potentially "drop-in" system has not been properly investigated [19].

In fact, several investigators have identified that FGR has a negative impact on plant efficiency, and have proposed methods to reduce it [12,20,21]. For instance, Prof. Spliethoff's group in TU Munich has tried using a controlled non-stoichiometric burner design to reduce the flue gas recycle to as low as 50% [21], and Kobayashi and Bool discuss the challenges and several potential strategies for oxy-fuel power plant design with minimal to no flue gas recycle [22]. The SPOC process [12,23,24] is an example of a process that is designed to reduce recycle in pressurized oxy-coal combustion. All these process concepts are essentially various methods proposed to overcome the challenge of a higher oxygen concentration in the combustor—as the FGR is reduced—through various novel burner and process design solutions. However, to the best of our knowledge, the benefits of reducing FGR in oxy-combustion have neither been fully understood, nor systematically quantified.

Often the goal of reducing FGR is justified only on the grounds of reducing fan-power requirements. However, in this chapter, we will show that while the fan power loss is significant, it is not the most important reason for the plant efficiency reduction caused by high FGR. This chapter mainly focuses on dry flue gas recycle, where the flue gas is recycled downstream of the gas cleanup unit operations, such as particulate filters, flue gas desulfurization units, and moisture condensers [10,25,26]. Wet recycling, on the other hand, involves recycling of flue gas prior to the gas cleanup unit, where it is still hot, contains acid gases and ash particles. While wet recycling could avoid a significant amount of exergy losses described in this chapter, it is associated with several practical challenges like corrosion and erosion and will not be discussed in this chapter. Rather, since the proportion of studies and demonstration plants using dry recycle is much more than wet recycle, in this chapter we will focus on the impact of dry FGR on the efficiency and performance, for both atmospheric and pressurized oxy-combustion. Additionally, to keep the analysis focused on the thermodynamic impact of recycle we have combined the primary and secondary recycle as one recycle stream. Various proposed combinations of primary and secondary recycle can be understood using the same methodology. Similarly, the advantage of reduced air-ingress in pressurized oxy-combustion—with the potential to delivery higher purity CO_2, reducing the cost of CPU—is also not discussed in this work, as it deviates from the focus of this work. The impact of reduced air-ingress can easily be added on top of the gains / losses discussed herein.

Finally, it is important to note that the scope of the manuscript is to clarify the impact of the critical parameter of flue gas recycle ratio on the efficiency of oxy-combustion power plants—both atmospheric and pressurized—using thermodynamic analysis. The novelty of this work comes from clearly and quantitatively explaining the fundamental reason for the reduction in plant

efficiency with FGR. This comes at a time when there is significant interest in reducing flue gas recycle in oxy-combustion, without a clear explanation or quantification of the benefit of FGR reduction. This work yields a set of simple algebraic equations that can be used in the optimization of FGR for any oxy-combustion plant concept. For completeness, the results from a detailed plant model developed in ASPEN Plus are also presented—as a confirmation of the accuracy of the thermodynamic analysis.

7.2 Methodology

7.2.1. Parallel heat exchangers (PHX): Quantifying heat integration capacity

A simplified process flow diagram for the gas side of a first-generation oxy-combustion plant is shown in Figure 7.1. As described previously, the fuel is combusted with a mixture of oxygen and recycled flue gas within the boiler. The resulting flue gas heats the boiler tubes (carrying water/steam) and enters the preheater where it heats the cold RFG coming from the flue gas re-heater. The temperature of the flue gas stream into the preheater must be maintained above the acid dew point to avoid corrosion. From the preheater, the flue gas goes through various gas cleanup equipment, typically including an Electrostatic Precipitator (particulate removal), Flue Gas De-sulfurization (SO_x removal), and Direct Contact Cooler Polishing Scrubber (moisture and SO_x removal/conditioning). Around 60-80% of this flue gas from the DCCPS is typically recycled back to the boiler, and the rest is sent to the GPU for purification and compression.
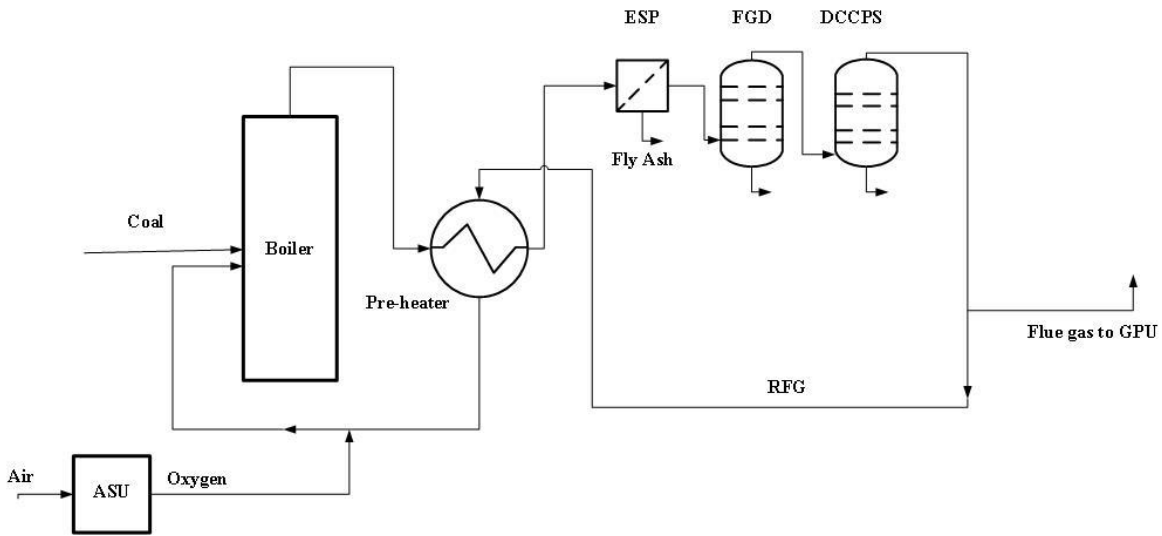
Figure 7.1. First-generation oxy-combustion process flow diagram. ESP: Electrostatic Precipitator; FGD: Flue Gas De-sulfurization; DCCPS: Direct Contact Cooler Polishing Scrubber.

To study both the integration of heat from the gas side to the steam side and the effect of FGR on plant efficiency, a base steam cycle, as shown in Figure 7.2, is constructed. The steam conditions are as in Gopan et al. [12], where the key assumptions and approaches follow the guidelines from the NETL's QGESS [27]. The steam cycle considered here is a single reheat supercritical Rankine cycle, with the main steam at 242 bar and 593 °C, and the reheat steam at 49 bar and 593 °C. The steam cycle parameters are presented in Table 7.1. Seven indirect feedwater heaters (FWH) and one direct feedwater heater for de-aeration are used in the steam cycle. This arrangement is typical in the power industry [28].
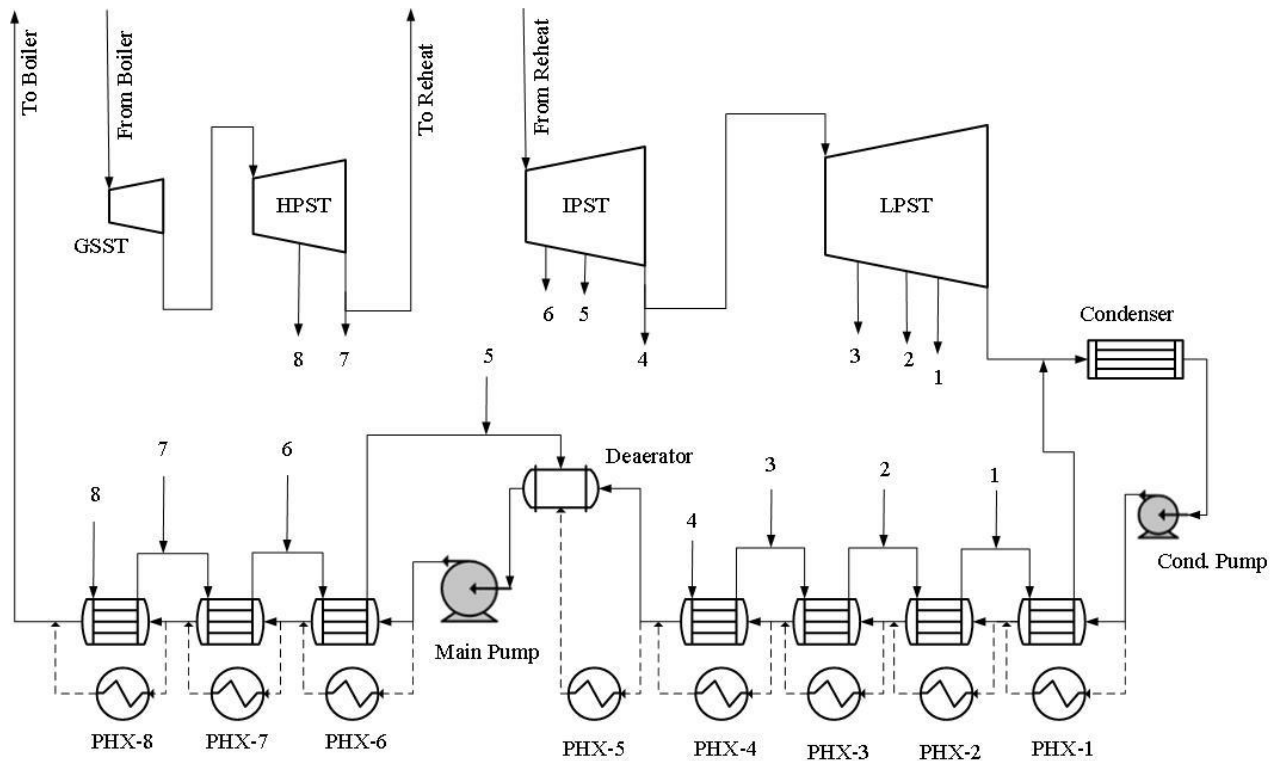
Figure 7.2. Simplified steam cycle with PHXs for thermal integration. GSST: Governing Stage Steam Turbine, HPST: High Pressure Steam Turbine; IPST: Intermediate Pressure Steam Turbine; LPST: Low Pressure Steam Turbine; PHX: Parallel Heat Exchanger.

Table 7.1 Key steam cycle process parameters

Parameter	Value
Governing stage efficiency	85 %
High-pressure efficiency	91.5 %
Intermediate-pressure efficiency	94 %
Low-pressure efficiency	89.2 %
Generator efficiency	98.8 %
Motor efficiency	97%
Condenser pressure	0.048 bar
Terminal temperature difference	11.7 °C

If additional heat is available from the flue gas stream or the ASU, and can be used for regeneration

of boiler feed water (BFW), the amount of steam bleeding from the turbine can be reduced and,

140

consequently, the gross power production increased. Depending on the temperature at which this additional heat is available, its integration will result in different amounts of increased electricity production, and thereby increases in net plant efficiency (NPE). To quantify the conversion efficiency from thermal to electrical energy for these heat sources, conceptual parallel heat exchangers (PHXs) are employed [26] (as shown in Fig. 7.2). The thermal to electrical energy conversion ratio for each of the PHXs is defined as the marginal efficiency of the FWH [26]. The concept of marginal efficiency is the manifestation of the 2nd law of thermodynamics in the form of heat integration principles. Since, the exergy of the heat integrated to the FWHs operating at different temperature ranges is different, the work produced from these FWHs for the same amount of heat integration will be different as well. Consequently, the FWHs operating at higher temperature—having a higher exergy or availability—have higher marginal efficiency. This methodology makes it easier to conceptualize and calculate the amount of electric work that can be produced by any given energy source if the temperature and the quantity of thermal energy are known. In this study, the concept of PHXs and marginal efficiency is extended to include the temperature range for the boiler, and the steam generator, superheater, reheater, and economizer can be lumped into a single unit—the boiler. It should be noted that marginal efficiency is a function of the steam cycle rating and configuration. Mathematically, it can be represented as

$$\eta(T) = \frac{\Delta W_{el}}{\Delta Q_{th}} \tag{1}$$

Figure 7.3 presents the marginal efficiency as a function of temperature. In this work, the steam cycle modelling for heat integration and the calculation of marginal efficiency are performed using Aspen Plus (v8.8) for a 550 MW_e power plant. The marginal efficiency of the other FWHs was calculated and is presented in Figure 3. They were found to be the same as found in Hagi et al. [26]. Additionally, the marginal efficiency of the thermal energy transferred by the boiler was

calculated to be 54%. The total work obtained from the integration of all the heat sources can be

represented as

$$\Delta W_{int} = \sum_i^n \eta_i Q_i \tag{2}$$

The change in net plant efficiency due to exergy losses caused by recycling flue gas is then given

by

$$\%\Delta NPE = \frac{\Delta W_{int}}{Q_{coal}} \tag{3}$$

where Q_{coal} is the higher heating value (HHV) of the coal.

	Temperature Range (C)
PHX1	32—67
PHX2	67—102
PHX3	102—137
PHX4	137—172
PHX5	172—205
PHX6	231—240
PHX7	240—280
PHX8	280—310
Boiler	> 330
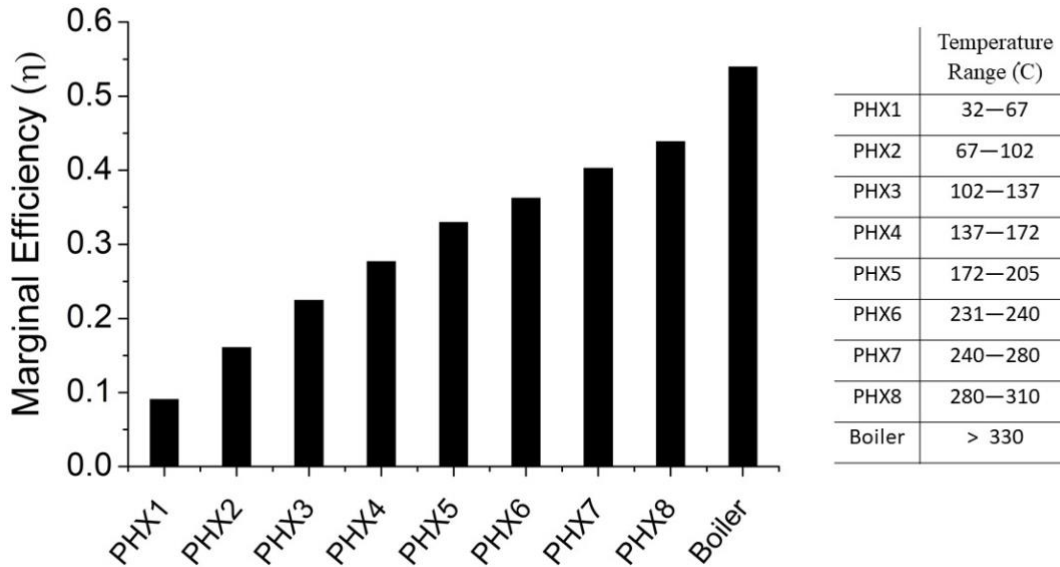
Figure 7.3 Marginal Efficiency as a function of temperature

It is important to note that there is a limit to the amount of heat that can be integrated to each

parallel heat exchanger. Starting from a well-designed steam cycle with no integration, the steam

bleeding ratio from the turbines decreases as the amount of heat integrated through a PHX

increases. Once sufficient heat is integrated—such that the bleed ratio directed to the

corresponding FWH becomes zero—no additional heat can be integrated to that PHX, and the remaining heat must be integrated into a PHX at a lower temperature.

7.2.2. Simplification of a power plant: Quantifying the effect of FGR

For illustration purposes, as shown in Figure 4, we conceptualize the power plant as being made up of a High Temperature (HT) block—including the boiler, superheater, reheater, and economizer—and a Low Temperature (LT) block, which is comprised of a flue gas pre-heater. The demarcation between the HT and LT blocks is based on the practical integration of heat into the steam cycle. Typically, in first-generation oxy-combustion power plants, only heat from the HT block is integrated into the steam cycle [10]. However, for an efficiently valorized oxy-combustion power plant, the excess heat from the LT block can also be integrated into the steam cycle as LT economizing heat [29]. Additionally, a Loss block is added to the model to lump all unit operations that primarily lose heat from an energetic viewpoint. In first generation oxy-combustion power plant, the loss block includes FGD, DCCPS, etc. which operate at flue gas temperatures below its acid dew point. As these unit operations run at relatively low temperatures, the recovery of heat using BFW or steam is economically infeasible—rendering these unit operations as essentially heat loss units. The temperature at which the flue gas comes out of the economizer in a power plant is typically in the range of 330–350 °C, and hence this temperature is used to distinguish between the HT and LT blocks. Due to acid-dew-point considerations, a temperature of 140 °C is used to separate the LT block from the Loss block.

143
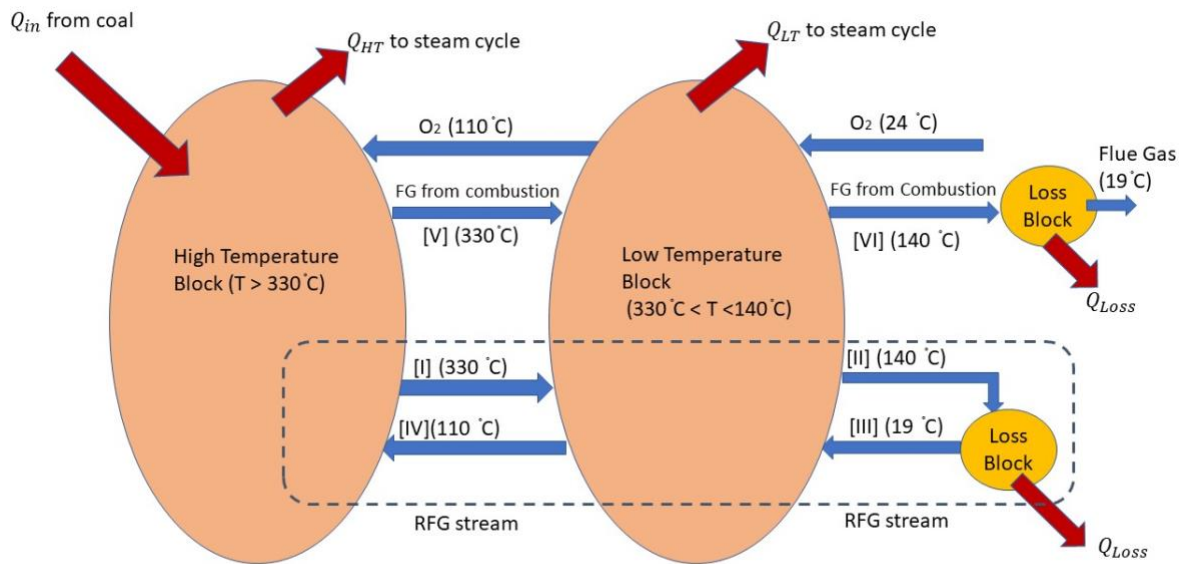
Figure 7.4 Simplified block diagram to understand the effect of flue gas recycle on cycle efficiency.

To understand the effect of FGR on power plant efficiency, the recycled flue gas is treated separately from the oxygen stream. In this way, the oxy-combustion plant can be considered to be made up of two "streams", as depicted in Figure 7.4. The first stream, which is shown in the top part of the figure, is the "oxygen stream"—which is the stream that would exist if there were no FGR. This stream includes the incoming oxygen preheated by the LT block, which is mixed and combusted with coal in the HT block, and the flue gas resulting from the oxygen/coal combustion that flows from the HT block to the LT block and then to the Loss block. The second stream, shown at the bottom of the diagram, consists of the recycled flue gas, which circulates between the High Temperature, Low Temperature, and the Loss blocks. As can be seen, the RFG stream essentially transports part of the heat from the HT block to the LT block, and further downstream to the Loss block. In practice, part of the heat from the RFG may be required for coal drying,

however it is negligible compared to the overall recycle. Also, following the work of [29], the maximum temperature of preheating the RFG in the preheater (LT block) is assumed to be 110 °C. Since the National Energy Technology Lab (NETL) assumes an even lower temperature of 55 °C [13,14], this lower temperature will also be considered for comparison. Due to such constraints in preheating, surplus heat is available in the flue gas after heating the incoming RFG. In a valorized oxy-combustion power plant, this heat is integrated into the steam cycle. In a non-valorized plant, the flue gas in the LT block is simply cooled using cooling water to a temperature of 140 °C before entering the Loss block (FGD, DCCPS, etc.) [15,20,29].

For the baseline assumption of zero flue gas recycle (ZR), an energy balance equation on the HT block can be written to obtain the energy available to the steam cycle from that block as:

$$Q_{ZR,HT}^{out} = m_c HHV_c + m_{o_2} c_{O_2,HT} \Delta T_{O_2,HT} - m_{FG} c_{p,I} \Delta T_I, \tag{4}$$

where m_c and m_{o_2} are the mass flow rates of the coal and oxygen fed into the HT block respectively, m_{FG} is the mass flow rate of flue gas coming out of it, HHV_c is the higher heating value of the coal, and $c_{p,O_2,T_{in}}$ and $c_{p,I}$ are the average specific heats of the oxygen into and the flue gas out of the HT block, respectively, and the deltas for temperature are the difference from a reference temperature.

For a fixed exhaust gas temperature from the HT block (herein assumed to be 330 °C), the heat available from the HT block to the steam cycle reduces with increasing RFG because part of the heat of combustion is used to increase the temperature of the RFG entering the HT block (Stream IV) to the exit gas temperature. If Q_{HT}^{out} is the amount of thermal energy obtained from the boiler when the mass flow rate of the recycled flue gas is m_{RFG}, the change in the thermal input to the

steam cycle from the HT block—compared to a case without flue gas recycle—can be expressed

as

$$\Delta Q_{HT} = Q_{ZR,HT}^{out} - Q_{HT}^{out} = m_{RFG}(c_{p,IV}T_{IV} - c_{p,I}\,T_I), \tag{5}$$

where, T_{IV} is the temperature at which RFG enters the HT block (stream IV), and T_I is the

temperature at which flue gas exits the HT block. If the marginal efficiency of the HT Block is

η_{HT}, the change in the electrical work produced from the HT block can be written as

$$\Delta W_{elec,HT} = \eta_{HT}\left(Q_{ZR,HT}^{out} - Q_{HT}^{out}\right) = \eta_{HT}\,m_{RFG}(c_{p,IV}T_{IV} - c_{p,I}\,T_I), \tag{6}$$

A similar analysis for the LT block will yield the heat available for the steam cycle (assuming

valorization) for the case of zero FGR as

$$Q_{ZR,LT}^{out} = m_{FG}\left(c_{p,V}T_V - c_{p,VI}\,T_{VI}\right) - m_{O_2}\left(c_{p,O_2}T_{IV} - c_{p,O_2}T_{O_2}\right), \tag{7}$$

where $c_{p,i}$ is the specific heat capacity of stream i and T_{O_2} is the temperature of oxygen entering

the LT block. When FGR is introduced, the change in heat available to the steam cycle from the

LT block is

$$\Delta Q_{LT} = Q_{ZR,LT}^{out} - Q_{LT}^{out} = m_{RFG}\left[\left(c_{p,I}T_I - c_{p,II}\,T_{II}\right) - \left(c_{p,III}T_{III} - c_{p,IV}\,T_{IV}\right)\right] \tag{8}$$

If the marginal efficiency of the LT Block is η_{LT}, the change in the electrical work produced from

the LT block is

$$\Delta W_{elec,LT} = \eta_{LT}\,m_{RFG}\left[\left(c_{p,I}T_I - c_{p,II}\,T_{II}\right) - \left(c_{p,III}T_{III} - c_{p,IV}\,T_{IV}\right)\right] \tag{9}$$

Neglecting fan losses, the change in the net plant efficiency due to flue gas recycle can be

expressed in terms of the changes in electrical work output from the HT and the LT blocks

$$\%\Delta NPE = \frac{\left(\Delta W_{elec,HT} + \Delta W_{elec,LT}\right)}{Q_{coal}} = \frac{\left(\eta_{HT}\Delta Q_{HT} + \eta_{LT}\Delta Q_{LT}\right)}{Q_{coal}} \tag{10}$$

Note that equation (4), (5), (7), and (8) are the manifestation of the first law of

thermodynamics—quantifying the change in energy transferred to the steam cycle as a function

of the amount of flue gas recycle. Equations (6) and (9) then multiply that heat (first law) with the marginal efficiency (second law of thermodynamics) to finally quantify the useful work done by the heat, *i.e.*, electricity produced, and consequently the net plant efficiency in equation (10).

7.3 Results and Discussions

7.3.1. Understanding the Effect of Recycle

There are two means by which efficiency is reduced (exergy is destroyed) when flue gas is recycled. As the HT block represents the highest temperature region, any transport of energy from the HT block to a lower temperature region will destroy some exergy and produce less electricity, as expected from the marginal efficiency curve (Fig. 3). Only a part of the energy transported from the HT block by FGR is exchanged in the LT block, either as gas pre-heating or as steam cycle integration. The remainder is transported to the Loss block, which has a conversion efficiency of zero. This transport of energy to the Loss block with zero conversion efficiency is the first means of exergy destruction. However, even the part of the energy transported from the HT block, which is exchanged with steam in the LT block (LT block heat valorization case), the significant difference in marginal efficiency between the HT and the LT block adds to the loss in efficiency due to FGR. In a non-valorized power plant—as is typical in first generation oxy-combustion design—this loss gets further exacerbated due to zero conversion in the LT block—leaving only the recovery due to pre-heating of RFG.

Figures 7.5 and 7.6 show the heat available from the HT and LT block to the steam cycle as a function of FGR. It is interesting to note that decreasing the recycle ratio from 80% to 70% halves

the loss of heat from the HT block (RFG flow rate halves), while the loss is nearly linear with recycle ratio in the 0–40% range. As is evident from these figures, the change in the amount of energy available to the steam from the HT block due to FGR, ΔQ_{HT}, is a linear function of the RFG flow rate. However, the relationship between ΔQ_{HT} and the more commonly used parameter, flue gas recycle ratio, is not linear, and ΔQ_{HT} falls sharply at high recycle ratios. The reason for this non-linear behavior is the often-overlooked hyperbolic relationship between recycle ratio and RFG flow rate, which is shown in Figure 7.7.
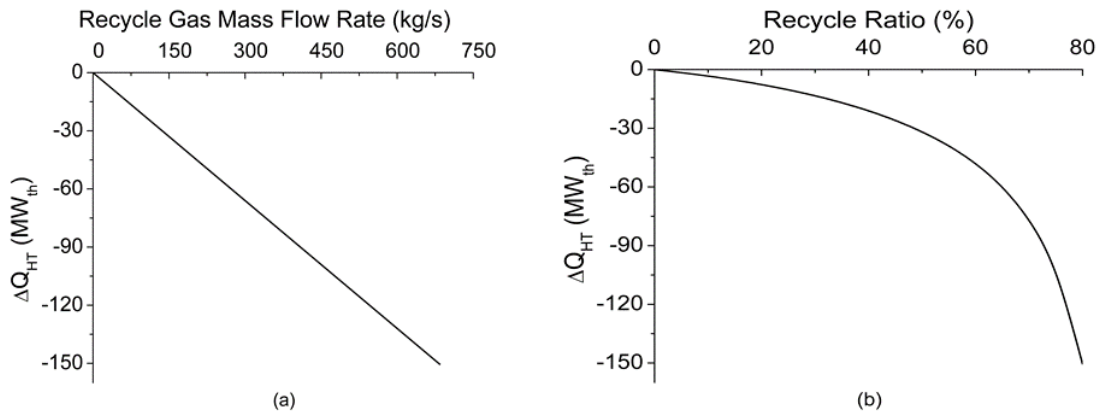
Figure 7.5 Change in the thermal energy transferred to steam cycle from HT block.
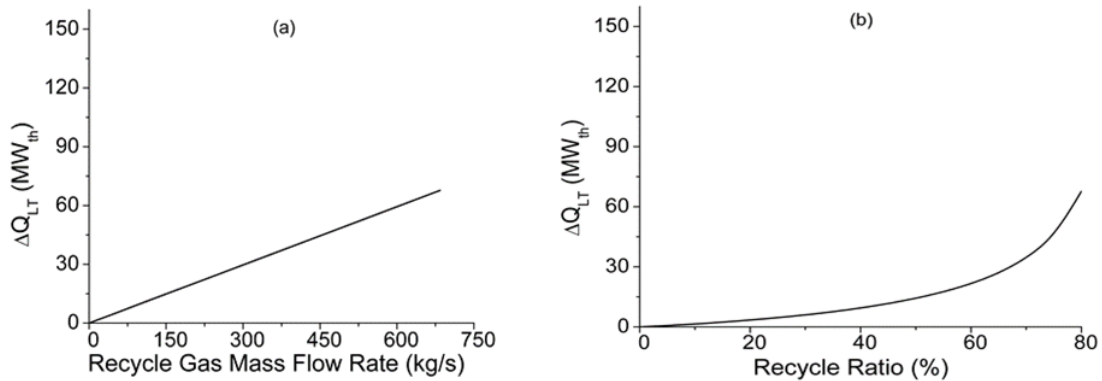
Figure 7.6 Change in the thermal energy transferred to steam cycle from LT block.
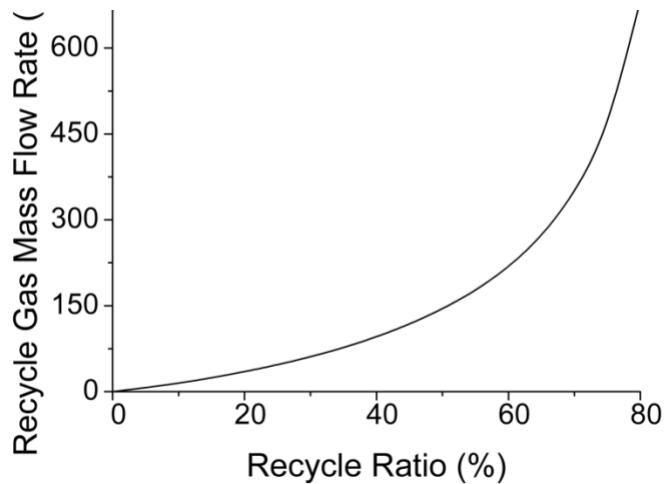
Figure 7.7 Flue gas mass flow rate as a function of recycle ratio.

The effect of this non-linearity is not only evident in the non-linear exergy destruction at high recycle ratios but also in fan power losses. Fan power as a function of recycle ratio and recycle mass flow rate is shown in Figure 7.8. This is derived using a simplifying assumption of fan power being proportional to the momentum flux, and scaling the fan power requirement from that presented in [10]. For low recycle—up to 40% recycle ratio—the fan power does not affect plant

efficiency because the mass flow rate of the flue gas being recycled is low. The NETL report accounting for the power requirement for the induced and forced draft fans indicate that the fan power losses for close to 60% recycle ratio is also negligible compared to other auxiliary loads in the system [30]. On the other hand, at very high recycle ratios (say, in flameless combustion) a significant loss in plant efficiency would result due to fan power requirements. This loss would be exacerbated for high temperature (wet) recycle due to the lower density associated with high temperature and the presence of water vapor in the flue gas.
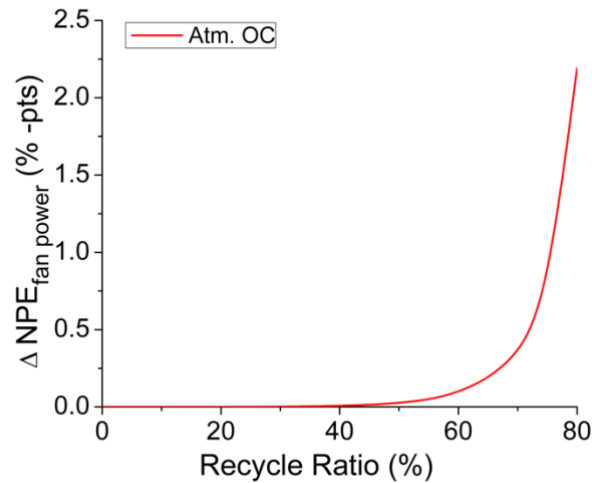
Figure 7.8 Change in net plant efficiency due to fan power requirements as a function of recycle ratio.

NOTE: The efficiency loss due to fan power is not considered further in this work. Also, only the efficiency loss due to exergy destruction caused by dry recycle of flue gas is presented.

The change in the net plant efficiency of the first-generation oxy-combustion plant with increasing recycle ratio (from zero—a conceptual plant, to 80%—as in a flameless concept) and the flow rate

is shown in Figure 7.9. The efficiency is seen to decrease sharply at the higher recycle ratios for both valorized and non-valorized cases, with a higher loss for the non-valorized case. As expected, the temperature to which the RFG is heated in the preheater (LT block) has an impact on the NPE, with the lower temperature case (55 °C, NETL) resulting in a larger loss in efficiency compared to the higher temperature (110 °C, EDF) case. This is because, for the lower temperature (NETL) process, even though more heat is available to the steam cycle from the LT block (less heat is spent in pre-heating RFG), the reduction in exergy—and thus electricity—is much more, and results in a lower net plant efficiency. However, once again, due to the low RFG mass flow rate at recycle ratios below 33%, the impact of pre-heat temperature is also limited at low recycle ratios.
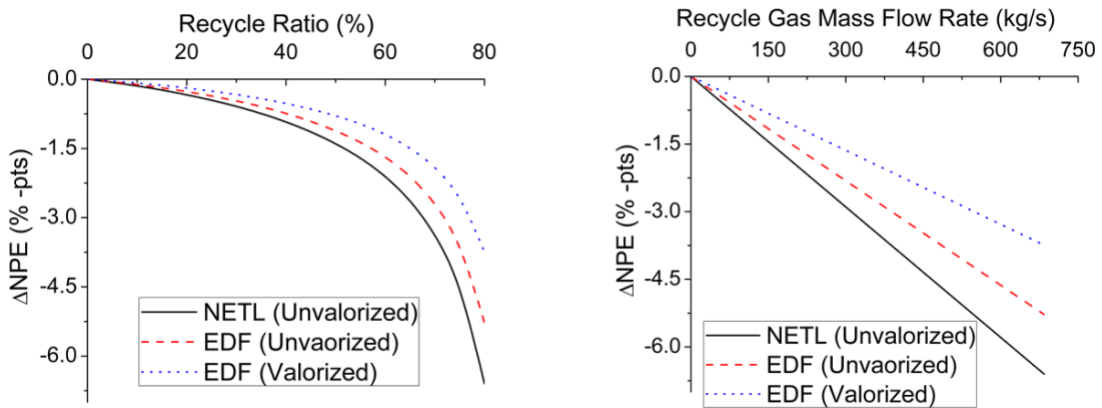
Figure 7.9 Change in Net Plant Efficiency as a function of recycle ratio and recycle flue gas flow rate.

As noted above, only the efficiency loss due to exergy destruction is considered here. The fan power consumption for recycling the flue gas reduces the NPE by an additional 0.5 percentage points for 70% recycle. The combination of these two effects (exergy and mechanical losses) results in a significant efficiency penalty associated with FGR, particularly at high FGR.

7.3.2. Effect of Flue Gas Recycle on Pressurized Oxy-Combustion
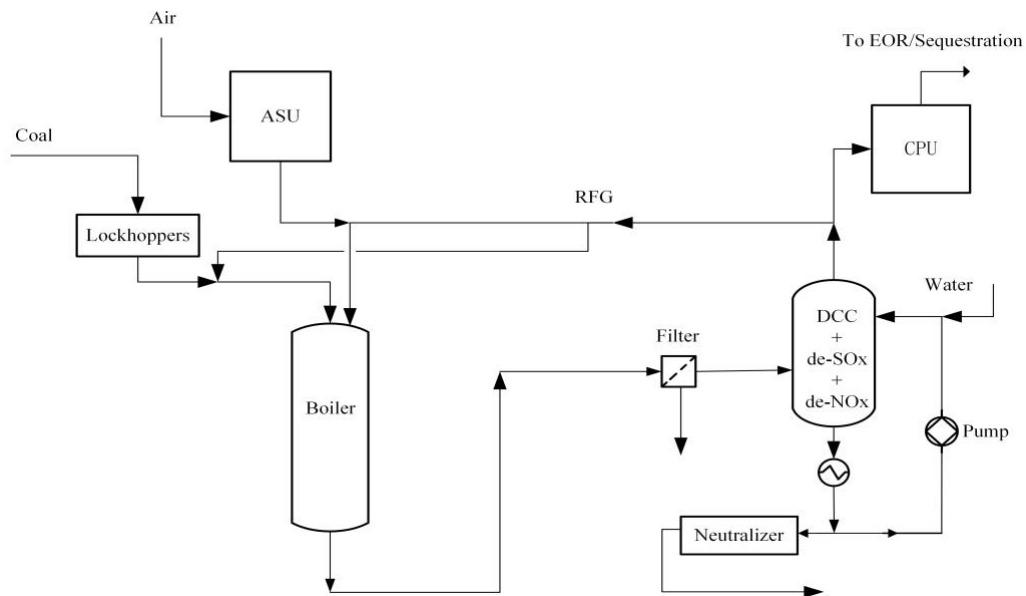
Figure 7.10 Pressurized oxy-combustion process flow diagram. ASU: Air Separation Unit; DCC: Direct Contact Cooler; RFG: Recycle Flue gas; CPU: Compression and Purification Unit.

As mentioned in Section 7.1, pressurized oxy-combustion (POC) has several advantages over atmospheric oxy-combustion. Notably, the plant efficiency is higher because at higher pressure the moisture in the flue gas condenses at a higher temperature, such that the latent heat of condensation of the moisture can be integrated into the steam cycle, unlike with atmospheric oxy-combustion where the latent heat is completely lost (in the Loss block). The power plant considered for pressurized oxy-combustion is presented in Figure 7.10. The HT block of the POC process is the same as for atmospheric pressure oxy-combustion, however, the LT block includes the latent heat of the flue gas moisture, in addition to the sensible heat from the flue gas (available at atmospheric pressure). The heat available from the flue gas in the LT block (latent and sensible) can be integrated into the steam cycle using either an indirect heat exchanger (IDHX)—where the

boiler feed water and the flue gas do not contact each other, or a Direct Contact Column (DCC)—

a reactive absorption column that employs direct contact with cooling water to recover both the

latent heat and sensible heat from the flue gas [12]. Although an IDHX is more attractive

thermodynamically than a DCC, it poses corrosion risks due to acid condensation on the tube

surfaces, which would require the use of expensive alloy materials. The DCC, on the other hand,

in the process of latent heat recovery, the DCC also removes most of the acids from the flue gas

[32,33]. However, as the acids are naturally diluted by the cooling water, the DCC does not pose

the same corrosion risks as an IDHX, potentially reducing cost. The cooling water coming out of

the DCC is at an elevated temperature and can be integrated with the steam cycle in a liquid-liquid

heat exchanger. It is assumed here—with a significant safety factor due to lack of experimental

data at these conditions—that flue gas temperatures below 330 °C could lead to acid condensation

[12]. Hence, the flue gas temperature at the inlet of either the IDHX or DCC is set to 330 °C. With

better prediction of acid dew point under pressurized oxy-combustion conditions (with variable

recycle) lower DCC inlet conditions could be assumed, and the exact amount of exergy destruction

due to the DCC would change. However, the broader conclusions of this work should be

unaffected.

The impact of the IDHX and DCC on the efficiency of the power plant also changes with recycle

ratio. Figure 7.11 shows the change in electric work obtained from both IDHX and DCC due to

flue gas cooling and moisture condensation as a function of the recycle ratio for a pressurized oxy-

combustion power plant operating at 15 bar. As with the atmospheric pressure cases, the change

in efficiency is measured by comparing it to a conceptual atmospheric pressure oxy-combustion

plant with zero flue gas recycle. Note that this does not represent the net change in plant efficiency

with recycle ratio for POCs, but only the additional electricity made available due integration of the latent and sensible heat of the flue gas. As expected, the total electric work from the LT block increases with increasing FGR for both the DCC and the IDHX. However, the electric work increases more sharply for the IDHX than the DCC because when the flue gas recycle ratio is increased in the DCC, the requirement of cooling water increases to avoid drying up the column stages. This requirement lowers the temperature of the cooling water outlet from the column. The lower temperatures lead to lower marginal efficiencies when integrated into the steam cycle. The marginal efficiency of the heat from the DCC decreases by about 20% as the recycle ratio increases from 0 to 80%. This change in marginal efficiency explains the trend that, although the total amount of heat recovered is not very different between the two cases, the electric work is lower for the DCC, including a lower increment with increasing recycle, *i.e.*, a smaller slope in the curve.
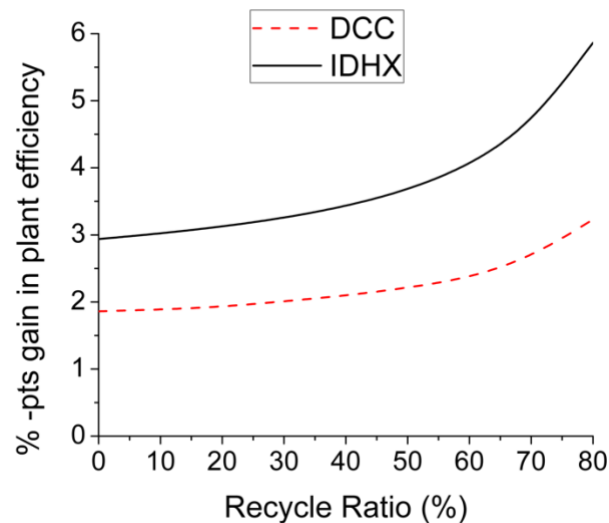
Figure 7.11 Gain in plant efficiency (percentage point) from Direct and Indirect integration of latent heat as a function of recycle ratio.

This effect of recycle on the DCC and IDHX can be coupled with the effect of recycle on the HT block (which remains the same as with first-generation oxy-combustion) to understand the overall effect of recycle on the efficiency of pressurized oxy-combustion. Figure 7.12 shows the change in NPE as a function of recycle ratio for both types of LT valorization in pressurized oxy-combustion. For the IDHX case, the difference with atmospheric pressure remains constant over the recycle range due to the similarity in configuration. However, with a DCC, the difference decreases at higher recycle flow rates due to the reduction in the marginal efficiency of the integration, as discussed above. Practically, this might be somewhat offset by the fact that with increasing recycle ratio there will be a reduction in the concentration of acid gases in the flue gas, and consequently the dew point temperature, allowing for a reduction in the DCC inlet temperature. However, the difference will not be significant at low recycle (up to 40%). The dotted line above 40% recycle for the DCC case, represents the theoretical analysis if the RFG temperature at the DCC inlet is kept constant.
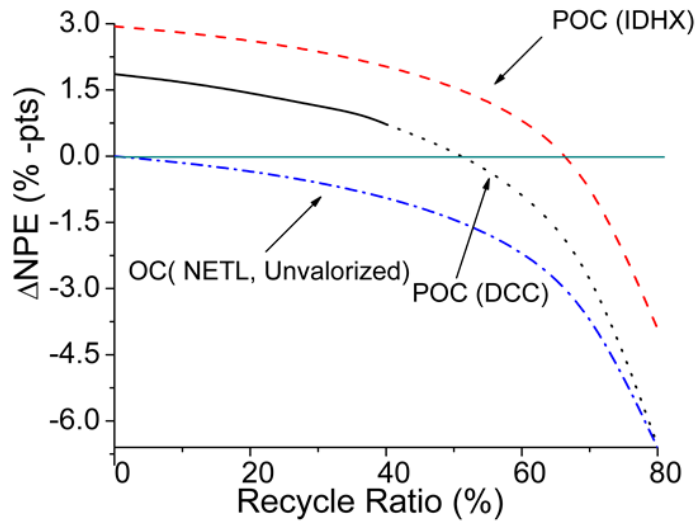
Figure 7.12 Change in NPE with flue gas recycle ratio for a POC power plant using an IDHX or DCC compared to an atmospheric pressure oxy-combustion power plant.

7.3.3. The effect of recycle on various proposed oxy-combustion systems

A succinct summary of the above thermodynamic analyses and how it applies to various proposed oxy-combustion systems is shown in Figure 7.13, where the efficiencies for select oxy-combustion strategies available in the literature are compared. The two curves represent the change in NPE with recycle ratio for pressurized oxy-combustion and atmospheric pressure oxy-combustion (Atm. OC). For illustration purposes, the NPE for POC considers the IDHX integration. As is evident from this figure, pressurized oxy-combustion with low-recycle significantly outperforms all other conceptual designs. The so-called Staged, Pressurized Oxy-Combustion (SPOC) process is an example of a pressurized oxy-combustion process with low recycle. The SPOC process uses fuel staging as a strategy for controlling the combustion and heat transfer processes when operating with low recycle [12,24]. Pressurizing a 1st generation atmospheric oxy-combustion process can be considered an example of high (traditional) FGR, whereas a flameless oxy-combustion system with dry FGR is an example of very high FGR. Figure 13 clearly shows that even with the

156

advantages of POC, if the recycle ratio is very high (> 80%), the POC process will be less efficient than a 1st generation atmospheric oxy-combustion process (60–70% recycle).
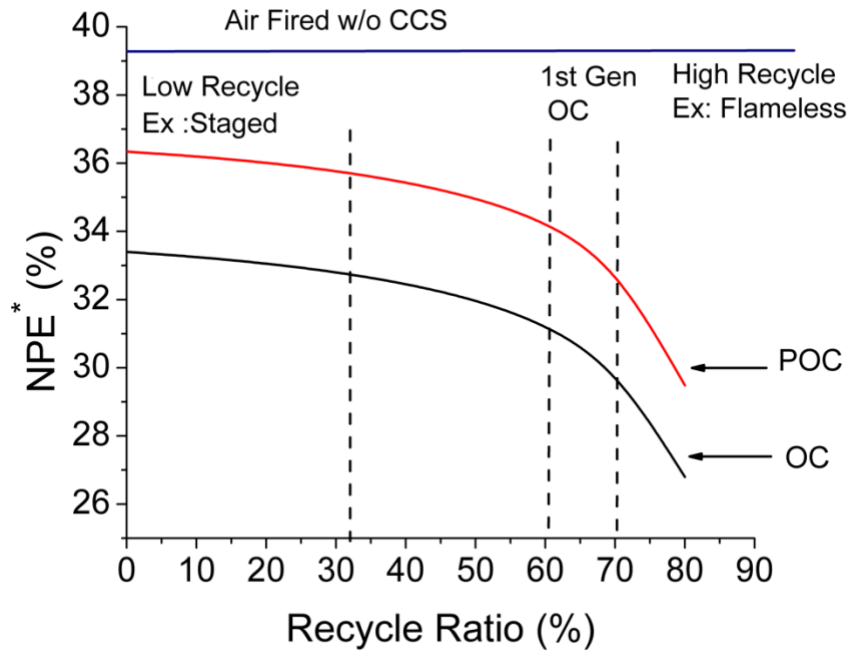
The impact of fan power on efficiency is not considered in this figure.

Figure 7.13 Comparison of Net Plant Efficiency of POC and Atm. OC for different regions of the recycle ratio space. POC is considered with IDHX.

7.4 Conclusions

It is known that reducing flue gas recycle increases the net plant efficiency of oxy-fuel combustion processes, and this has been the motivation for industrial and academic research to facilitate, with varying success, low recycle strategies for oxy-combustion. The novelty of this work is in clarifying, quantifying, and simplifying our understanding of the efficiency loss; in other words, to identify the main cause for the reduction in efficiency with recycle ratio, to understand how it varies with recycle ratio, and to identify what levels of recycle ratios are allowable without a significant loss in efficiency.

This work revealed that there is a strongly non-linear relationship between net plant efficiency and recycle ratio, with changes in recycle having a nearly-linear impact on efficiency at low recycle, and an almost exponential impact at high recycle. This is because recycle ratio—though a commonly used parameter—is misleading when trying to understand the impact of FGR. Recycle mass flow rate is the controlling parameter, and plant efficiency is linearly dependent on it. This work has also clarified that the loss in efficiency, especially at low recycle ratios, is primarily due to exergy destruction, with the flue gas carrying heat from a high grade to low grade with increasing recycle. Fan power loss, also being dependent on recycle mass flow rate, is negligible at low recycle, but becomes significant at high recycle ratios. Nonetheless, fan power plays a smaller role than exergy destruction. Wet recycle—which entails practical challenges due to the corrosive, erosive nature of wet recycle—has much lower exergy destruction, but fan power losses increase.

This work also demonstrated that pressurized oxy-combustion—touted to increase efficiency—may fail to do so if the flue gas recycle is kept as high as in 1st gen. oxy-combustion or flameless

oxy-combustion. On the other hand, at low recycle ratios, the marginal utility of further reduction in recycle may be low, and recycle ratios of 30–40% may be more practical than 0–30%.

Clearly, one of the most important points arising out of this work is the need to focus on developing methods to implement low recycle oxy-combustion systems with low cost and high reliability. Low recycle, pressurized oxy-combustion processes, such as SPOC, indicate a potential to increase the efficiency of carbon capture processes by more than 6%-pts. over 1st generation approaches, bridging the efficiency gap between non-CCUS and CCUS processes. This bridging could make CCUS a viable and attractive low carbon solution.

7.5 References

[1]   IPCC, Climate Change 2007 Synthesis Report.

[2]   EIA. Annual Energy Outlook 2018 with projections to 2050. Washington, D.C.: Energy Information Administration, United States Department of Energy, 2018.

[3]   F.L. Horn, M. Steinberg, Control of carbon dioxide emissions from a power plant (and use in enhanced oil recovery), Fuel. (1982).

[4]   R. Stanger, T. Wall, R. Spörl, M. Paneru, S. Grathwohl, M. Weidmann, G. Scheffknecht, D. McDonald, K. Myöhänen, J. Ritvanen, S. Rahiala, T. Hyppänen, J. Mletzko, A. Kather, S. Santos, Oxyfuel combustion for CO2 capture in power plants, Int. J. Greenh. Gas Control. (2015).

[5]   B.J.P. Buhre, L.K. Elliott, C.D. Sheng, R.P. Gupta, T.F. Wall, Oxy-fuel combustion technology for coal-fired power generation, Prog. Energy Combust. Sci. 31 (2005) 283–307.

[6]   G. Scheffknecht, L. Al-Makhadmeh, U. Schnell, J. Maier, Oxy-fuel coal combustion-A review of the current state-of-the-art, Int. J. Greenh. Gas Control. 5 (2011).

[7]   F. Carrasco-Maldonado, R. Spörl, K. Fleiger, V. Hoenig, J. Maier, G. Scheffknecht, Oxy-fuel combustion technology for cement production - State of the art research and technology development, Int. J. Greenh. Gas Control. 45 (2016) 189–199.

[8]   L. Chen, S.Z. Yong, A.F. Ghoniem, Oxy-fuel combustion of pulverized coal: Characterization, fundamentals, stabilization and CFD modeling, Prog. Energy Combust. Sci. 38 (2012) 156–214.

[9]   D. McDonald, D. DeVault, R. Varagani, Oxy-Combustion in Pulverized Coal Power Plants for Carbon Dioxide Concentration, Electr. Power Conf. (2007) 1–9.

[10]   Pulverized coal oxycombustion power plants. Bituminous Coal to Electricity, rev. 2, Report DOE/NETL-2007/1291, vol. 1. US Department of Energy, National Energy Technology Laboratory (2008).

[11]   J. Hong, G. Chaudhry, J.G. Brisson, R. Field, M. Gazzino, A.F. Ghoniem, Analysis of oxy-fuel combustion power cycle utilizing a pressurized coal combustor, Energy. 34 (2009) 1332–1340.

[12]   A. Gopan, B.M. Kumfer, J. Phillips, D. Thimsen, R. Smith, R.L. Axelbaum, Process design and performance analysis of a Staged, Pressurized Oxy-Combustion (SPOC) power plant for carbon capture, Appl. Energy. 125 (2014) 179–188.

[13]   L. Zheng, ed., Oxy-fuel combustion for power generation and carbon dioxide (CO2) capture.

[14]   A. Gopan, B.M. Kumfer, R.L. Axelbaum, Effect of operating pressure and fuel moisture on net plant efficiency of a staged, pressurized oxy-combustion power plant, Int. J. Greenh. Gas Control. 39 (2015) 390–396.

[15]   J. Hong, R. Field, M. Gazzino, A.F. Ghoniem, Operating pressure dependence of the pressurized oxy-fuel combustion power cycle, Energy. 35 (2010) 5391–5399.

[16]   P.R. S, S. G, Oxyfuel CO2 Capture for pulverized coal: An evolutionary approach, (2007) Document16.

[17]   B. Giancarlo, M. Massimo, G. Girardi, Innovative Oxy-coal Combustion process suitable for future and more efficienct zero emission power plants, (2008).

[18]   Eriksson TSippu OHotta AFan ZMyöhänen KHyppänen TPikkarainen TSee fewer, Oxyfuel CFB Boiler as a route to near zero CO2 emission coal firing, (2007) 1–23.

[19]   International Energy Agengy, Oxy Combustion Processes for CO 2 Capture from Power Plant, IEA Greenh. Gas R&D Program. (2005) 212.

[20]   T. Ochs, D. Oryshchyn, R. Woodside, C. Summers, B. Patrick, D. Gross, M. Schoenfield, T. Weber, D. O'Brien, Results of initial operation of the Jupiter Oxygen Corporation oxy- fuel 15 MWth burner test facility, Energy Procedia. 1 (2009) 511–518.

[21]   V. Becher, J.P. Bohn, A. Goanta, H. Spliethoff, A combustion concept for oxyfuel processes with low recirculation rate - Experimental validation, Combust. Flame. 158 (2011) 1542–1552.

[22]   H. Kobayashi, L.E. Bool, 12 - Direct oxy-coal combustion with minimum or no flue gas recycle, in: L.B.T.-O.-F.C. for P.G. and C.D. (CO2) C. Zheng (Ed.), Woodhead Publ. Ser. Energy, Woodhead Publishing, : pp. 259–272.

[23]   Z. Yang, D. Khatri, P. Verma, P. Du, R.L. Axelbaum, Characteristics of pressurized oxy-coal combustion in a 100 kWth, 15 bar combustor, in: 44th Int. Tech. Conf. Clean Energy, .

[24]   F. Xia, Z. Yang, A. Adeosun, A. Gopan, B.M. Kumfer, R.L. Axelbaum, Pressurized oxy-combustion with low flue gas recycle: Computational fluid dynamic simulations of radiant boilers, Fuel. 181 (2016) 1170–1178.

[25]   Advancing oxycombustion technology for bituminous coal power plants: An R&D guide. Report DOE/NETL - 2010/1405, US Department of Energy, National Energy Technology Laboratory (2012).

[26]   H. Hagi, T. Neveux, Y. Le Moullec, Efficiency evaluation procedure of coal-fired power plants with CO2 capture, cogeneration and hybridization, Energy. 91 (2015) 306–323.

[27]   Quality Guidelines for Energy System Studies: Process modeling design parameters. Report DOE/NETL - 341/042613. US Department of Energy, National Energy Technology Laboratory (2013).

[28]   H. Hagi, M. Nemer, Y. Le Moullec, C. Bouallou, Towards second generation oxy-pulverized coal power plants: Energy penalty reduction potential of pressurized oxy-combustion systems, Energy Procedia. 63 (2014) 431–439.

[29]   H. Hagi, M. Nemer, Y. Le Moullec, C. Bouallou, Optimal Integration of the flue gas heat for the minimization of the energy penalty of oxy-fired power plants, Energy Procedia. 63 (2014) 7359–7366.

[30]   M. Matuszewski, M.J. Turner, M. Woods, S. Chen, R.D. Brasington, J.L. Haslbeck, C. Zhang, Advancing Oxycombustion Technology for Bituminous Coal Power Plants: An R&D Guide, (2012).

[31]   B. Coal, E.F. Report, O.I. Date, Pulverized Coal Oxycombustion Power Plants Volume
       1 : Bituminous Coal to Electricity Final Report (Original Issue Date , August 2007),
       October. 1 (2007).

[32]   S. Ajdari, F. Normann, K. Andersson, F. Johnsson, Reduced Mechanism for Nitrogen and
       Sulfur Chemistry in Pressurized Flue Gas Systems, Ind. Eng. Chem. Res. 55 (2016)
       5514–5525.

[33]   S. Ajdari, F. Normann, K. Andersson, F. Johnsson, Modeling the nitrogen and sulfur
       chemistry in pressurized flue gas systems, Ind. Eng. Chem. Res. 54 (2015) 1216–1227.

[34]   M. Matuszewski, Cost and Performance for Low-Rank Pulverized Coal Oxycombustion
       Energy Plants, (2010) 442.

Chapter 8.   Process design and analysis of a novel carbon-capture-ready process for flexible-load power generation: Modular Pressurized Air Combustion

8.1 Introduction

The rapid socio-economic growth throughout the world is closely tied to the availability and reliability of electricity, especially in developing countries such as India, China, and Indonesia [1]. While electricity has been traditionally supplied from reliable sources such as fossil fuels, nuclear or hydro, grids are now experiencing a significant influx of intermittent renewable energy (IRE) sources, specifically wind and solar [2]. These weather- and time-dependent sources of energy are not dispatchable and thus, the penetration of IRE sources can lead to uncertainties in the reliability and stability of the grid.

In parallel with IRE integration, existing fossil-based power plants, especially coal-fired power plants, are being retired at alarming rates without replacement, especially in the U.S. and Europe. These plants are increasingly relied on as load-following resources to back up the IREs, as well as to provide critical ancillary services to the grid, such as grid inertia. Since traditional coal-fired power generation technologies were designed and optimized for baseload operations, these cycling requirements are causing deleterious effects on their thermal and environmental performance, maintenance costs, and integrity, potentially compromising their lifetimes [3]. Over the long-term,

wide-scale retirements of the existing fleet of coal-fired power plants may lead to the significant undermining of the reliability of the electricity supply [4].

The need for reliable, dispatchable generation, critical ancillary services and energy security, combined with uncertainties in natural gas prices, have created the potential for advanced coal-fired generation. Deployment of new coal plants requires a different perspective from that of today's utility-scale baseload power plant. To meet market and environmental needs, the future coal power plant should have high flexibility in addition to high efficiency, low cost, and near-zero-emissions (including carbon dioxide).

In the past decades, significant efforts have been extended in the development of coal-based technologies with carbon capture. Oxy-combustion is a promising approach for carbon capture. In oxy-combustion, the nitrogen is removed from the air such that the flue gas is primarily composed of CO_2 and H_2O, and CO_2 can be easily captured after condensing out the H_2O. While atmospheric oxy-combustion has been extensively explored the relatively low efficiencies stemming from penalties associated with the parasitic load of the ASU and high flue gas recycle has discouraged its implementation[5]. To improve the performance of oxy-combustion, pressurized oxy-combustion has been proposed in recent years and received much attention. Pressurized oxy-combustion offers several benefits over atmospheric oxy-combustion, the most important of which is the fact that the moisture in the flue gas condenses out at a higher temperature at high pressure. Hence, the latent heat can be recovered and integrated into the steam cycle, increasing the efficiency of the plant [6]. Additionally, the gas volume at high pressure is significantly reduced, which reduces the size of the equipment and potentially capital costs. Pressurization also reduces the costs of flue gas cleanup because at high pressure SOx and NOx can be scrubbed during the process of latent heat recovery. These advantages have enabled the introduction of several

pressurized oxy-combustion technologies, including staged, pressurized oxy-combustion (SPOC). The SPOC process further improves the efficiency and operational flexibility of the plant by minimizing flue gas recirculation and incorporating a modular boiler design. This process has been supported by the U.S. Department of Energy's Coal FIRST (Flexible, Innovative, Resilient, Small, and Transformative) initiative, and considered as one of the promising future coal plant concepts.

Despite the important role of carbon capture in fighting climate change globally, the demonstration and commercialization of the carbon capture technologies has been slow, due to their higher costs compared with conventional coal plants without carbon capture. Without incentives for CO_2 capture, the risk associated with these high-cost technologies will continue to impede investment for large-scale demonstration, which in return limits the chances for these technologies to reduce their initial costs by technological learning. For example, the wet FGD technology had an 11% learning rate (i.e., a decrease in capital cost of 11% for each doubling of installed capacity) in the first 20 years' implementation[7]. In the present environment, a carbon capture ready process, which has competitive performance and economics with conventional coal plants without carbon capture, as well as critical components that are also part of a carbon capture system, would be very attractive. The benefits of such a process are twofold: 1) once this process is commercialized, the capital costs of those critical components that are shared by a carbon capture process can gradually drop due to the power of learning-by-doing; 2) when regulations or economic opportunities for CO_2 capture are in place, the installed carbon capture ready plants can be retrofit to carbon-capture plants at relatively low cost, which reduces the investment risk by minimizing the impact of future regulations or policy changes.

With the demand for carbon capture ready technologies and the recognition that pressurized oxy-combustion holds great promise for carbon capture, the need exists to evaluate the potential of pressurized air combustion as a carbon capture ready technology. Consequently, this chapter aims to develop a conceptual design for such a plant that addresses the contemporary needs of coal-fired power plants, which include: 1) flexible operation, 2) high efficiency, 3) low cost, and 4) carbon-capture ready). The pressurized air combustion system will have two critical components that shared with a pressurized oxy-combustion system: 1) the pressurized PC boiler, and 2) SOx and NOx removal unit. The ultimate goal is to understand and quantify the potential benefits of the process. The proposed process - the modular pressurized-air combustion (MPAC) process - is found to yield a very high-efficiency flexible plant with a modular design, which allows for ease of construction and low-cost manufacturing, while being designed to be easily retrofit into the staged, pressurized, oxy-combustion (SPOC) process [8].

8.2 Process Description

The MPAC concept incorporates pressurized combustion of coal with air, in modular boiler design. A high-level process flow diagram for the proposed concept is presented in Figs. 8.1 and 8.2. The process consists of multiple combustion boilers, typically four. Air is compressed with a single- or multi-stage compressor before entering the boilers with pulverized coal (PC). The coal and air are distributed among the boilers in nearly equal amounts and the boilers are arranged in parallel such that all boilers have nominally the same design and operating conditions. Downstream of the pressurized boilers, the flue gas streams are combined and fed into a high-pressure heat recovery (HPHR) unit. In this unit, heat is extracted and integrated into the power cycle (Fig. 8.2). After the pressurized heat recovery unit, the flue gas is cooled to slightly above the acid dew point temperature and a particle filter is utilized to remove the fly ash particles.
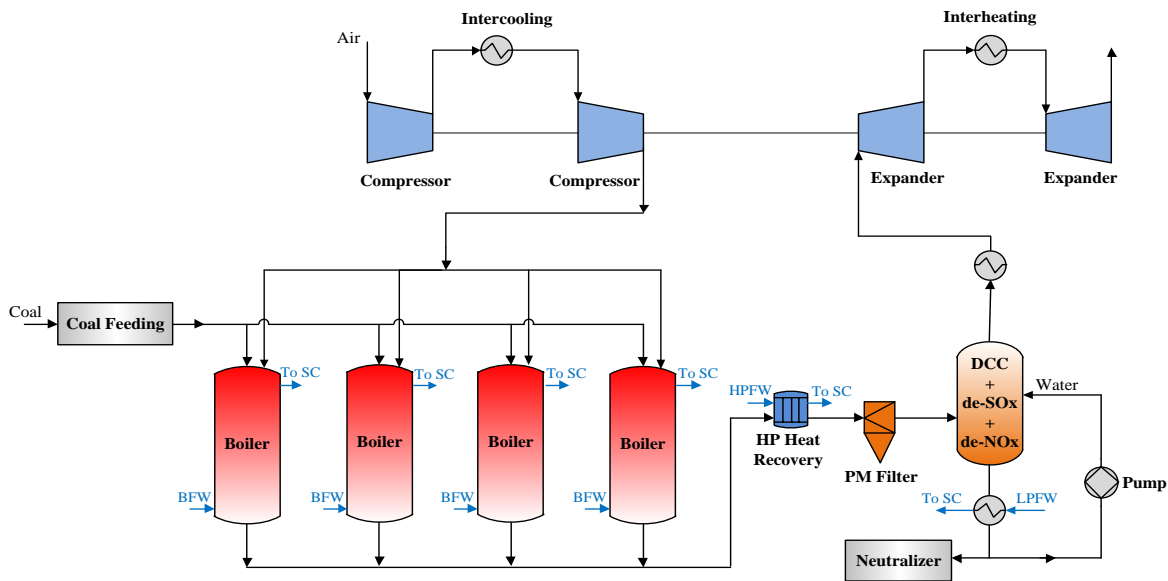
Figure 8.1 Gas-side process flow diagram for the MPAC process. SC: Steam Cycle; BFW: Boiler Feed Water; HPFW: High Pressure Feed Water; DCC: Direct Contact Column; LPFW: Low Pressure Feed Water
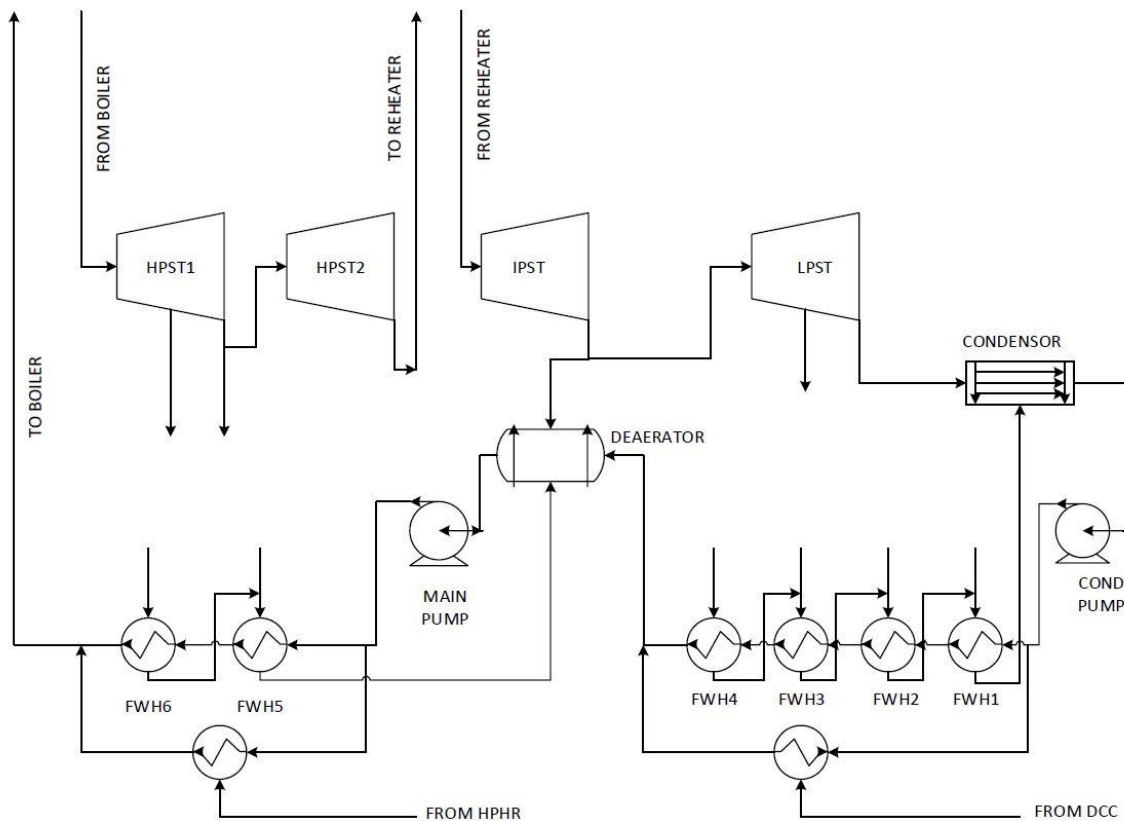
Figure 8.2 Steam-side process flow diagram of the MPAC process. FWH: Feed Water Heater; HPST: High Pressure Steam Turbine; IPST: Intermediate Pressure Steam Turbine; LPST: Low Pressure Steam Turbine; HPHR: High Pressure Heat Recovery; DCC: Direct Contact Column.

After particulate removal, the flue gas is further cooled in a concomitant pollutant removal (CPR) unit. The CPR unit is a direct-contact cooling (DCC) column, in which the flue gas flows against a stream of cooling water, thereby reducing the flue gas temperature and resulting in condensation of the flue gas moisture. Since the process is pressurized, the latent heat released from the moisture condensing in the flue gas is at a sufficiently high temperature that it can be used for boiler feed water heating (Fig. 8.2). The ability to utilize the heat of condensation from the flue gas moisture allows for an increase in plant efficiency over atmospheric-pressure systems. In addition, under

169

high pressure, sulfur- and nitrogen-containing species in the flue gas can be easily dissolved in the cooling water and removed. A detailed mechanism of this process is discussed in a later section. This process of SOx and NOx removal is much simpler and more cost-effective than traditional approaches for pollutant removal: flue-gas desulfurization (FGD) for removing SOx and selective catalytic reduction (SCR) for removing NOx.

After the CPR unit, the clean, particle-free flue gas is heated back to a higher temperature using part of the CPR heat. The heated flue gas then goes through a single- or multi-stage expansion turbine to produce power. If multi-stage compressors and multi-stage expansion turbines are employed, the compression heat is recovered by intercooling and used to heat the flue gas between turbine stages to increase the power output. In this way, most of the work consumed by the compressors is recovered by the power generated from the expansion turbines. The remaining part of the compressor work becomes the auxiliary load of the plant.

Compared with a conventional coal-fired plant, potential benefits of the MPAC plant include: 1) higher efficiency with comparable capital cost; 2) improved flexibility in load-following; 3) convertible to an advanced carbon capture plant with modest cost. The primary goal of this work is to evaluate the thermodynamic performance of the proposed plant. Other benefits will also be discussed here briefly and qualitatively. Detailed analyses of the economics and flexibility of the new plant will be presented in subsequent works.

Improved flexibility

Since demand can vary significantly hour-to-hour and day-to-day, as well as seasonally, flexibility has become one of the most sought-after characteristics of new dispatchable systems. Such systems should support efficient, baseload operation, as well as load following without significant loss in efficiency. Compared with a conventional PC power plant, the proposed MPAC plant potentially has much better flexibility, mainly due to three reasons: 1) the multiple, parallel-boiler configuration could allow for deeper turndown. The minimum load for a conventional PC plant is around 40%, constrained by combustion instability. However, the proposed MPAC plant could easily achieve even 12% load shutting down three boiler modules and turning the remaining boiler down to half load– a number that has never been achieved by existing industrial-scale coal-fired technologies; 2) Unlike the SCR unit used for NOx removal in conventional PC plants, the performance of the DCC is not constrained by load variation. In conventional PC plant, the temperature of the flue gas entering the SCR decreases when the plant operates at lower loads, which adversely affects the removal efficiency of the SCR. However, in the proposed plant, the removal efficiency of DCC increases at lower loads due to higher gas residence time. This feature makes it easier for the MPAC plant to operate at very low load; 3) the ramp rate and cold/warm start-up speeds of the proposed MPAC plant are potentially higher than a conventional PC plant because the size of each boiler module is much smaller than that of a conventional PC plant with comparable power output – e.g., for a 550 MWe MPAC plant, each boiler module is envisioned to have a 4.2-m diameter, while a PC boiler for a comparable-sized plant can be ~20 m x 20 m.

Higher Efficiency

The flue gas generated from coal combustion contains a considerable amount of moisture. The latent heat associated with this flue gas moisture is discarded in conventional coal power plants,

often referred to as the 'moisture loss'. This is an inherent loss because, at atmospheric pressure, the condensation temperature of this moisture is around 55°C, which is too low to be utilized in the steam cycle. The heat that is exhausted with the flue gas is typically 10–20% of the total heat input to the boiler. As the condensation temperature is strongly dependent on operating pressure, when the combustion process is pressurized, the moisture in the flue gas condenses out at a higher temperature, making it feasible to recover almost all the latent heat in the flue gas and utilize this heat to improve plant efficiency. If the additional power produced by this extra energy is higher than the net auxiliary load for pressurization (power consumed by pressurization minus power generated by expansion), which is true for the proposed MPAC plant as will be shown in the later sections, the pressurized combustion plant can have a higher net plant efficiency compared with existing coal plants. In this work, a comprehensive process model is built to evaluate the thermodynamic performance of the MPAC plant.

Competitive Cost

The proposed plant differs from a conventional coal plant mainly on the combustion side (i.e., fuel and oxidizer delivery, boiler, and flue gas cleanup systems). The steam cycle system for conventional coal plants can be used by the MPAC plant with only small changes. A detailed economic analysis for the MPAC plant is beyond the scope of this study, but an estimation can be made based on the economic analysis for a SPOC plant performed by the Electric Power Research Institute (EPRI) because major equipment is shared by both plants[9]. Cost scaling methods from the Capital Cost Scaling Methodology developed by the National Energy Technology Laboratory are used for this cost estimation. The capital costs of the fuel and oxidizer delivery systems for the MPAC plant are higher than those of a conventional coal plant due to the elevated pressure.

However, the cost of the boiler is lower because pressure can greatly enhance radiative and convective heat transfer, leading to reduced heat transfer surfaces in the boiler. By scaling from ERPI's cost data, the estimated total capital cost of the fuel and oxidizer delivery system and boiler for the MPAC plant is 29% higher than that of a conventional plant. The capital cost of the flue gas cleanup system for the MPAC plant is significantly lower than that of a conventional coal plant (64% reduction if scaled from the EPRI's result), due to the reduced flue gas volume at a higher pressure and the compact SOx and NOx simultaneous removal system (i.e., DCC). Considering the total plant cost, the MPAC plant has only 2% higher capital cost than a conventional coal plant.

It should be noted that the boilers and flue gas cleanup units for the MPAC plant are small enough to be manufactured in factories and then shipped to the power plant location to assemble [10]. This type of modular construction can potentially reduce the equipment manufacturing cost and plant construction costs, which has not been included in the above cost estimation. In addition, the modular design can facilitate on-time and within-budget plant construction, which is particularly important in the U.S., where recent coal power plant projects have encountered construction delays and cost overruns due to the lack of experienced labors locally.

Carbon Capture Ready

The proposed MPAC process can be retrofitted, with modest modifications, to be a SPOC process, which is one of the most promising carbon capture technologies for coal power generation [8]. The high efficiency of the SPOC process is achieved through the recovery of the latent heat of the flue-gas moisture, as it is in the MPAC process, plus fuel staging, which reduces the need for high flue gas recycle (FGR), which in turn can significantly reduce the efficiency of oxy-combustion

processes [11]. Figure 8.3 shows the SPOC process retrofitted from the MPAC process. The following modifications are made:

1) An air separation unit (ASU) is added between compressor stages to produce oxygen. Note that in a cryogenic ASU, the air is compressed before flowing into the separation column. Since air is already compressed in the MPAC process, the equipment cost for the air compressors can be avoided.

2) The expansion turbines are replaced by a CO_2 compression and purification unit (CPU) to produce CO_2 that is ready for transportation, utilization, and/or storage. Since the expansion turbines are removed, the compression heat extracted from the multi-stage compressors can then be integrated into the power cycle to increase power output.

3) The boilers are connected into a series-parallel configuration, unique to the SPOC process, in which a small portion of the flue gas coming out of the last-stage boiler is recycled back into the first stage. This FGR is used to dilute the oxygen entering the first-stage boiler. Then part of the flue gas coming out of the first-stage boiler is fed into the second stage to dilute the oxygen flow in this stage. By utilizing the flue gas from the first stage, instead of FGR, the total amount of FGR is reduced. The same process occurs for all downstream stages (i.e., oxygen is always mixed with part of the flue gas from the previous stage before it enters the present stage). In an atmospheric-pressure oxy-combustion process, around 70% flue gas is recycled back to the boiler to control combustion temperature, causing ~3% point efficiency loss [12]. The above unique mode of operation that SPOC utilizes minimizes FGR and maximizes efficiency. By adjusting the flow rates of the flue gas entering each stage, all stages can have similar operating conditions. Therefore, the plant

174

still maintains high flexibility, since the low load can be achieved by shutting down one or more boilers.
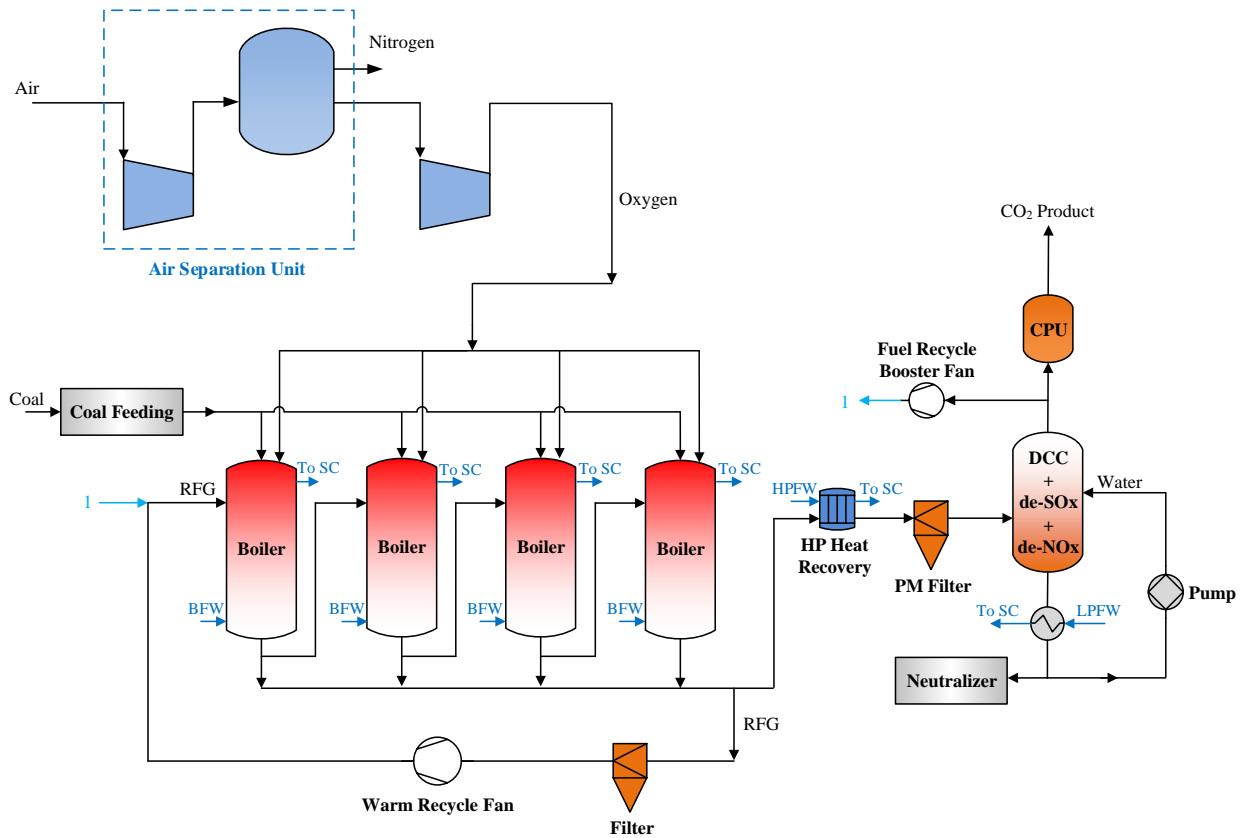
Figure 8.3 Retrofit process flow diagram of the SPOC process. SC: Steam Cycle; BFW: Boiler Feed Water; HPFW: High Pressure Feed Water; DCC: Direct Contact Column; LPFW: Low Pressure Feed Water; RFG: Recycle Flue Gas; CPU: Compression and Purification Unit.

More details of the SPOC process can be found in[8,9]. The majority of the equipment present in MPAC can be readily modified to accommodate the operation of the SPOC process. The boiler, HPHR, particulate filter, and the DCC remain integral to both systems, with a slight change in flow configuration. When retrofitting for carbon capture, the system also allows for additional load-following capability through energy storage (Fig. 8.3), in which pressurized, liquid oxygen can be stored in times of low demand and utilized in times of peak demand[13]. This mode of operation, with onsite storage, ensures that the system can operate closer to design capacity by

175

reducing the ramping of the power plant. This also improves the overall economics of the plant because the sale of electricity can be maximized during times of high prices, and since there is less cycling, this mode of operation yields less wear and tear on the plant.

Other benefits of both the MPAC and SPOC process include 1) enhanced combustion performance due to the higher partial pressure of oxygen and CO_2; and 2) suitability for low-rank, high-moisture coals because by recovering the latent heat of the moisture, the fuel is effectively "upgraded".

8.3 Methodology for Process Analysis

8.3.1 Modeling Approach

Aspen Plus™ (v9) software was employed for modeling the MPAC process. The property method used for gas-side modeling was Peng-Robinson, and Steam-TA (steam tables) was used for modeling the steam cycle. For the reactive absorption modeling of the DCC, the ELECNRTL method was used. Illinois #6 bituminous coal was assumed, and the design characteristics of the coal are provided in Table 8.1. To make a comparison with established air-fired combustion and oxy-combustion processes, the modeling assumptions and parameters were taken in accordance with the National Energy Technology Laboratory (NETL) studies [14–16]. A 550 MWe (net) MPAC power plant is modeled with a supercritical Rankine cycle – 241 bar/593°C/593°C (3500 psig/1100°F/1100°F). The site conditions of a generic Midwest ISO location were used, as shown in Table 8.2. The parameters of the steam-cycle modeling are detailed in Table 8.3. The motor efficiencies of the generator and steam turbine were taken from the DOE process modeling guideline [16]. The steam cycle was slightly modified from the generic NETL case to integrate the

low-grade heat from the flue gas side. Two additional parallel heat exchangers were attached with the traditional feedwater heaters to make use of heat from the HPHR system and the DCC (Fig. 8.2). This also ensures the lowest exergy loss of the heat integrated to the steam cycle. The design, operating, and performance characteristics of the key components of the MPAC process are shown in Table 8.4.

Table 8.1 Design Coal Characteristics: Illinois #6

Proximate Analysis	Wet Basis, %
Moisture	11.12
Ash	9.70
Volatile Matter	34.99
Fixed Carbon	44.19
Total	*100.00*
Heating Value	**Wet Basis**
HHV, kJ/kg	27,113
Ultimate Analysis	**Wet Basis, %**
Carbon	63.75
Hydrogen	4.50
Nitrogen	1.25
Sulfur	2.51
Chlorine	0.29
Ash	9.70
Moisture	11.12
Oxygen (by difference)	6.88
Total	*100.00*

Table 8.2 Site Conditions

Site Conditions	Midwest ISO
Elevation, m	0
Barometric pressure, MPa	0.101
Design ambient dry bulb temperature, °C	15
Design ambient wet bulb temperature, °C	10.8

Design ambient relative humidity, %	60
Cooling water temperature, ℃	15.6
Air composition, mass %	
H_2O	0.616
Ar	1.280
CO_2	0.050
O_2	22.999
N_2	75.055
Total	100

Table 8.3 Key Steam Cycle Process Parameters

Parameter	Value
High-pressure efficiency, %	91.5
Intermediate-pressure efficiency, %	94
Low-pressure efficiency, %	89.2
Generator efficiency, %	98.8
Motor efficiency, %	97
Condenser pressure, bar	0.048 (0.7)
Terminal temperature difference, ℃	11.7 (21.1)

Table 8.4 Key Component Data

Component/Subsystem	Technology type, basis for design and performance	Operating Condition			
		Inlet		**Outlet**	
		Temp (℃)	Pressure (MPa)	Temp (℃)	Pressure (MPa)
Air compression unit	NETL Guidelines	15	0.1	117	1.6
Coal milling	Vendor data/Commercial Design	25	0.1	49.5	0.1
Coal feeding	Pneumatic dry feed	49.5	0.1	53	1.6
Boilers (I-IV)	Vendor data/Self-defined	Coal: 50 Air: 117	1.6	340	1.6

HP heat recovery	Vendor data/Commercial design	340	1.57	200	1.54
Particulate filter	Candle Filter, Vendor data/Commercial design	200	1.54	200	1.52
DCC	Counter-flow packed bed	200	1.52	55	1.47
Flue gas heater	Vendor data/Commercial design	55	1.47	110	1.46
Expander unit	NETL Guidelines	110	1.46	15	0.1
Steam turbine	NETL Guidelines	593	24.2	32.2	0.005

8.3.2 Boiler and HPHR

For modeling the combustion of coal in Aspen Plus, solid modeling guidelines from ASPEN were followed and the coal was modeled as a non-conventional solid. The outlet temperature from each combustor was kept at 340°C. A heat loss of 1% from the boiler section was taken into account based on the NETL guidelines[16]. The flue gas enters the HPHR unit at 340°C and leaves at 200°C. The temperature of 200°C for the outlet of the HPHR was selected based on the assumed acid dew point temperature. Although there is no experimental data on acid dew point under pressure (at 15 bar), the empirical estimation of SO_3 formation in pressurized air combustion from studies at atmospheric pressure suggests that the dew point should be close to 200°C [17–19]. The sensitivity study shows that the net plant efficiency decreases marginally (close to 0.2% points) if the acid dew point increases to 250°C from 200°C. The energy from the HPHR is utilized in the boiler feedwater (BFW) heater added in parallel to the high-pressure BFW heaters (Fig. 2). The HPHR system keeps the exergy of the heat integration high before it is lowered significantly in the DCC, enhancing the overall efficiency of the steam cycle.

8.3.3. Direct-Contact Cooler

The DCC is a counter-current reactive-absorption column that recovers the latent heat of moisture as well as sensible heat from the flue gas. The flue gas is scrubbed and cooled using circulating water entering the column at a temperature of 42°C (part of which is recycled) to cool the flue gas and condense the moisture in it. The circulating water exits at a temperature higher than 127°C. This water is neutralized, and the thermal energy is used in two places, the steam cycle and to heat the outlet flue gas to a high temperature before expansion. In the steam cycle, the energy from the DCC replaces the energy that would typically need to be extracted from the steam taps of the low-pressure steam turbine, which in turn increases the overall efficiency of the cycle.

The other critical function of the DCC is that it can remove SOx and NOx from the flue gas. The main acidic gases that are formed in coal combustion are SO_2, SO_3, NO, and NO_2. SO_3 and NO_2 have a high solubility in water and are easy to remove. The gases that are most difficult to remove from the flue gas are SO_2 and NO. In a conventional air-fired coal power plant, an SCR is used to remove NO and an FGD is used to remove SO_2.

Under elevated pressure, the rate of conversion of NO to NO_2 is very high as compared to atmospheric pressure. The experiment by Timothy et al.[20] to estimate the conversion of NO to NO_2 under different pressure provides clear evidence of this phenomenon, where the conversion of NO increases 8 fold as the pressure is increased from 1 bar to 15 bar. This provides a means to remove all four gases in the same column [21]. The kinetics of integrated SOx and NOx removal in a pressurized combustion environment has been studied in detail by several groups [22–24]. The optimized kinetic model suggests that the reaction mechanism can be characterized by a mechanism of five reactions [25], as shown in Table 5. The mechanism primarily includes: 1) the oxidation of NO to NO_2; 2) its subsequent dissolution in water to form HNO_2 and HNO_3; 3) the

dissolution of SO_2 in water to form HSO_3^-; and 4) the interaction of HNO_2 and HSO_3^- in the liquid phase to form H_2SO_4 and HADS. The main parameters that control the removal of SOx and NOx from the flue gas are: 1) the reaction rate for the oxidation of NO to NO_2; 2) the ratio of NOx/SOx in the flue gas; 3) the temperature profile in the DCC; and 4) the operating conditions of the DCC, including inlet temperatures and pH.

Table 8.5 Reactions Mechanism and Kinetics

	Reaction	References
1	$2NO + O_2 \rightarrow 2NO_2$	[26]
2	$2NO_2 + H_2O \rightarrow HNO_2 + HNO_3$	[27]
3	$SO_2 + H_2O \leftrightarrow HSO_3^- + H^+$	[22]
4	$HNO_2 + HSO_3^- \rightarrow HSO_4^- + \frac{1}{2} N_2O + 0.5 H_2O$	[28]
5	$HNO_2 + 2HSO_3^- \rightarrow HADS + H_2O$	[28]

The reactions described in Table 8.5 are used for the simulation, with the equilibrium reactions handled directly within Aspen Plus. The kinetics of Reactions 1, 2, 4, and 5 were provided in the form of a power-law expression in Aspen Plus, while Reaction 3 was treated as an equilibrium reaction. The packing material for gas-liquid contact was considered to be metal Raschig rings. The circulating water flow rate required for recovery of latent and sensible heat from the flue gas was based on the outlet flue gas moisture concentration with the target moisture concentration kept to less than 1.5% v/v. Depending on the ease of transportation and the design of the column, a single column or two columns in parallel can be employed. In this work, a single column was used as an example.

8.3.4 Air Compression and Flue Gas Expansion Unit

A systematic study on the effect of pressure on latent heat of moisture recovery similar to the one conducted by Akshay et al. [11] suggests that there is a marginal net plant efficiency gain above 16 bar. Hence, the combustion pressure was selected as 16 bar and the air is compressed to 2.5 bar, 6.3 bar, and 16 bar, successively in three stages. Intercoolers are employed between each compression stage to keep the compression work to a minimum. The heat extracted from the intercoolers is synced with the flue gas expanders, where heating is required after each stage expansion. Since this unit provides the highest parasitic load to the system, the optimal pressure ratios for the compression-expansion unit is used to keep the extra work to a minimum [29]. The temperatures and pressures for compression and expansion are provided in Table 8.6.

Table 8.6 Compression and Expansion Parameters

Compression Stage	Pressure (bar)		Temperature (℃)	
	Inlet	Outlet	Inlet	Outlet
1st	1.01	2.54	12.0	113.5
2nd	2.54	6.37	18.0	117.5
3rd	6.37	16.00	18.0	117.8
Expansion Stage				
1st	15.00	6.10	114.0	37.7
2nd	6.10	2.48	77.9	14.4
3rd	2.48	1.01	101.9	27.3

8.4. Result and Discussion

8.4.1. Plant Performance

Efficiency and Auxiliary Load Comparison

The net plant efficiencies for the MPAC plant and the NETL base case air-fired power plant are provided in Table 8.7. The net plant efficiency (HHV) for the MPAC process is 1.7% higher than that of the NETL base case. Note that the steam cycle employed in the NETL base case and the current MPAC case does not represent the state-of-the-art design. But as the concept of recovering the latent heat of moisture in the flue gas is not affected by the power cycle of the plant, the above efficiency gain will still hold, indicating that the MPAC process is effectively the most efficient PC combustion process available. Table 8.7 shows that almost 60% of the auxiliary load in the MPAC process is from compression, indicating that minimizing the net compression loss by choosing appropriate pressure ratios among stages of compressors is important. Additionally, since the air is already under pressure, the fuel and air delivery fans in the MPAC process are not required, reducing the total parasitic load. The rest of the load remains equivalent to the NETL base case. However, the total electricity production is increased as compared to the atmospheric pressure process.

Table 8.7 Auxiliary Load and Performance Comparison

Performance Parameter	Units	MPAC	Air Fired	SPOC [5]	1st Gen. Oxy. *
Gross Power Output (after generator loss)	MWe	601.9	584.1	729.1	787.8
Compression loss	MWe	29.0	-	-	-
Total Oxygen Production load	MWe	-	-	127.0	126.7
Total clean up and CPU load	MWe	4.9	4.5	19.4	77.35
Other auxiliaries and miscellaneous balance of plant	MWe	18.0	25.18	31.6	33.53
Total Auxiliary Power	MWe	51.9	29.68	178.0	237.8
Net Power Output	MWe	550	554.4	555.1	550.0
Net Plant Efficiency (HHV)	%	41.4	40.7	36.7	29.3
Thermal Input (HHV)	MWth	1328.5	1349.57	1511.8	1879.2

The calculated boiler efficiency is 86.5% for the MPAC power plant and 87.7% for the SPOC power plant. The value remains comparable because in the SPOC process, the oxygen concentration in each boiler is 30%. Existing studies have found that, to match the adiabatic flame temperature of oxy-combustion with that of air-combustion, the burner inlet oxygen mole fraction of oxy-combustion needs to be increased to 28% and 35% for wet and dry recycle respectively, to compensate for the higher heat capacities of H_2O and CO_2 compared with N_2. Therefore, the adiabatic flame temperature in the furnace of the SPOC process should be comparable to that of the MPAC process. In terms of heat transfer, air combustion may have a slightly lower radiative heat transfer rate than oxy-combustion (the radiative heat transfer in pressurized coal combustion is expected to be dominated by particle emission and absorption), but the convective heat transfer rate of air combustion should be a little higher due to a higher volumetric flow rate. Overall, the gas temperatures in the furnace and boiler are expected to be comparable between the MPAC and SPOC systems and hence similar boiler efficiencies.

The auxiliaries for the carbon-capture counterparts of the two power plants, namely, SPOC and first-generation oxy-combustion, are higher because of the load from the air separation unit. However, the efficiency of the SPOC system is almost 7% points higher than that of first-generation oxy-combustion, mainly because of latent heat capture in the DCC and staged combustion, which allows for operation with minimal FGR, thus minimizing exergy loss in the boiler.

Efficiency Breakdown

184

As mentioned above, the main parasitic load to the MPAC system comes from compression and expansion. Although thermodynamically the energy produced from the expansion of one mole of CO_2 is 40% greater than that to compress one mole of oxygen, the overall isentropic efficiency of compression and expansion makes the process energy-intensive. The compression and expansion process costs almost 2% points to the MPAC process compared to the atmospheric air combustion process. The efficiency of the MPAC process is improved by the DCC, which helps increase the efficiency by 2.71% points through the recovery of the latent heat of moisture and the sensible heat of the flue gas, resulting in an overall efficiency gain of 0.7% points. The breakdown can be seen in Fig. 8.4.
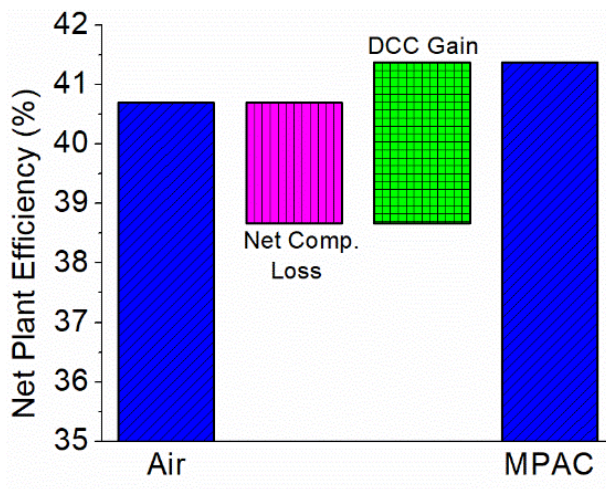
Figure 8.4 MPAC efficiency comparison with air

Integrated SOx and NOx Removal

The modeling results suggest that all of the SO_3 and NO_2 present at the inlet of the column is removed in the first few stages of the column. The removal of NO from the flue gas is limited by the slow oxidation of NO to NO_2 and this reaction controls the total flue gas residence time in the column. The removal of SO_2 is governed by the two liquid-phase reactions between HNO_2 and

HSO_3^-. Although there is evidence that the NO concentration decreases with pressure, for the purposes of this study we have performed a conservative estimation of the NO concentration assuming an NO emission intensity of an atmospheric PC boiler[30–32]. The residence time of the column for an NO outlet concentration of less than 100 ppm is estimated and compared with the removal in oxy-combustion for the same residence time. For SO_2, depending on the amount of sulfur in coal, retention and SO_3 formation, a low-temperature polisher may be required for complete removal. Table 8.8 presents the flue gas composition before entering the DCC. The results suggest that a residence time of 110 seconds is required to remove NO to an acceptable level. The comparison between removal efficiency for pressurized air and pressurized oxy-combustion is presented in Figure 8.5. Since the flue gas flow rate is reduced in oxy-combustion the removal is much higher for NO with higher residence time in the same column. It should be noted that, in practice, the pressurized air combustion plant may incorporate two DCC columns in parallel to ensure each column is small enough to be manufactured in a factory. When the plant is converted to a pressurized oxy-combustion plant, one of the columns can be removed. In this way, the change of the gas flow rate in the DCC from air-mode to oxy-mode is much smaller.

Table 8.8 Flue gas concentration entering DCC

Component	N_2	CO_2	H_2O	O_2	NO	NO_2	SO_2
Concentration (% v/v)	74.45	15.54	8.51	0.94	0.062	0.01	0.15
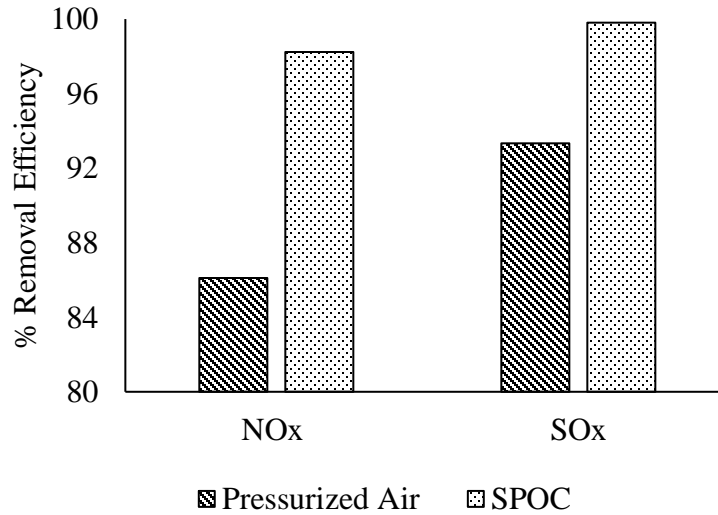
Figure 8.5 Comparison of SO_x and NO_x removal efficiencies in pressurized air and oxy-combustion

8.4.2. Effect of plant size on net plant efficiency

Table 8.9 Summary of net efficiency of MPAC plants with different scales

Supercritical steam cycle gross power (MW$_e$)	100	200	350	600
Steam Cycle Efficiency	46.5%	49.0%	51.5%	51.5%
Plant Net Power (MW$_e$)	92	183	321	550
MPAC Plant Net Efficiency:	37.5%	40.0%	41.4%	41.4%

The target output for the MPAC process in this work is 550 MWe (approx. 600 MWe gross), however it is important to understand the impact of plant size on the NPE of the power plant. To address this question, more cases with net plant outputs of 92, 183 and 321 MWe were simulated, which correspond to total steam cycle gross output of 100, 200, and 350 MWe, respectively. It is assumed that the change of net plant efficiency at different scale is primarily caused by the efficiency change of the steam cycle. The efficiency data of steam cycles at various scales were obtained from industry (Doosan Babcock Ltd). The results are shown in Table 8.9. Data shows that the efficiency drop of the steam cycle remains negligible until the gross output decreases to

below 350 MWe. As a result, the plant efficiency remains the same when the plant scale decreases from 550 to 321 MWe. At 183 MWe and 92 MWe scales, the net efficiency drops by 1.4% and 3.9% respectively.

8.4.3. Optimization

DCC Heat Integration to Heat the Exit Flue Gas from the DCC

The flue gas coming out of the DCC at 55°C is clean with less than 1.5 % v/v of H_2O. To maximize the work obtained from the first stage of the expander and to maintain operational constraints, the flue gas is heated to 110°C. The heating can be accomplished by drawing heat from various places in the system such as the boiler, the HPHR unit, and/or the DCC. Two integrations methods were considered to optimize the efficiency of the system. In Case A, presented in Figure 8.6a, the hot water from the DCC which exits at 127°C was used to heat the flue gas from the DCC outlet, and in Case B, presented in Figure 8.66b, the flue gas heat from the HPHR unit was used. Although both systems are operationally feasible, the results presented in Figure 8.7, suggest that when the heat from the DCC water outlet is used (Case A), the system has a higher net plant efficiency by 0.31% points. The reason for this can be understood by considering the exergy of the heat integrated into the steam cycle. The energy integrated from the HPHR system has higher availability than the energy integrated from the DCC outlet water (temperature of 340°C vs. 127°C). Hence, using the high-grade heat from the HPHR unit for such low-grade heating results in higher exergy destruction, whereas using the DCC outlet water, which is at 110°C, to heat the exit flue gas minimizes exergy destruction. Thus, the first option was utilized in the final modeling.
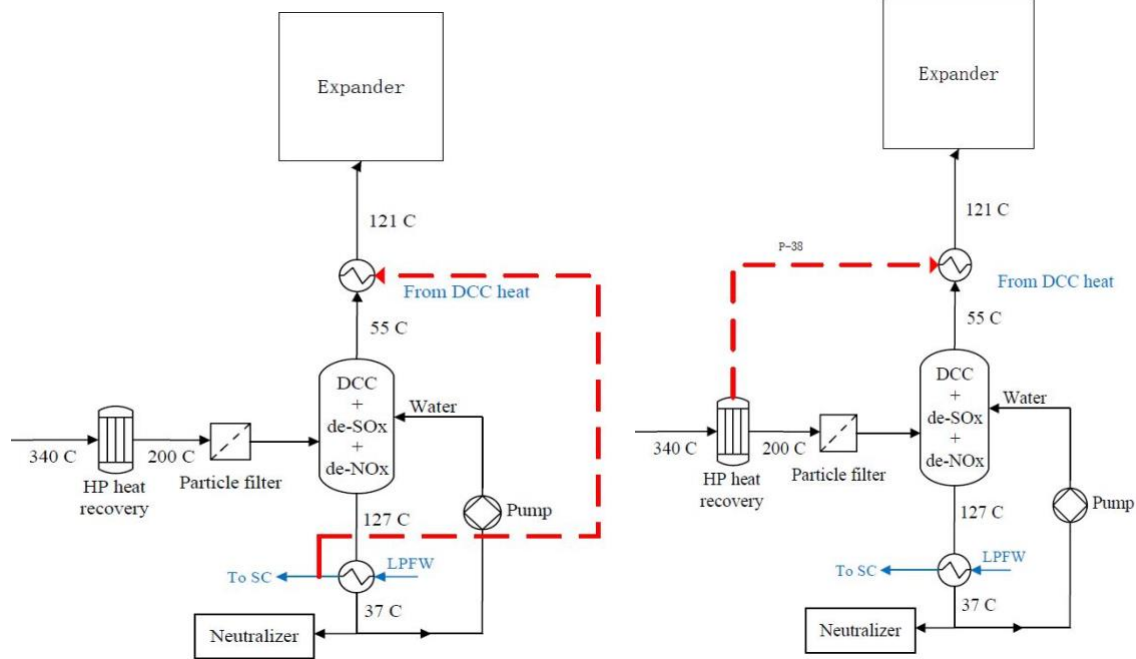
a. Case A   **b. Case B**

Figure 8.6 Heat integration methodology for MPAC.
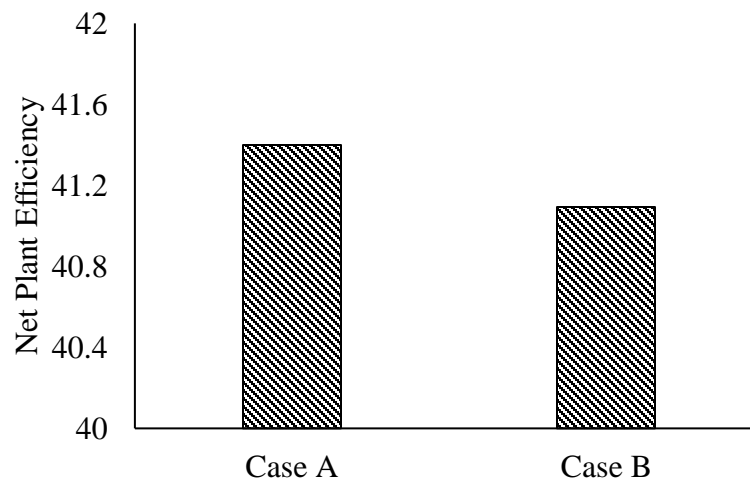
Figure 8.7 Comparison of Net plant efficiency from heat integration cases.

Inlet Air Temperature

Utilizing high-temperature air for combustion, as compared to room-temperature air, ensures that the exergy destruction in the boiler is minimized. After being compressed in the third-stage compressor (16 bar), the air is already at a temperature of 117°C, hence it is convenient to supply high-temperature air to the boiler. This also effectively removes the need for a pre-heater, since neither the MPAC nor SPOC processes require raising the inlet gas temperature. Since the high-temperature compressed air is effectively saving heat from the DCC, which is the temperature range of the hot flue gas conventionally used for pre-heating, the overall efficiency gain for the process has been accredited to the DCC.

8.5 Conclusions

The traditional utility perspective of coal power being produced from large, baseload power plants, is undergoing a paradigm shift due to market forces and environmental considerations. The growing demand for dispatchable generation capable of flexible load operation and low-cost, rapid construction, opens up the opportunity for alternative designs that are not only possible but promise to be economical, and in the process, offer a stable, secure, and reliable source of power to the grid that can be retrofitted for carbon capture. Under this backdrop, the design of the optimum coal plant of the future will require a different approach, and the proposed MPAC power plant is an ideal candidate. By operating the combustion system under pressure and thus increasing the condensation temperature of the moisture in the flue gas, the MPAC process is capable of recovering the latent heat of the flue gas moisture and integrate this heat into the steam cycle. The extra power generated can overcome the net losses caused by pressurization, resulting in a net

efficiency gain. The MPAC process promises a flexible, high efficiency, low-cost solution that can be retrofitted for carbon capture. The modular design addresses the economic challenges that have plagued new coal plants by allowing cheaper construction costs and promises to transform how coal technologies are designed and manufactured. As the combustion system consists of multiple modular boilers operated in a parallel configuration, the plant can achieve an ultra-low load, which is not feasible for any other existing technology. The ramp rate of the plant is also expected to be higher than the existing PC plants. The MPAC power plant of the future fits into the sweet spot of meeting the future needs of the grid while being built from established technologies or concepts, thus offering a high probability of success.

8.6 References

[1]   Sajal Ghosh. Electricity Consumption and Economic Growth in South Asia. Energy Policy 2002;30:125–9. https://doi.org/10.1177/1391561416649721.

[2]   Administration USEI. Annual Energy Outlook 2018 with projections to 2050. J Phys A Math Theor 2018;44:1–64. https://doi.org/DOE/EIA-0383(2017).

[3]   Kumar N, Besumer P, Lefton S, Agan. D, Hilleman D. Power Plant Cycling Costs. NREL 2012.

[4]   Abang R, Weiß S, Krautz HJ. Impact of increased power plant cycling on the oxidation and corrosion of coal-fired superheater materials. Fuel 2018;220:521–34. https://doi.org/10.1016/j.fuel.2018.02.047.

[5]   Scheffknecht G, Al-Makhadmeh L, Schnell U, Maier J. Oxy-fuel coal combustion-A review of the current state-of-the-art. Int J Greenh Gas Control 2011;5:16–35. https://doi.org/10.1016/j.ijggc.2011.05.020.

[6]   Hagi H, Nemer M, Le Moullec Y, Bouallou C. Towards second generation oxy-pulverized coal power plants: Energy penalty reduction potential of pressurized oxy-combustion systems. Energy Procedia 2014;63:431–9. https://doi.org/10.1016/j.egypro.2014.11.046.

[7]   Rubin ES, Taylor MR, Yeh S, Hounshell DA. Learning curves for environmental technology and their importance for climate policy analysis. Energy 2004;29:1551–9. https://doi.org/10.1016/j.energy.2004.03.092.

[8]   Gopan A, Kumfer BM, Phillips J, Thimsen D, Smith R, Axelbaum RL. Process design and performance analysis of a Staged, Pressurized Oxy-Combustion (SPOC) power plant for carbon capture. Appl Energy 2014;125:179–88. https://doi.org/10.1016/j.apenergy.2014.03.032.

[9]   Hume S. Enabling Staged Pressurized Oxy-Combustion: Improving Flexibility and Performance at Reduced Cost. 2019.

[10]   Corp CT, Station M. Small, Modular, low-cost coal-fired power plants for the International Market n.d.

[11]   Gopan A, Kumfer BM, Axelbaum RL. Effect of operating pressure and fuel moisture on net plant efficiency of a staged, pressurized oxy-combustion power plant. Int J Greenh Gas Control 2015;39:390–6. https://doi.org/10.1016/j.ijggc.2015.05.014.

[12]   Gopan A, Verma P, Wang Z, Axelbaum R. Quantitative analysis of the impact of flue gas recirculation on the efficiency of oxy-coal power plants. Int J Greenh Gas Control 2019.

[13]   Liu W, Li Q, Liang F, Liu L, Xu G, Yang Y. Performance analysis of a coal-fired external combustion compressed air energy storage system. Entropy 2014;16:5935–53. https://doi.org/10.3390/e16115935.

[14]   Advancing oxycombustion technology for bituminous coal power plants: An R&D guide. Report DOE/NETL - 2010/1405, US Department of Energy, National Energy Technology Laboratory (2012). 2012.

[15]   NETL. Cost and Performance Baseline for Fossil Energy Plants Volume 1a: Bituminous Coal (PC) and Natural Gas to Electricity Revision 3. Natl Energy Technol Lab 2015;1a:240. https://doi.org/DOE/NETL-2010/1397.

[16]   Black J. Process Modeling Design Parameters in NETL Studies. NETL 2014;DOE/NETL-2.

[17]   Wang X, Liu Z-H, Han X, Chen Y, Tan H-Z, Axelbaum R. Dynamic Mechanism Investigation on the Formation of SO3 During Pressurized Oxy-Fuel Combustion. J Eng Thermophys 2017;38.

[18]   Fleig D, Normann F, Andersson K, Johnsson F, Leckner B. The fate of sulphur during oxy-fuel combustion of lignite. Energy Procedia 2009;1:383–90. https://doi.org/10.1016/j.egypro.2009.01.052.

[19]   Zuo W, Zhang X, Li Y. Review of flue gas acid dew-point and related low temperature corrosion. J Energy Inst 2020;93:1666–77. https://doi.org/10.1016/j.joei.2020.02.004.

[20]   Ting T, Stanger R, Wall T. Laboratory investigation of high pressure NO oxidation to NO2 and capture with liquid and gaseous water under oxy-fuel CO2compression conditions. Int J Greenh Gas Control 2013;18:15–22. https://doi.org/10.1016/j.ijggc.2013.06.016.

[21]   Stanger R, Ting T, Spero C, Wall T. Oxyfuel derived CO2 compression experiments with NOx, SOx and mercury removal-Experiments involving compression of slip-streams from the Callide Oxyfuel Project (COP). Int J Greenh Gas Control 2015;41:50–9. https://doi.org/10.1016/j.ijggc.2015.06.022.

[22]   Normann F, Jansson E, Petersson T, Andersson K. Nitrogen and sulphur chemistry in pressurised flue gas systems: A comparison of modelling and experiments. Int J Greenh Gas Control 2013;12:26–34. https://doi.org/10.1016/j.ijggc.2012.11.012.

[23]   Ajdari S, Normann F, Andersson K, Johnsson F. Modeling the nitrogen and sulfur chemistry in pressurized flue gas systems. Ind Eng Chem Res 2015;54:1216–27. https://doi.org/10.1021/ie504038s.

[24]   Ajdari S, Normann F, Andersson K, Johnsson F. Reduced Mechanism for Nitrogen and Sulfur Chemistry in Pressurized Flue Gas Systems. Ind Eng Chem Res 2016;55:5514–25. https://doi.org/10.1021/acs.iecr.5b04670.

[25]   Verma P, Gromotka Z, Yablonsky G, Stokie D, Constales D, Kumfer B, et al. Optimizing complexity in the kinetic modelling of integrated flue gas purification for pressurized oxy-combustion. Chem Eng J 2020. https://doi.org/10.1016/j.cej.2019.122875.

[26]   Tsukahara H, Ishida T, Mayumi M. Gas-phase oxidation of nitric oxide: Chemical kinetics and rate constant. Nitric Oxide - Biol Chem 1999;3:191–8. https://doi.org/10.1006/niox.1999.0232.

[27]   Lee YN, Schwartz SE. Reaction kinetics of nitrogen dioxide with liquid water at low partial pressure. J Phys Chem 1981;85:840–8. https://doi.org/10.1021/j150607a022.

[28]   Axelbaum R, Stokie D, Verma P, Kumfer B, Min Y, Zhu Y, et al. Integrated Flue Gas Purification and Latent Heat Recovery for Pressurized Oxy-Combustion. 2019.

[29] Cengel Y, Boles M. Thermodynamics: An Engineering Approach. Fifth. McGraw Hill; n.d.

[30] Lu Y, Jahkola A, Hippinen I, Jalovaara J. The emissions and control of NOx and N2O in pressurized fluidized bed combustion. Fuel 1992;71:693–9. https://doi.org/10.1016/0016-2361(92)90174-M.

[31] Svoboda K, Pohořelý M. Influence of operating conditions and coal properties on NOx and N2O emissions in pressurized fluidized bed combustion of subbituminous coals. Fuel 2004;83:1095–103. https://doi.org/10.1016/j.fuel.2003.11.006.

[32] John S. Nordin, Merriam NW. Nox Emissions Produced With Combustion of Powder River Basin Coal in a Utility Boiler 1997.

Chapter 9.   Summary and Future Work

9.1   Summary

1.   In the combustion experiments conducted in a $100\,kW_{th}$ pressurized oxy-combustor, 1) the concentration of CO in the flue gas decreases with pressure and residence time in the combustor and decreases with excess O_2 in the flue gas, 2) the concentration of NO in the flue gas decreases with pressure, but increases with excess O_2 concentration in the flue gas, and 3) the concentration of SO_2 in the flue gas decreases with increase in pressure, and increase in O_2 in the flue gas concentration.

2.   The reaction rate between HNO_2 and HSO_3^- in acidic conditions, increases with decrease in pH and also increases with increase in liquid temperature. Moreover, with decreasing pH, the product formed from the reaction slowly shifts from HADS towards the formation of HSO_4^-. Increasing temperature does not seem to have an impact on selectivity of the products.

3.   The kinetics model reaction inside the DCC can be reduced to 5-reaction system. The disintegration of HNO_2 is not significant and the liquid phase mechanism can be reduced to two major reactions. The reduced model only contains species that could be easily measured.

4.   The experiments in DCC suggest that at 15 bar and 1-3% excess oxygen in the flue gas, it is possible to remove most of the SO_2 and higher than 80% of NO. The removal of NO is mainly limited by the residence time in the column because of the comparatively slow NO oxidation to NO_2.

5.   The removal of SO_2 is enhanced by the liquid phase interaction with absorbed NO_2 i.e. reaction between HNO_2 and HSO_3^-. The reaction enhancement of SO_2 removal goes up with

higher NO inlet concentration. Moreover, even though the overall removal of SO_2 goes down with increase in temperature, the fraction of SO_2 removed through the liquid phase reaction with HNO_2 increases. Finally, the impact of L/G ratio is significantly higher on SO2 than on NO. SO2 removal foes down shapely with reducing L.G ratio compared to NO removal.

6.   The reduced model is able to predict the removal efficiencies to a high accuracy (within 5% of error), over a range of parameters.

7.   An optimized DCC full scale model with multiple water inlet is able to remove higher 9% NO and 3% higher SO_2. This is mainly achieved by faster cooling and condensation of moisture in the flue gas, giving the gas a higher residence time in the column which results in higher removal of NO and consequently higher SO_2. The final flow rate of water and the inlet stage can be optimized for any given coal with varying amount of moisture.

8.   Reducing flue gas recycle reduces the energy penalty for a power plant, by decreasing the exergy destruction in the high temperature zone of the power plant. This is true for both atmospheric pressure and pressurized oxy-combustion power plant. The impact on net plant efficiency is highly non-linear with the recycle ratio, the efficiency reduces significantly for a recycle ratio of 60-70% but remains small and linear up to 30%.

9.   A modular, pressurized air-combustion power plant with expansion turbines to recover the energy of pressurization has a higher efficiency than conventional air combustion power plant. Such a power plant can be easily retrofitted to SPOC by adding an ASU and CPU when economics of such a move are supportive.

9.2   Suggestion for future work

The following are the suggestions for future work in development of stages pressurized oxy-combustion process,

1.   A thorough understanding of sulfur balance in the combustion process is required. A systematic analysis of sulfur in ash and SO_3 in the flue gas is needed to close the sulfur balance. Additionally, the impact of pressure on both ash retention and SO_3 formation should be systematically investigated. A model should be developed to validate the results.

2.   Measurement of other nitrogen compounds that may exists in the flue gas is needed, especially N_2O to better understand the NOx formation in the combustion process.

3.   A different coal with higher sulfur and nitrogen should be tested to further understand the formation process of SO_x and NO_x.

4.   For SPOC process, there is also a need to understand the transformation of SO_x, NO_x and CO in staging flames. Studies have shown that reburning may result in different species because it changes the radical pool.

5.   In the lab scale experiment to understand the kinetics of interaction between HNO_2 and HSO_3^-, experiments should be designed to measure the disintegration of HADS at higher temperature. This is required to understand if there is a significant impact of that reaction, but also to design a treatment process for the water coming out of DCC.

6.   There is also a need to understand the impact of other acids, such as Hcl, which may exists in the flue gas on the kinetics of the process.

7.   The direct contact column (DCC) needs to be operated at higher SO_2 concentration to understand the limits of removal in the liquid phase and to understand the impact of pH more

significantly. Additionally, there is a need to measure the concentration of N_2O in the exhaust of the column to collaborate the model.

8.   More studies on the treatment of water coming out of the DCC should be performed to understand the most effective way to design the process.

9.   A DCC experiments with flue gas containing moisture and ash particles is required to confirm the heat transfer in the column and to see if condensation of moisture has an impact in removal of SO_x and NO_x. Moreover, there is a need to understand the impact of recycling the water from the sump to see the impact of recycled water on removal of SO_x and NO_x, since recycling can reduce the water usage. Following this, an impact of caustic injection in the inlet water should also be investigated.

10.   To verify the optimized heat transfer profile, temperature profile measurements on the column is required to confirm the heat transfer. This would also corroborate the temperature profile from the model.

11.   There is also a need to analyze the optimized design for optimization of SO_x removal and plant efficiency for high sulfur coal. This implies that if a change in L/G ratio is required to remove a higher amount of SO_2, what impact does that has on net plant efficiency of the power plant.

12.   In understanding the impact of flue gas recycle, a detailed analysis of the impact on plant efficiency and operational issues of wet flue gas recycle needs to be discussed. Several new systems have proposed wet flue gas recycle; however only limited analysis exists.

Appendix A: Normann et al. mechanism.

#	Reaction	Kinetic rate expression (mol m^3 s^{-1})
1	$2NO + O_2 \rightarrow 2NO_2$	$r = 1.197 \times 10^{-3} \times exp\left(\dfrac{530.4}{T}\right) \times C_{NO}^2 \times C_{O_2}$
2	$2NO_2 + O_2 \rightarrow 2NO$	$r = 1.632 \times 10^6 \times exp\left(\dfrac{-13109.67}{T}\right) \times C_{NO_2}^2$
3	$NO + NO_2 \leftrightarrow N_2O_3$	$r = 5.625 \times \left(C_{NO} \times C_{NO_2} - \dfrac{C_{N_2O_3}}{K(3)}\right)$
4	$NO_2 + NO_2 \leftrightarrow N_2O_4$	$r = 5.625 \times \left(C_{NO_2}^2 - \dfrac{C_{N_2O_4}}{K(4)}\right)$
6	$NO + NO_2 + H_2O \leftrightarrow 2HNO_2$	$r = 1.6 \times 10^{-4} \times \left(C_{NO} \times C_{NO_2} \times C_{H_2O} - \dfrac{C_{HNO_2}^2}{K(6)}\right)$
10	$NO_2 + SO_2 \leftrightarrow SO_3 + NO$	$r = 6.32 \times 10^6 \times exp\left(\dfrac{-13587}{T}\right) \times C_{NO_2} \times C_{SO_2}$
11	$SO_2 + H_2O \leftrightarrow HSO_3^- + H^+$	$r = k_{inst} \times \left(C_{SO_2} - \dfrac{C_{HSO_3^-} \times C_{H^+}}{K(11)}\right)a$
14	$2NO_2 \leftrightarrow N_2O_4$	$r = 4.5 \times 10^5 \times \left(C_{NO_2}^2 - \dfrac{C_{N_2O_4}}{K(14)}\right)$
15	$NO + NO_2 \leftrightarrow N_2O_3$	$r = 1.1 \times 10^6 \times \left(C_{NO} \times C_{NO_2} - \dfrac{C_{N_2O_3}}{K(15)}\right)$
16	$2NO_2(N_2O_4) + H_2O \rightarrow HNO_2 + HNO_3$	$r = 6.5 \times 10^4 \times C_{NO_2}^2$
17	$NO + NO_2(N_2O_3) + H_2O \rightarrow 2HNO_2$	$r = 7.4 \times 10^3 \times C_{NO} \times C_{NO_2}$
18	$3HNO_2 \rightarrow HNO_3 + 2NO + H_2O$	$r = \dfrac{1}{3} \times 10.267 \times 10^{\left(-\frac{6200}{T}+20.19\right)} \times \dfrac{C_{HNO_2}^4 \times H_{NO}^2}{C_{NO}^2}$
19	$HNO_3 \leftrightarrow NO_3^- + H^+$	$r = 8534 \times C_{NO_2}^2 \times C_{HSO_3^-}$
20	$HNO_2 \leftrightarrow NO_2^- + H^+$	$r = k_{inst} \times \left(C_{HNO_2} - \dfrac{C_{NO_2^-} \times C_{H^+}}{K(20)}\right)a$
23	$HSO_4^- \leftrightarrow SO_4^{2-} + H^+$	$r = k_{inst} \times \left(C_{HSO_4^-} - \dfrac{C_{SO_4^{2-}} \times C_{H^+}}{K(23)}\right)a$
24	$HNO_2 + HSO_3^- \rightarrow NOSO_3^- + H_2O$	$r = 2.4 \times C_{HNO_2} \times C_{HSO_3^-}$
25	$NOSO_3^- + H^+(+H_2O) \rightarrow HNO + H_2SO_4$	$r = 50 \times C_{NSS} \times C_{HSO_3^-}$
26	$NOSO_3^- + HSO_3^- \rightarrow 2HNO(SO_3)_2^{-2}$	$r = 85 \times C_{NSS} \times C_{HSO_3^-}$
27	$HNO + HNO \rightarrow N_2O + H_2O$	$r = 3 \times 10^4 \times C_{HNO}^2$
28	$HNO(SO_3)_2^{-2} + H^+ \rightarrow HNOHSO_3^- + H^+ + HSO_4^-$	$r = 1.9 \times 10^{-2} \times C_{HADS} \times C_{H^+}$
32	$CO_2 + H_2O \leftrightarrow H_2CO_3$	$r = k_{inst} \times \left(C_{CO_2} - \dfrac{C_{H_2CO_3}}{K(32)}\right)a$
33	$H_2CO_3 \leftrightarrow HCO_3^- + H^+$	$r = k_{inst} \times \left(C_{H_2CO_3} - \dfrac{C_{HCO_3^-} \times C_{H^+}}{K(33)}\right)a$

a: As a specific rate for the equilibrium controlled reaction is not available, k_{inst} of 100,000 is used for instantaneous reaction.

Appendix B: Reduced mechanisms proposed by Ajdari et al.

List of Reactions in the Detailed Mechanism

#	Reactions
	Gas Phase Reactions
R_g1_f	$2NO + O_2 \rightarrow 2NO_2$
R_g1_b	$2NO_2 \rightarrow 2NO + O_2$
	Liquid Phase Reactions
R_l1	$2NO_2 + H_2O \rightarrow HNO_2 + HNO_3$
R_l3_f	$2HNO_2 \rightarrow NO + NO_2 + H_2O$
R_l3_b	$NO + NO_2 + H_2O \rightarrow 2HNO_2$
R_l12	$2NO_2 + HSO_3^- + H_2O \rightarrow SO_4^{2-} + 3H^+ + 2NO_2^-$
R_l14	$HNO_2 + HSO_3^- \rightarrow NSS + H_2O$
R_l16	$NSS + H_2O \rightarrow HNO + HSO_4^-$
R_l17	$HNO + HNO \rightarrow N_2O + H_2O$
R_l30	$HNO_2 + HSO_3^- \rightarrow HSO_4^- + 0.5N_2O + 0.5H_2O$
R_l31	$HNO_2 + 2HSO_3^- \rightarrow HADS + H_2O$
	Equilibrium Reactions
R_l6	$HNO_2 \leftrightarrow H^+ + NO_2^-$
R_l7	$HNO_3 \leftrightarrow H^+ + NO_3^-$
R_l25	$SO_2 + H_2O \leftrightarrow H^+ + HSO_3^-$
R_l27	$HSO_4^- \leftrightarrow H^+ + SO_4^{2-}$

List of Reactions in the Reduced Mechanism[a]

Mechanism	Kinetic reactions										Equilibrium reactions				no. of reactions	no. of species
	R_g1	R_l1	R_l3	R_l12	R_l14	R_l15	R_l16	R_l17	R_l30	R_l31	R_l6	R_l7	R_l25	R_l27		
Reduced pH 1-5	×	×	×	×[e]	×	×	×	×			×	(×)	×	×	12	20
Reduced pH 1	×	×	×		(×)		(×)	(×)	×			(×)	×	×	7	16
Reduced pH 2	×	×	×		(×)	(×)	(×)	(×)	×	×		(×)	×	×	8	17
Reduced pH 4	×	×	×		(×)	(×)				×	×	(×)	×		7	14

| Reduced pH 5 | × | × | | × | (×) | (×) | | | × | | × | (×) | × | | × | 7 | 14 |

Appendix C: Curriculum Vitae

Piyush Verma

Ph.D. Candidate

Department of Energy, Environmental & Chemical Engineering

Washington University in Saint Louis

One Brookings Drive, Campus Box 1180, Saint Louis, MO 63130

Office: +1 314-295-0701

E-mail: piyush.k.verma@wustl.edu

Education

Ph.D., Department of Energy, Environmental & Chemical Engineering	2016 – Present
Washington University in Saint Louis, U.S.A.	
Bachelor of Technology, Department of Chemical Engineering	2010 – 2014
Indian Institute of Technology, Varanasi, India	

Research Experience

Ph.D. Washington University in St Louis, U.S.A.	2016 – Present

Reaction mechanism and chemical kinetics development

- Optimizing the reaction mechanism for the co-removal of SO_x and NO_x from the flue gas of pressurized oxy-combustion.

- Development of liquid-phase kinetics for the interaction of dissolved SO_x and NO_x in a lab-scale reactor.
- Understanding the impact of temperature and pH on the reaction rate and mechanism.

Pilot-scale testing and model validation

- Pilot-scale testing of a 100 kW_{th} DCC (packed bed absorption column) using synthetic flue gas to study the parameters for efficient scrubbing.
- Validating the model and kinetics developed in the lab-scale reactor over a range of parameters in the pilot-scale scrubber.
- Process design and modeling a novel direct contact cooler (DCC) to remove SO_x and NO_x from pressurized flue gas.

Pilot-scale studies on the formation of SO_x and NO_x in 100 kW_{th} pressurized oxy-combustion of solid fuel

- Understanding the impact of oxygen concentration, pressure, and residence time on SO_x and NO_x formation in pressurized oxy-combustion.
- Design of measurement technique for SO_3 at high pressure and temperature.
- Development of post-flame kinetics for understanding the formation of SO_x and NO_x at high pressure.

Development and optimization of pressurized combustion processes

- Process Design and Analysis of novel carbon capture ready process flexible load power generation: Modular pressurized air combustion.
- Development of the relationship between the amount of recycle flue gas used and the change in net plant efficiency for both atmospheric and pressurized oxy-combustion power plants.

Work Experience

Reliance Industries Limited., Process Design Engineer   July 2014- June 2016

- Development of a dynamic Reactor Network Model for a pressurized Entrained Flow Gasifier.
- Parametric studies on the model to understand the start-up and shut down behavior.
- Studying the impact of fly ash addition on the slagging characteristics of ash.

Skills

- Software: Aspen Plus, Aspen Custom Modeler, Matlab
- Languages: C++, C
- Instruments: Ionic Exchange Chromatography (IC); Thermogravimetric Analyzer (TGA); Scanning Electron Microscopy with Energy Dispersive X-ray (SEM/EDX)

Selected research paper

1. *Quantitative analysis of the impact of flue gas recirculation on the efficiency of oxy-coal power plants*, P Verma, A Gopan, Z Yang, RL Axelbaum, International Journal of Greenhouse Gas Control, 2020.
2. *Optimizing complexity in the kinetic modelling of integrated flue gas purification for pressurized oxy-combustion*, P Verma, Z. Gromotka, RL Axelbaum, Chemical Engineering Journal, 2020.
3. *Process design and analysis of a novel carbon-capture-ready process for flexible-load power generation: Modular pressurized air combustion*, P Verma, Z Yang, S Hume, A Maxson, RL Axelbaum, Energy Conversion and Management, 2021
4. *Pilot-scale testing of direct contact cooler for the removal of SOx and NOx from the flue gas of pressurized oxy-coal combustion*, D Stokie, P Verma, B Kumfer, G Yablonsky, AK Suresh, RL Axelbaum, Chemical Engineering Journal, 2021
5. *Experimental study and demonstration of pilot-scale, dry feed, oxy-coal combustion under pressure.* Z Yang, D Khatri, P Verma, T Li, A Adeosun, BM Kumfer, RL Axelbaum, Applied Energy, 2021
6. *A process to simultaneously recover latent heat and remove SOx and NOx from pressurized flue gas.* P Verma, Z Yang, RL Axelbaum, 12th International Conference on Applied Energy (ICAE2020)

Patents

1. *Modular pressurized coal combustion (mpcc) for flexible generation.* P Verma, Z Yang, R Axelbaum - US Patent App. 16/938,725, 2021
2. *Simultaneous recovery of latent heat and removal of SOx and NOx from pressurized flue gas.* P Verma, Z Yang, R Axelbaum – Provisional, 2020

Appendix D: Transcript

E44 501 01	FL2016	A	3	Transport Phenomena in EECE
E44 503 01	FL2016	A+	3	Mathematical Methods in Engineering
E44 504 01	FL2016	A	3	Aerosol Science and Technology
E44 507 01	SP2017	A	3	Kinetics and Reaction Engineering Principles
E44 502 01	SP2017	A	3	Advanced Thermodynamics in EECE
E44 576 01	SP2017	A	3	Chemical Kinetics and Catalysis
E44 512 01	FL2017	A+	3	Combustion Phenomena
E37 5412 01	FL 2018	B	3	Computational Fluid Dynamics
E37 5424 01	FL 2020	A+	3	Thermo-Fluid Modeling of Renewable Energy Systems
E44 514 01	SP 2021	A	3	Atmospheric Science and Climate

Cumulative GPA: 3.9